State of Oregon
Oregon Department of Geology and Mineral Industries
Brad Avy, State Geologist

GEOLOGIC MAP 124

GEOLOGIC MAP OF THE BIGGS JUNCTION AND RUFUS 7.5' QUADRANGLES, SHERMAN AND GILLIAM COUNTIES, OREGON

by Ian P. Madin[1] and Jason D. McClaughry[2]

2019

[1]Ian.Madin@oregon.gov, Oregon Department of Geology and Mineral Industries, 800 NE Oregon Street, Suite 965, Portland, Oregon 97232
[2]Oregon Department of Geology and Mineral Industries, Baker City Field Office, Baker County Courthouse, 1995 3rd Street, Suite 130, Baker City, Oregon 97814

NOTICE

Cover photograph:
Missoula Flood-scoured cliffs of Basalt of Sand Hollow and Basalt of Ginkgo east of Rufus.
Photograph by Ian Madin, 2018.

Expires: 5/31/2020

Oregon Department of Geology and Mineral Industries Geologic Map 124
Published in conformance with ORS 516.030.

For additional information:
Administrative Offices
800 NE Oregon Street, Suite 965
Portland, OR 97232
Telephone (971) 673-1555
Fax (971) 673-1562
https://www.oregongeology.org
https://www.oregon.gov/dogami

TABLE OF CONTENTS

LIST OF FIGURES

LIST OF TABLES

GEOGRAPHIC INFORMATION SYSTEM (GIS) DATA

See the digital publication folder for files.

GEODATABASE

BJR2019_GeMS_v10.6.gdb

See the appendix for geodatabase description.
Geodatabase is Esri® version 10.6 format.

SHAPEFILES AND SPREADSHEETS (ALSO SEE APPENDIX)

Shapefiles
BJR2019_Geochemistry.shp
BJR2019_RefMap
BJR2019_WaterWells.shp
BJR2019_XSectionLines.shp

Spreadsheets (Microsoft® Excel®)
BJR2019_DATA.xls master file contains sheets:
BJR2019_Geochemistry.xls
BJR2019_WaterWells.xls

Metadata is embedded in the geodatabase and shapefiles
and is also provided as separate .xml format files.

MAP PLATE

Plate 1. Geologic map of the Oregon portions of the Biggs Junction and Rufus 7.5' quadrangles, Sherman and Gilliam Counties, Oregon

FULL-RESOLUTION OUTCROP IMAGES

In order to capture the detail and scope of large outcrops shown in eight of the figures (Figures 5-8, 5-22, 5-27, 5-30, 5-34, 5-35, 5-36, and 5-51), multiple overlapping photographs were taken in the field and processed using Agisoft Metashape structure from motion software. Photographs were taken with an Apple® iPhone® SE or iPad® 2 with a native resolution of 12 megapixels, and photo locations were recorded using the camera GPS system. The photos for the outcrop were aligned in Metashape, and the aligned photos were used to generate a high-resolution point cloud and 3D model. The 3D models were oriented with a view direction that was perpendicular to the outcrop and horizontal, and that orientation was used as the plane of projection for an orthomosaic image. The resulting orthomosaics retain detail in the centimeter range.

1.0 INTRODUCTION

The geology of the Oregon portions of the Biggs Junction and Rufus 7.5' quadrangles was mapped by the Oregon Department of Geology and Mineral Industries (DOGAMI) during 2018 and 2019 through USGS STATEMAP Award G18AC00136. Additional funds were provided by the State of Oregon. The objective of this mapping project is to provide an updated and spatially accurate geologic framework for northern Sherman County, as part of a multi-year study of the geology of the larger Middle Columbia Basin (**Figure 1-1** and **Figure 1-2**). Detailed geologic mapping in the Middle Columbia Basin is a high priority of the Oregon Geologic Map Advisory Committee (OGMAC).

The core products of this study are this report, an accompanying plottable geologic map and cross sections, and an Esri ArcGIS™ ArcMap™ geodatabase. The geodatabase presents the new geologic mapping in a digital format consistent with the Geologic Map Schema (GeMS), version 2.7 (USGS National Cooperative Geologic Mapping Program, 2010, 2018). The geodatabase contains spatial information about geologic polygons, contacts, and structures, and basic data about each geologic unit such as age, lithology, mineralogy, and structure. Digitization at scales of 1:8,000 or better was accomplished by using a combination of 1-m lidar DEMs and 1-m 2011, 2014, and 2016 National Agriculture Imagery Program (NAIP) digital orthophoto mosaics. Nominal 1-m DEMs were produced from 1954 aerial photographs using Agisoft Photoscan™ Structure from Motion software. Photoscan was also used to produce a nominal 1-m orthomosaic from the 1954 photos, and an additional orthomosaic from 1947 aerial photos. Additional structural insight was derived from an unpublished high-resolution aeromagnetic survey image provided by Dr. Rick Blakely of the USGS (written communication, 2018). Surficial and bedrock geologic units contained in the geodatabase are depicted on Plate 1 at a scale of 1:24,000. Plate 1 also includes two interpretive cross sections derived from the digital data included in the geodatabase. Both the geodatabase and associated plottable map are supported by this report describing the geology in detail, and digital appendices with geochemical and water well data.

This report, digital geologic maps, and cross sections refine our understanding of geologic conditions that control the distribution, quantity, and quality of groundwater resources, the distribution of terrain susceptible to landslides, the nature of seismic hazards, and the distribution of potential aggregate sources and other mineral resources in the Oregon portions of the Biggs Junction and Rufus 7.5′ quadrangles. New detailed geologic data presented here also provide a basis for future geologic, geohydrologic, and geohazard studies in the greater Middle Columbia Basin.

Figure 1-1. Location of the Middle Columbia Basin in north-central Oregon and adjacent physiographic features. Study area shown by black outline (upper right). Solid orange line corresponds to the watershed hydrologic boundary of the Middle Columbia Basin. The Columbia River, flowing from east to west, separates the states of Oregon on the south and Washington on the north. The Deschutes River marks the boundary between Sherman County on the east and Wasco County on the west. Label abbreviations are as follows: OR – Oregon; WA – Washington.

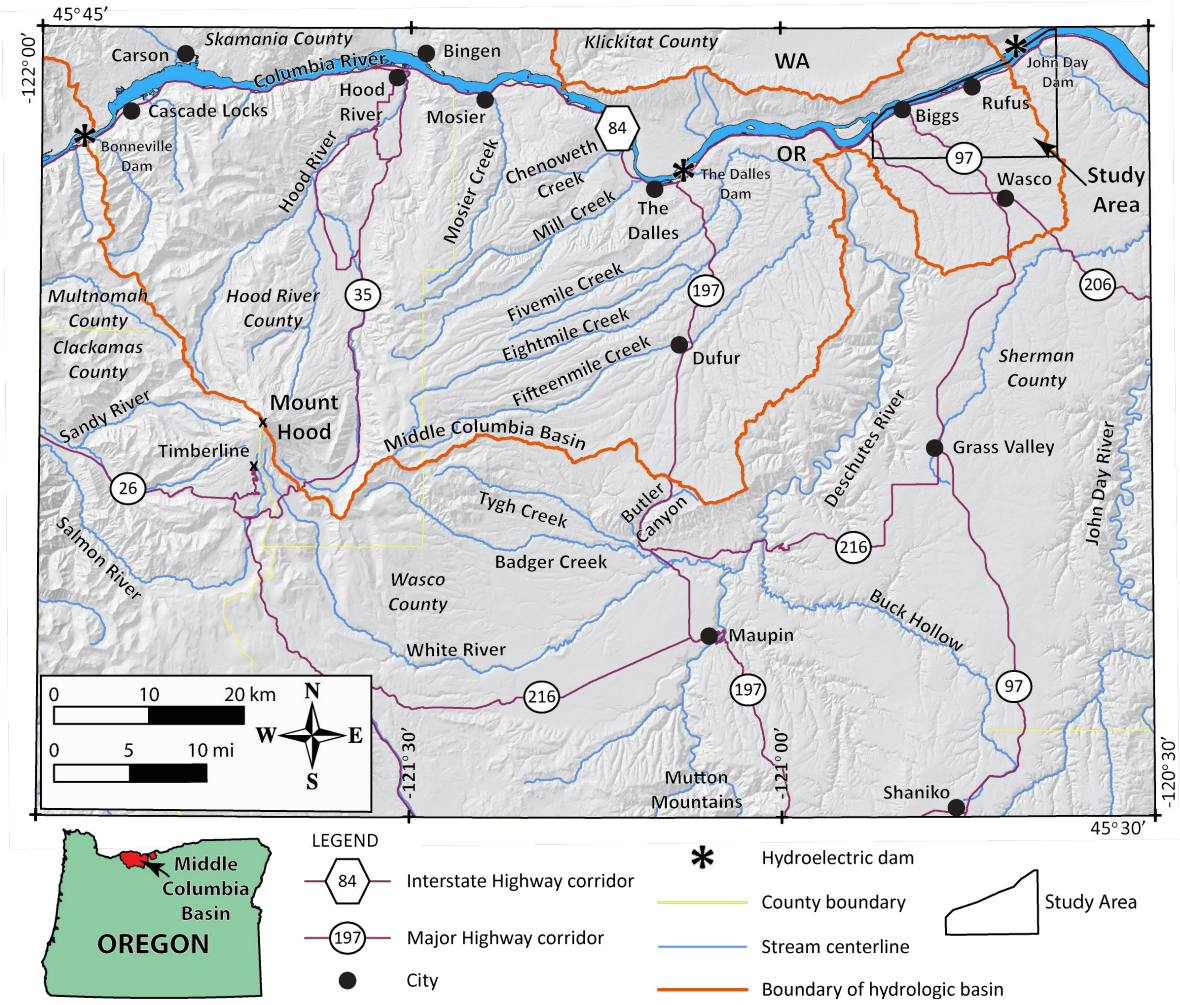

Figure 1-2. Status map of geologic mapping completed, in progress, and planned in the Middle Columbia Basin. Yellow-shaded area encompasses geologic mapping in the Oregon portions of the Biggs Junction and Rufus 7.5′ quadrangles completed for this report. Dark blue-shaded quadrangles include areas where geologic mapping is currently being conducted by the USGS (FEDMAP). Orange-shaded quadrangles include areas that have been mapped by DOGAMI with funding from OWRD and STATEMAP between 2014 and 2017. Dog River 7.5′ quadrangle was mapped for STATEMAP during 2017 and 2018. Purple- and light blue-shaded quadrangles include targets of future geologic mapping by DOGAMI. Label abbreviations are as follows: BD—Bonneville Dam; CL—Cascade Locks; C—Carson; HR—Hood River; B—Bingen; TD—The Dalles; TDD—The Dalles Dam; D—Dufur; OR—Oregon; WA—Washington; R—Rufus; W—Wasco; JDD—John Day Dam; GV—Grass Valley.

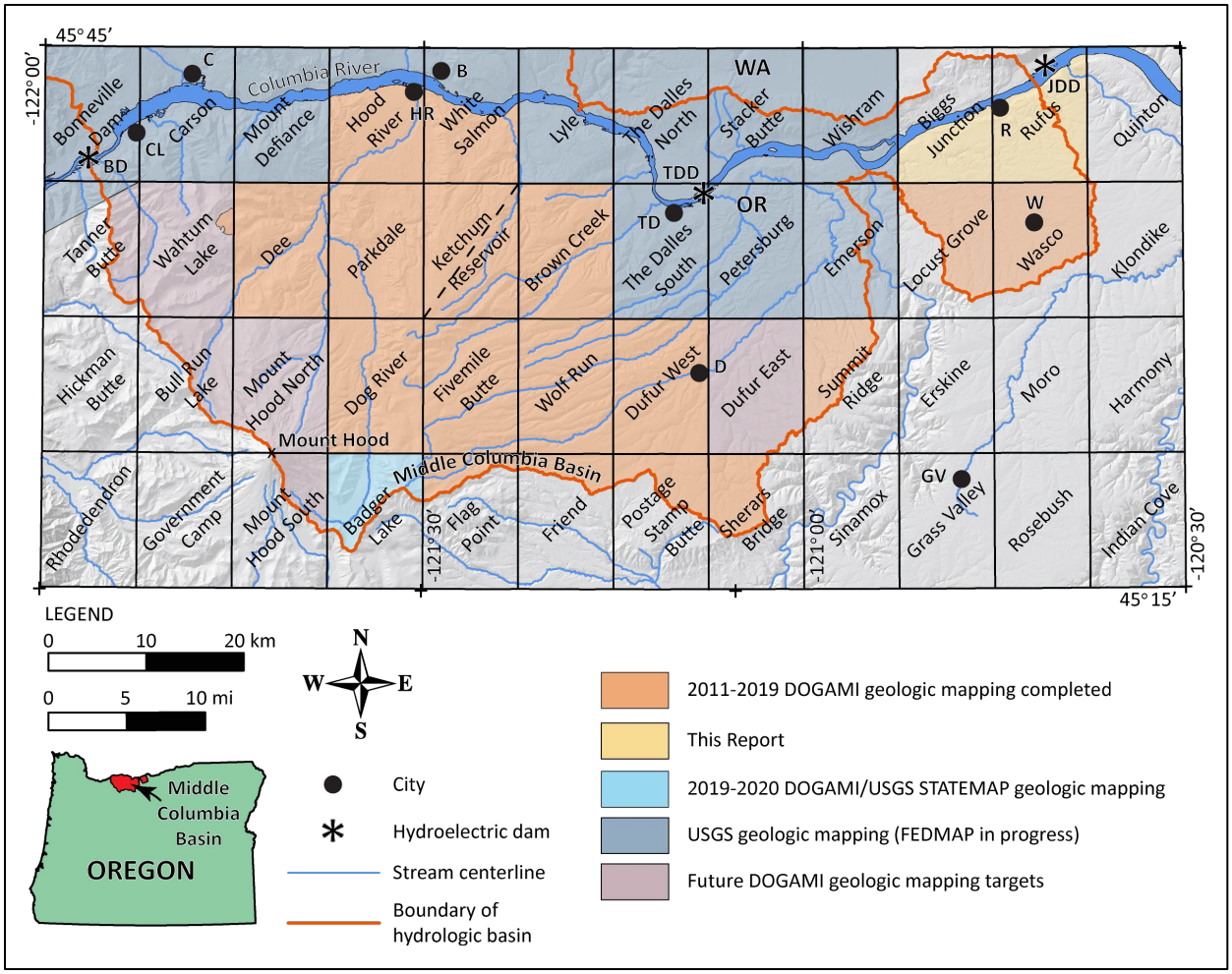

2.0 GEOGRAPHIC AND GEOLOGIC SETTING

The Oregon portions of the Biggs Junction and Rufus 7.5' quadrangles encompass an area of ~165 km^2 (64 mi^2) in the northeast part of the Middle Columbia Basin in north-central Oregon (**Figure 1-1** and **Figure 1-2**). The Middle Columbia Basin extends from the city of Wasco and the John Day Dam on the east to Mount Hood and Bonneville Dam on the west and to Butler Canyon on the south. The northern part of the basin is bound by the Columbia River Gorge. Major tributaries to the Columbia River include Hood River, Mosier Creek, Mill Creek, Fivemile Creek, Eightmile Creek, Fifteenmile Creek, the Deschutes River,

and Frank Fulton, Spanish Hollow, Scott, and Helm canyons and the John Day River (**Figure 1-1** and **Figure 1-2**). This part of north-central Oregon is topographically varied, transitioning from the steep mountainous terrain of the Cascade Range on the west to broad plateaus and ridges incised by the deep canyons of the Columbia and its tributaries on the east. Topographic relief in the Middle Columbia Basin is substantial, ranging from 3,428 m (11,244 ft) at the summit of Mount Hood along the crest of the Cascade Range to 23 m (75 ft) at the Columbia River at Bonneville Dam (**Figure 1-1**). Farther east, in the Oregon portions of the Biggs Junction and Rufus 7.5' quadrangles, elevations range from ~450 m (1,480 ft) in the southeast to ~50 m (160 ft) along the shores of the Columbia River. The Biggs Junction and Rufus quadrangles have two distinct landscapes. The majority of the area is a broad rolling plain almost entirely under cultivation with dryland wheat. Along the northern edge of the map area, the plateau is truncated by the steep to vertical walls of the Columbia River Gorge, here about 150–200 m (500–650 ft) deep. Tributary streams cut narrow, steep-walled canyons into the plateau as they near the Gorge, but the headwaters have very low relief and low gradients. Climate varies across the Middle Columbia Basin due to its transitional location between the wet marine airflow-dominated Cascade Range and the semi-arid continental climate of eastern Oregon. The upland and western parts of the basin have a relatively wet climate, averaging ~77 cm (30.5 in) of precipitation annually. The rain shadow of the Cascade Range reduces annual rainfall eastward, from ~48 cm (19 in) at Mosier to <35 cm (14 in) in the Biggs Junction-Rufus area.

The Biggs Junction-Rufus area is on the eastern flank of the Cascade Range, a chain of Quaternary and Pliocene volcanoes stretching from northern California to southern British Columbia. This volcanic arc is adjacent to the Cascadia subduction zone, an active continental margin, where oceanic crust obliquely subducted beneath the North American continental plate for much of the Cenozoic (**Figure 2-1**). Convergence along this plate boundary has produced a volcanic arc east of the subduction zone that has experienced a complex history since about 40 Ma (Lux, 1982; Phillips and others, 1986; Verplanck and Duncan, 1987; Conrey and others, 2002). From the Three Sisters north to Mount Adams (Washington State), the Quaternary to Pliocene High Cascades occupy an ~30-km-wide (18.6 mi), discontinuous and structurally segmented graben formed as a result of a northward propagating rift (**Figure 2-1**; Allen, 1966; Taylor, 1981; Williams and others, 1982; Smith and Taylor, 1983; Smith, 1987; Conrey and others, 2002; McClaughry and others, 2012). Between Mount Hood and Mount Adams, the structural depression occupied by the High Cascades coincides with the Hood River graben, a half-graben that forms the Hood River Valley (**Figure 2-1**). The eastern margin of this graben is defined by the north-northwest striking Hood River fault zone (Hodge, 1938; Newcomb, 1969; Timm, 1979; Korosec, 1987; Gray and others, 1996; Conrey and others, 1996; Sherrod and Smith, 2000; McClaughry and others, 2012), an en echelon succession of normal faults that began forming during the late Pliocene or early Pleistocene.

The axis of the High Cascades and the Hood River graben is superimposed in this area across the Yakima Fold Belt, a series of northeast-southwest-trending, asymmetric, locally overturned and faulted anticlinal ridges separated by broad synclinal valleys (Swanson and others, 1979b, 1981; Anderson, 1987; Watters, 1989; Reidel and Campbell, 1989; Tolan and Reidel, 1989; Anderson and others, 2013). This structurally deformed part of the Columbia Plateau began to develop during emplacement of the flood basalt flows of the Columbia River Basalt Group (CRBG) starting with the Grande Ronde Basalt around ca. 16 Ma (Reidel and others, 1989; Beeson and Tolan, 1990). Developing Yakima folds exerted a major influence on the location of paleodrainages of the ancestral Columbia River system during the early to middle Miocene as inferred from the increasingly restricted distribution of the younger parts of the Grande Ronde, Wanapum, and Saddle Mountains Basalts to synclinal troughs within the Columbia River Gorge (Vogt, 1981; Beeson and others, 1985; Fecht and others, 1987; Beeson and others, 1989; Beeson

and Tolan, 1990). Folds continued to develop in post-CRBG time as large accumulations of volcaniclastic and sedimentary detritus shed from the late Miocene and early Pliocene Cascades preferentially accumulated in depocenters coincident with topographically low synclinal structures. Compressional deformation in the Yakima Fold Belt has persisted beyond the Pliocene and into present day in the Middle Columbia Basin. Basaltic lavas, as young as 3 Ma, are broadly folded and structurally dismembered near Hood River, while in several locations across the Middle Columbia Basin modern drainages are redirected by north-northwest-trending strike-slip faults (McClaughry and others, 2012).

The Oregon portions of the Biggs Junction and Rufus 7.5' quadrangles are characterized by a shallow north-dipping section of Miocene volcanic rocks overlain by Quaternary surficial deposits. (**Figure 2-2**). The oldest exposed rocks in the area are tholeiitic basalt and basaltic andesite lava flows that are part of the regionally extensive early to middle Miocene CRBG. Members of the CRBG exposed in the map area include parts of the Priest Rapids Member (**Twpr**), the Roza Member (**Twr**), and parts of the Frenchman Springs Member (**Twfs**, **Twfh**, **Twfg**) of the Wanapum Basalt and the Sentinel Bluffs Member (**Tgsb**) of the Grande Ronde Basalt (Plate 1). Aggregate thickness of the CRBG in the Biggs Junction-Rufus area is at least 280 m (915 ft). Rocks older than the CRBG are not exposed in the map area.

The CRBG is overlain in most of the map area by poorly exposed fluvial volcaniclastic sedimentary rocks of the upper Miocene and lower Pliocene Dalles Formation up to ~ 50 m (164 ft) thick. The Dalles Formation is locally overlain by thin surficial deposits (up to ~ 20 m or 67 ft), including eolian (**Qe**), Missoula Flood bar and terrace (**Qm)**, loess (**Qlc**), fan deposits (**Qaf**), colluvium (**Qc**), stream channel alluvium (**Qa**) and terraces (**Qt**), Columbia River alluvium (**Qac**) and landslide deposits (**Qls**). Historical deposits include debris flows (**Hdf**), mined areas (**Hsm**), and fill (**Hcf**).

Figure 2-1. Tectonic setting of the Pacific Northwest region of the United States showing (A) the Cascadia subduction zone and regional plate boundaries, Quaternary faults in the North American plate, and the location of the study area near Biggs Junction-Rufus in north-central Oregon. The deformation front (barbed line) is defined by bathymetry where the abyssal plain meets the continental slope and is inferred to represent the surface projection of the Cascadia thrust fault. Modified from Nelson and others (2006). (B) Index map showing geographic locations, Middle Columbia Basin (orange shading), approximate extent of Western Cascades (tan shading) and High Cascades (brown shading), and some faults in the Oregon segment of the Cascade Range. Note that the names Western and High Cascades are not used in Washington or south of Mount Shasta in California. Modified from Sherrod and Smith (2000).

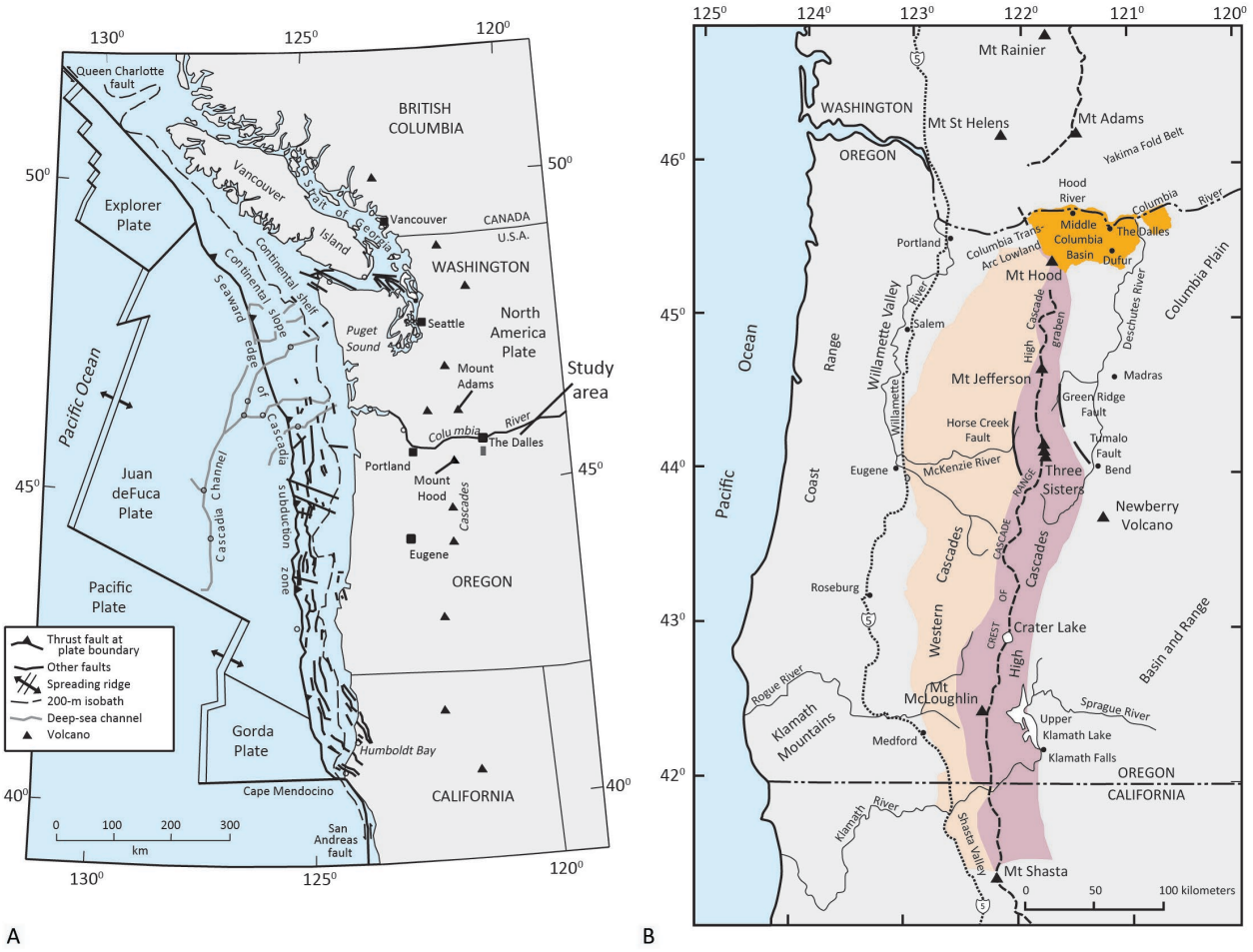

Figure 2-2. Generalized geology of north-central Oregon. Geology from OGDC-6 (Smith and Roe, 2015). Study area shown by black outline. Solid orange line corresponds to the watershed hydrologic boundary of the Middle Columbia Basin. Label abbreviations are as follows: BD—Bonneville Dam; TDD—The Dalles Dam; OR—Oregon; WA—Washington; JDD—John Day Dam.

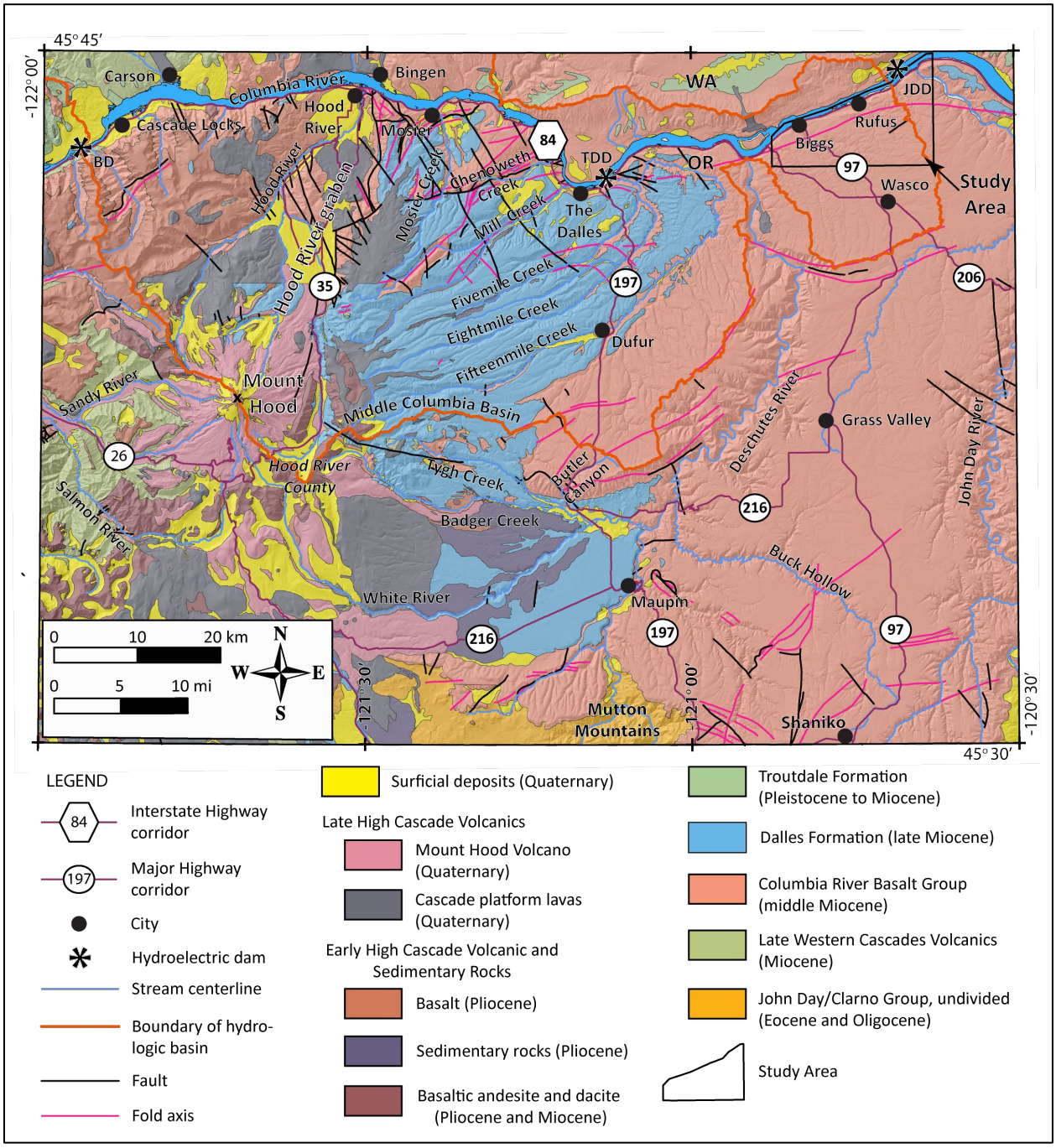

3.0 PREVIOUS WORK

Table 3-1 shows a list of previous regional geologic investigations useful for the current geologic study of the Biggs Junction-Rufus area. Reports listed in Table 3-1 are organized in chronological order; those shown in bold are geologic maps that intersect the study area. The index map shown in **Figure 3-1** summarizes the sources of mapping used for our geologic depiction and other sources consulted during the preparation of this report.

Table 3-1. Partial chronological listing of maps and reports on which this study builds. Bold titles are maps that intersect the Biggs Junction and Rufus 7.5' quadrangles.

Author	Year	Subject	Scale
Piper	1932	Geology and ground-water resources of The Dalles region	1:62,500
Allen	1932	Structure, stratigraphy, lower Columbia River Gorge	
Newcomb	**1966**	**Lithology and Eastward Extension of The Dalles Formation**	
Waters	1968	Geologic map of the Dufur quadrangle	1:62,500
Newcomb	**1969**	**Tectonic structure/groundwater the Dalles area**	**1:62,500**
Shannon and Wilson, Inc.	1973	Boardman nuclear project	1:250,000
Beaulieu	**1977**	**Geologic hazards of parts of northern Wasco County**	**1:62,500**
Swanson and others	**1981**	**Regional geologic map of the Columbia River Basalt Group**	**1:100,000**
Green	1981	Soil survey Hood River County	GIS
Bela	**1982**	**Geologic map Dalles 1 × 2-degree quadrangle**	**1:250,000**
Green	1982	Soil survey, Wasco County	GIS
Powell	**1982**	**Geology of the Columbia Hills**	**1:24,000**
Korosec	1987	Geologic map Hood River 30- × 60-minute quadrangle	1:100,000
Anderson	1987	Geologic map Columbia River Gorge area	1:24,000
Lite and Grondin	1988	Groundwater/geology Mosier area	1:24,000
Sherrod and Scott	1995	Geologic map Mount Hood 30- x 60-minute quadrangle	1:100,000
Conrey and others	1996	Isotopic ages Hood River/Mount Hood area	
Gray and others	1996	Isotopic ages Hood River/Mount Hood area	
Conrey and others	1997	Petrology Cascade arc	
Sherrod and Smith	2000	Geologic map of the Cascade Range in Oregon	1:500,000
Benito and O'Connor	2003	Missoula Flood deposits Columbia River Gorge	
Wells and others	1989	Columbia River Basalt, Columbia River Gorge	
Wells and others	2009	Columbia River Basalt, Columbia River Gorge	
Johnson	2011	Geologic map of Tygh Ridge and Dant areas	1:24,000
McClaughry and others	2012	Geologic map of the Hood River Valley	1:36,000
E. Burns and others	2012	Evaluation of basalt aquifers near Mosier	GIS
Martin and others	2013	Revisions to the stratigraphy of the Frenchman Springs Member	
Reidel and Tolan	2013	The Grande Ronde Basalt, Columbia River Basalt Group	
Lite	2013	Hydrogeology of the Mosier area	

Figure 3-1. Sources of regional geologic mapping used during the preparation of this report. See DataSourcePolys feature class in the geodatabase. Study area shown by green outline. Label abbreviations are as follows: BD—Bonneville Dam; TDD—The Dalles Dam; OR—Oregon; WA—Washington; JDD—John Day Dam.

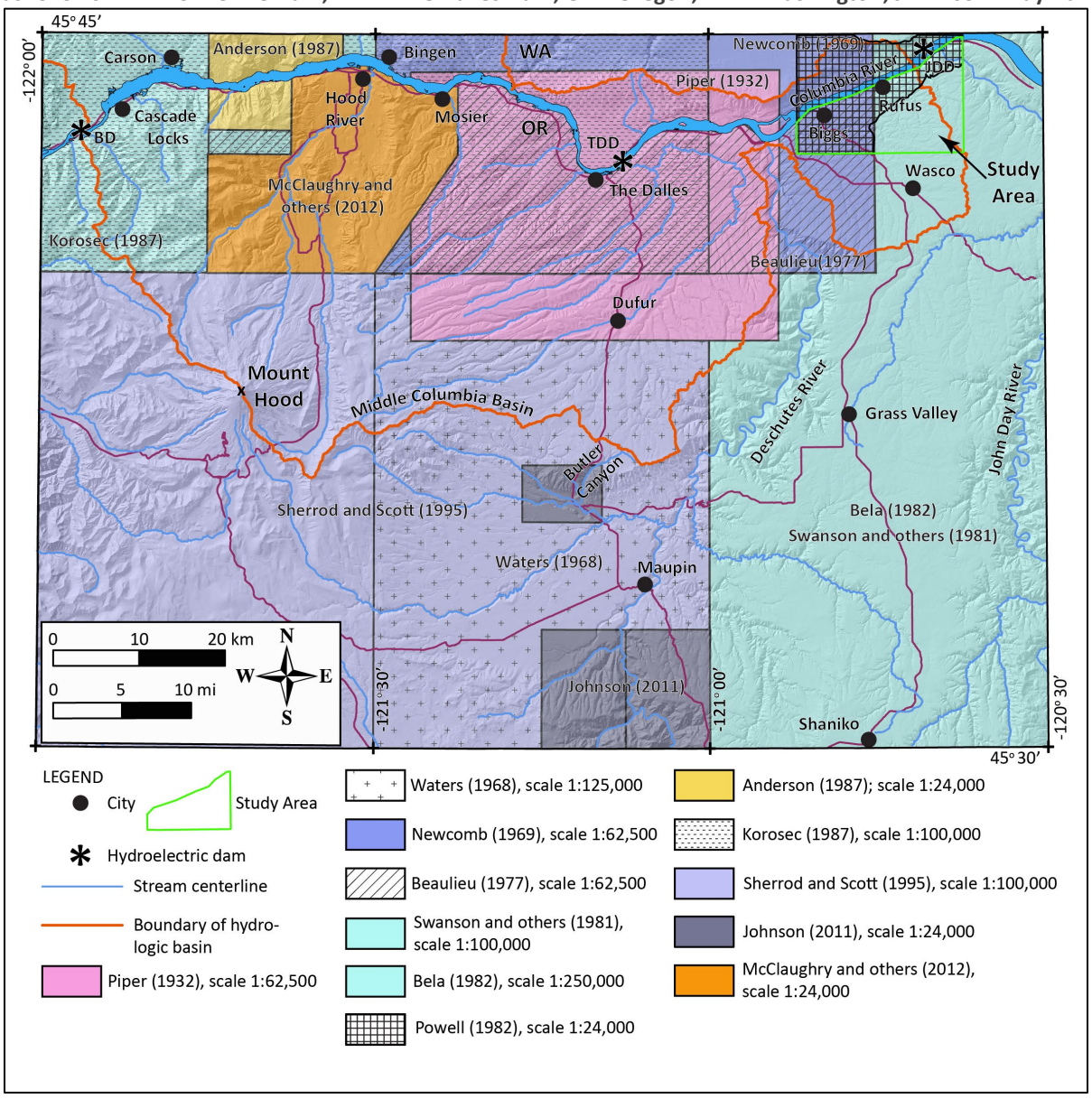

4.0 METHODOLOGY

Geologic data were collected digitally using an GPS-enabled Apple™ iPad™ mini 4 loaded with Esri™ Collector™, a field data collection extension of Esri ArcGIS™. Digital mapping used elevation-colored slopeshade raster images, derived from high-resolution (8 pts/m^2) lidar digital elevation models (DEMs) as basemaps (**Figure 4-1**). Additional basemap information was derived from digital orthophoto imagery (2011 NAIP). Fieldwork conducted during this study consisted of data collection along highways and roads, combined with a number of detailed traverses across public lands.

New mapping was compiled with published and unpublished data and converted into digital format using Esri ArcGIS ArcMAP™ 10.6 GIS software. On-screen heads-up digitizing was performed using georeferenced 1-m lidar DEMs, 2011, 2014, and 2016 NAIP imagery, and reference to fully 3D visualizations of lidar data with draped orthoimagery using QT Modeler™. No lidar data were available for a substantial portion of the Rufus quadrangle, so AgiSoft Photoscan™ Structure from Motion software was used to make a 66-cm-resolution DEM from 1954 1:28,400 scale aerial photographs obtained from the USGS. In addition, Photoscan was used to prepare orthomosaics derived from the 1954 aerial photography and 1947 1:27,700 aerial photographs, which were helpful in mapping areas now inundated by Lake Celilo and Lake Umatilla. Geologic interpretations were aided by GIS analyses based in part on the lidar and orthophoto imagery, aided by structural models based on surface outcrops and water well data, and regional aeromagnetic data (**Figure 4-2**) provided by Dr. Rick Blakely of the USGS (personal communication, 2018). Bedrock and surficial geologic units were created at a maximum use scale of 1:8,000. The geologic time scale used is the 2015 (v2015/01), version of the International Stratigraphic Commission International Stratigraphic Chart revised from Cohen and others (2013, http://www.stratigraphy.org/index.php/ics-chart-timescale).

Figure 4-1. The current extent of lidar coverage in the Middle Columbia Basin of north-central Oregon. Lidar coverage shown in orange shade. Study area shown by black outline. Label abbreviations are as follows: BD—Bonneville Dam; TDD—The Dalles Dam; OR—Oregon; WA—Washington; JDD—John Day Dam.

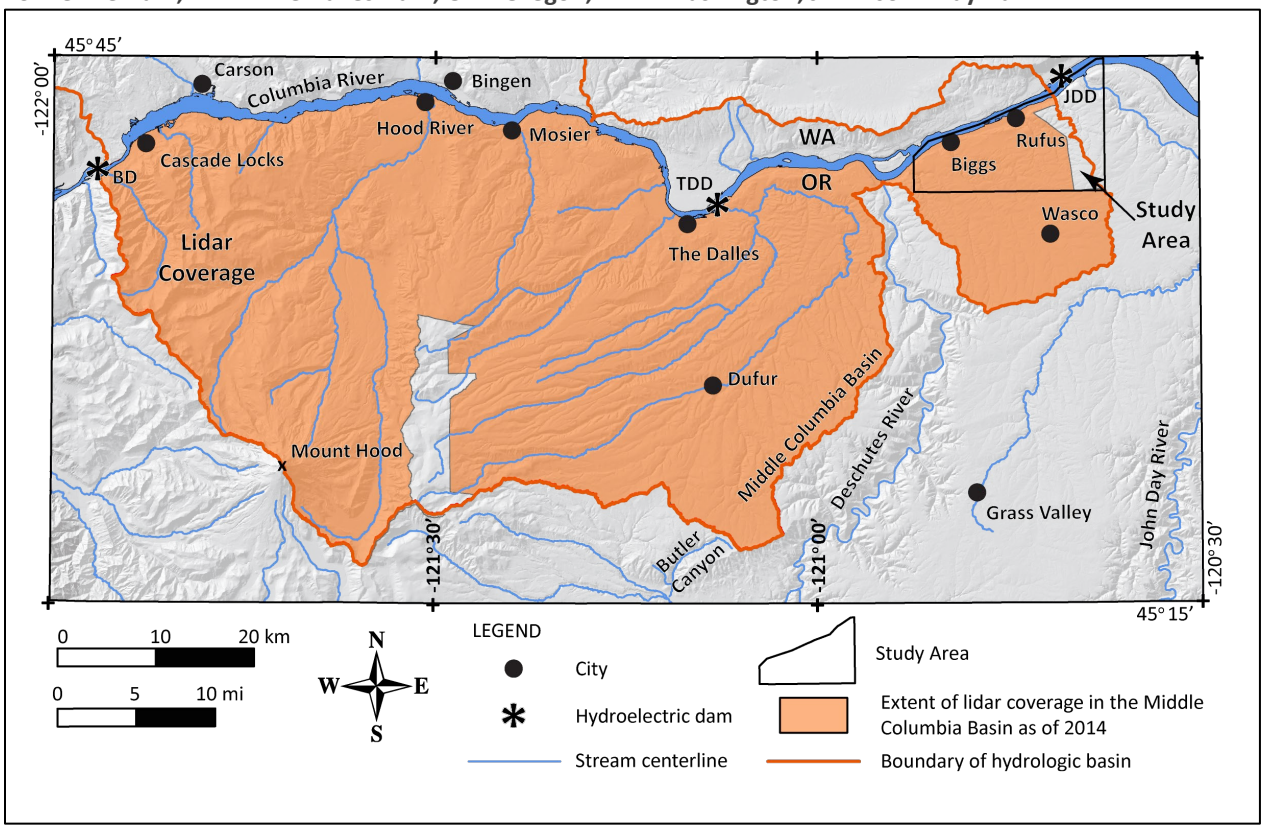

Figure 4-2 Regional aeromagnetic anomaly map. Airborne magnetic anomalies over south-central Washington and surrounding areas are shown as color-shaded relief. Rainbow colors represent the intensity of the Earth's magnetic field after subtraction of the International Geomagnetic Reference Field (IGRF). Color scale based on equal-area histogram. Flight lines and perpendicular tie lines were spaced 400 m and 4,000 m apart, respectively. Flight surface was developed in advance of the survey based on a digital elevation model and nominal 200-m terrain clearance. Actual surface altitude varied from the pre-planned surface as required for safety and FAA regulations. (Rick Blakely, USGS, personal communication, 2018).

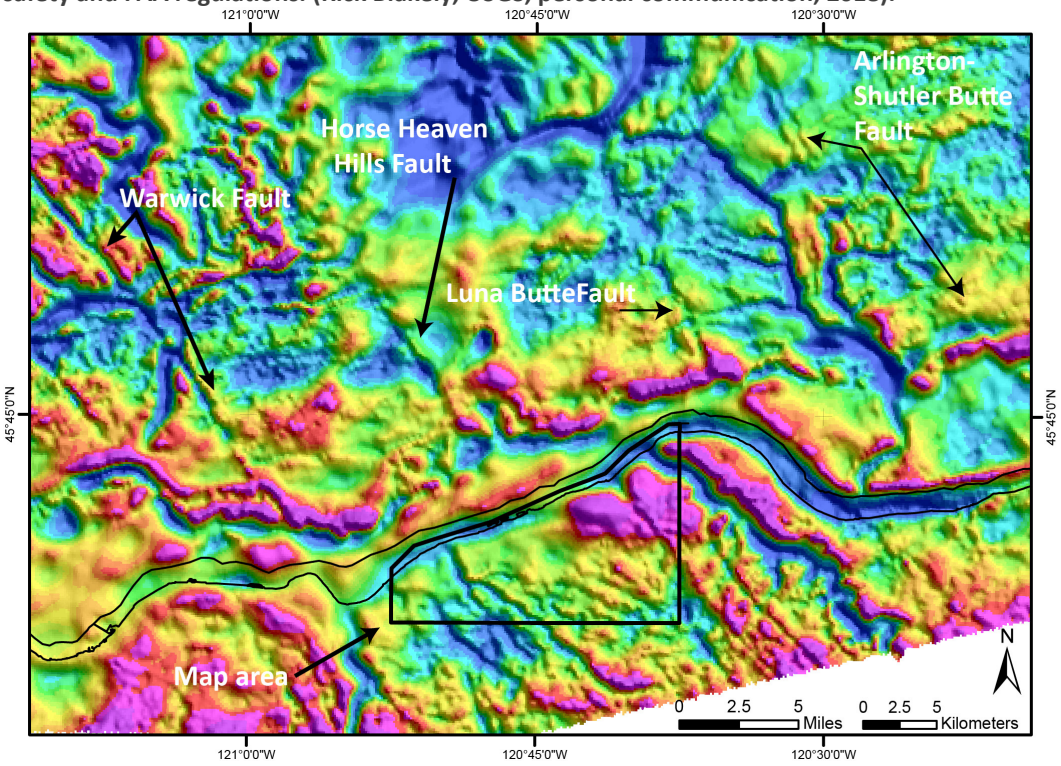

Structural analysis was aided by strike and dip measurements of inclined lava flows made using lidar DEMs visualized with QT Modeler software, which allows structural planes to be created and measured from selected topographic points. Mapping was supported by new and compiled X-ray fluorescence (XRF) geochemical analyses of whole-rock samples. Whole-rock geochemical samples were prepared and analyzed by X-ray fluorescence (XRF) at the Washington State University GeoAnalytical Lab, Pullman, Washington, under the direction of Dr. Scott Burroughs. Analytical procedures for the Washington State University GeoAnalytical Lab are described in Johnson and others (1999) and can be obtained online at https://environment.wsu.edu/facilities/geoanalytical-lab/. Major element determinations are normalized to a 100-percent total on a volatile-free basis and recalculated with total iron expressed as FeO*. Whole-rock chemical data are useful in classifying volcanic rocks, as many lavas are too fine grained and glassy to be adequately characterized by mineralogical criteria alone. Descriptive rock unit names for volcanic rocks are based in part on British Geological Survey classification schemes (Gillespie and Styles, 1999; Robertson, 1999; Hallsworth and Knox, 1999) and normalized major element analyses plotted on the total alkalis ($Na_2O + K_2O$) versus silica (SiO_2) diagram (TAS) of Le Bas and others (1986), Le Bas and Streckeisen (1991), and Le Maitre and others (1989, 2004).

In this report, volcanic rocks with fine-grained (<1 mm [0.04 in]; Mackenzie and others, 1997; Le Maitre and others, 2004), average crystal or particle size in the groundmass are characterized in the following manner:

- As having "coarse-grained groundmass" if the average size is <1 mm (0.04 in) and they can be determined using the naked eye (>~0.5 mm [0.02 in]).
- As having "medium-grained groundmass" if crystals of average size cannot be determined by eye but can be distinguished using a hand lens (>~0.05 mm [0.02 in]).
- As having "fine-grained groundmass" if crystals or grains of average size can only be determined using a microscope, or by hand lens recognition of phyllite-like sparkle or sheen in reflected light, indicating the presence of crystalline groundmass.
- As having a "glassy groundmass" if the groundmass has fresh, or originally had altered groundmass with the characteristics of glass (e.g., conchoidal fracture, sharp, transparent edges, vitreous luster, etc.).
- Mixtures of crystalline and glassy groundmass are described as intersertal.
- Ratios of glass to crystalline materials may be indicated by textural terms including holocrystalline, hypocrystalline, hyalophitic, and hyalopilitic.
- Microphenocrysts are defined as crystals larger than the overall groundmass and < 1 mm (0.04 in) across.

Subsurface geology shown in the geologic cross sections incorporates lithologic interpretations from water-well drill records available through the Oregon Water Resources Department (OWRD) GRID system (Plate 1; appendix). An attempt was made to locate water wells and other drill holes that have well logs archived by OWRD. Approximate locations were estimated using a combination of sources, including internal OWRD databases of located wells, Google Earth™, tax lot maps, street addresses, and aerial photographs. The accuracy of the locations ranges widely, from errors of 0.7 mi (1.1 km) possible for wells located only by section and plotted at the section centroid to a few tens of feet for wells located by address or tax lot number on a city lot with bearing and distance from a corner. For each well, the number of the well log is indicated in the database. This number can be combined with the first four letters of the county name (e.g., SHER 5473) to retrieve an image of the well log from the OWRD web site (http://apps.wrd.state.or.us/apps/gw/well_log/). A database of 42 water-well logs with interpreted subsurface geologic units is provided in the appendix.

Map coordinates are provided for outcrop photographs shown for report figures, allowing the interested reader to visit these sites in the field or to remotely visualize the area using Google Earth™. Coordinates are provided in Universal Transverse Mercator (UTM) Zone 10 (datum = NAD83, units = meters).

5.0 EXPLANATION OF MAP UNITS

The suite of terrestrial sedimentary and volcanic rocks in the Oregon portions of the Biggs Junction and Rufus 7.5' quadrangles is early Miocene to early Pliocene in age (**Figure 3-1** and **Figure 5-1**; Plate 1). Bedrock geologic units are locally covered by Pleistocene to Holocene surficial deposits. Lavas of the CRBG are assigned stratigraphic names following conventions established by Tolan and others (1989, 2009a) and Reidel and others (2013).

A time-rock chart showing age ranges for late Cenozoic bedrock and surficial units is depicted in **Figure 5-1**.

5.1 Overview of map units

QUATERNARY SURFICIAL DEPOSITS

Hcf constructed fill (Holocene)
Hsm surface mined land (Holocene)
Hdf debris flows (Holocene)
Qac Columbia River alluvium (Holocene and Upper Pleistocene)
Qe eolian deposits (Holocene and Upper Pleistocene)
Qa alluvium (Holocene and Upper Pleistocene)
Qaf fan deposits (Holocene and Upper Pleistocene)
Qls landslide deposits (Holocene and Upper Pleistocene)
Qc colluvium (Holocene and Upper Pleistocene)
Qt older alluvium (Holocene[?] and Upper Pleistocene[?])
Qm Missoula flood bars and terraces (Upper Pleistocene)
Qlc cultivated loess (Holocene and Pleistocene[?])

Unconformity

LOWER PLIOCENE AND UPPER MIOCENE VOLCANIC AND SEDIMENTARY ROCKS OF THE EARLY HIGH CASCADES

DALLES FORMATION

Tmdl Dalles Formation, undivided (Pliocene[?] and upper Miocene[?])

Angular unconformity to disconformity

LOWER AND MIDDLE MIOCENE VOLCANIC AND SEDIMENTARY ROCKS

COLUMBIA RIVER BASALT GROUP

Wanapum Basalt

Priest Rapids Member (middle Miocene)

Twpr Basalt of Rosalia (middle Miocene)

Roza Member (lower Miocene)

Twr Basalt of Roza (lower Miocene)

Frenchman Springs Member (lower Miocene)

Twfs Basalt of Sentinel Gap (lower Miocene)
Twfh Basalt of Sand Hollow (lower Miocene)
Twfg Basalt of Ginkgo (lower Miocene)

Disconformity—Vantage Member of the Ellensburg Formation

Grande Ronde Basalt

Normal-polarity (N2) magnetostratigraphic unit represented by:

Tgsb Sentinel Bluffs Member (lower Miocene)

Figure 5-1. Time-rock chart showing the 19 geologic units shown on the geologic map and in geologic cross sections in the Oregon portions of the Biggs Junction and Rufus 7.5' quadrangles. Note that depth of exposure in the map area does not extend beneath the Sentinel Bluffs Member (Tgsb).

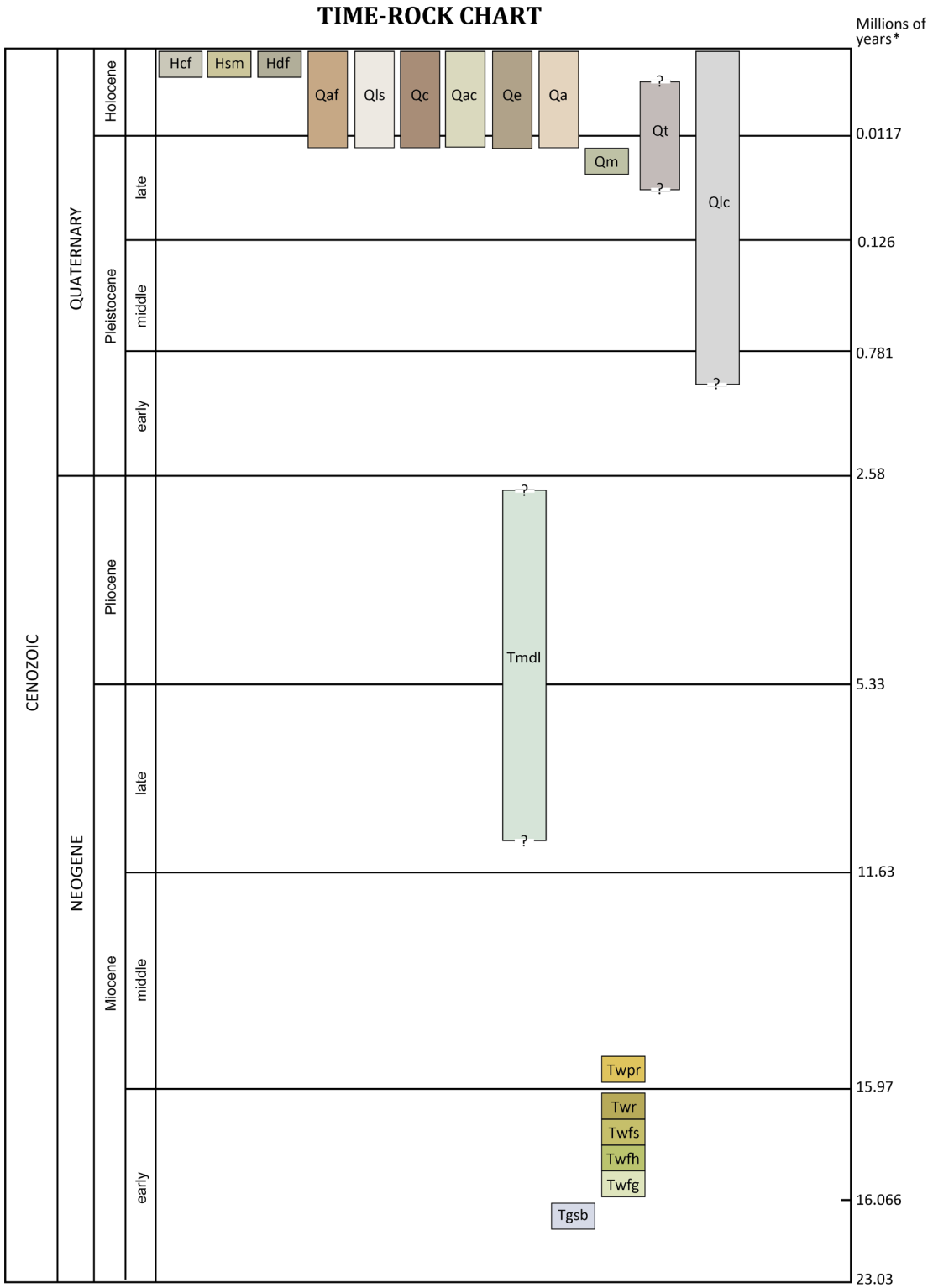

*International Chronostratigraphic Chart, International Stratigraphic Commission, v2015/01, Time scale after Gradstein and others (2004), Ogg and others (2008), Cohen and others (2013), and Kasbohm and Schoene (2018). http://www.stratigraphy.org/index.php/ics-chart-timescale

5.2 Upper Cenozoic surficial deposits

The early Miocene sedimentary and volcanic rocks of the Oregon portions of the Biggs Junction and Rufus 7.5' quadrangles are locally covered by Pleistocene and Holocene surficial deposits (**Figure 5-1**; Plate 1). Most of the upland areas in the two quadrangles are covered by a thin layer of mixed fine sediments, including loess, Missoula Flood silt and sand, and post-flood eolian deposits. Other important surficial units include Missoula Flood bar deposits, colluvium, alluvial fans, and alluvium in minor streams and along the Columbia River. Artificial fill is widespread along the I-84 corridor, and large areas near the Columbia River have been disturbed by surface mining. Surficial units within the project area are delineated on the basis of geomorphology as interpreted from a combination of field observations, 1-m lidar and 66-cm SfM DEMs (**Figure 4-1**), 2011, 2014, and 2016 NAIP orthophoto mosaics, and custom 1947 and 1954 orthophoto mosaics.

Hcf **constructed fill (Holocene)**—Sediment ranging from clay to boulder size placed by humans in a variety of locations and settings. Older constructed fill is commonly poorly sorted and compacted, while more modern fill is typically of uniformly sized material and engineered. Deposits mapped as constructed fill are generally associated with roadway and railroad grades, dams, and building sites. (Plate 1). Large areas of fill underlie the Interstate 84 right of way and adjacent railroad right of way. These areas appear to have been placed on causeways after the filling of Lake Celilo in 1957, which raised the water table and inundated some areas along the rights of way. Another large area of fill occupies the Oregon bank of the Columbia River from the John Day Dam to Rufus. Hundreds of small check dams have been constructed in gullies in the upland areas under cultivation (**Figure 5-2**) but they are mapped as part of unit **Qlc**. The thickness of fill-deposits varies widely and is poorly known. Thicknesses measured from larger embankments range up to ~10 m (33 ft). These deposits are assigned a late Holocene age, ranging in age from the late 1800s to recent times.

Hsm **surface mined land (Holocene)**—Surface mining disturbance, including pits, quarries, cuts, spoil piles, areas stripped of overburden, and areas covered during reclamation**.** Sediment moved or placed in these sites ranges from sand and silt to large boulders and is generally poorly sorted and highly variable in content and thickness. There are notable large areas of mining disturbance along the base of the cliffs between Rufus and the John Day Dam, where large amounts of Missoula Flood sediment, talus, and colluvium were excavated in the interval between 1954 and 1970, presumably for fill associated with construction of the John Day Dam (constructed 1968–1972) and the construction of I-84 (completed in 1964). These deposits are assigned a late Holocene age, ranging in age from the late 1800s to recent times.

Hdf **debris flow deposits (Holocene)**—Unconsolidated sediment ranging from clay to boulders deposited by debris flows triggered by intense rainfall. Several deposits are present along the base of the cliffs between Biggs Junction and Rufus. The deposits are clearly visible in lidar imagery and in recent orthophotos and originate at small scoured channels below the cliffs. The late Holocene age is based on the fact that the deposits are clearly not present in the 1954 orthophoto mosaic.

Figure 5-2. (A) Map and (B) perspective view of a landslide (Qls) in loess (Qlc) and Dalles Formation (Tmdl) located up Scott Canyon 2.6 km southeast of Rufus. Note the abundant small impoundments and marginal berms typical of cultivated loess (Qlc). In the map view, vegetation growing along the spring line that marks the upper contact of the Basalt of Sentinel Gap (Twfh) is visible. In the map view, the contact between the Basalt of Rosalia and the underlying Basalt of Roza makes a distinct bench.

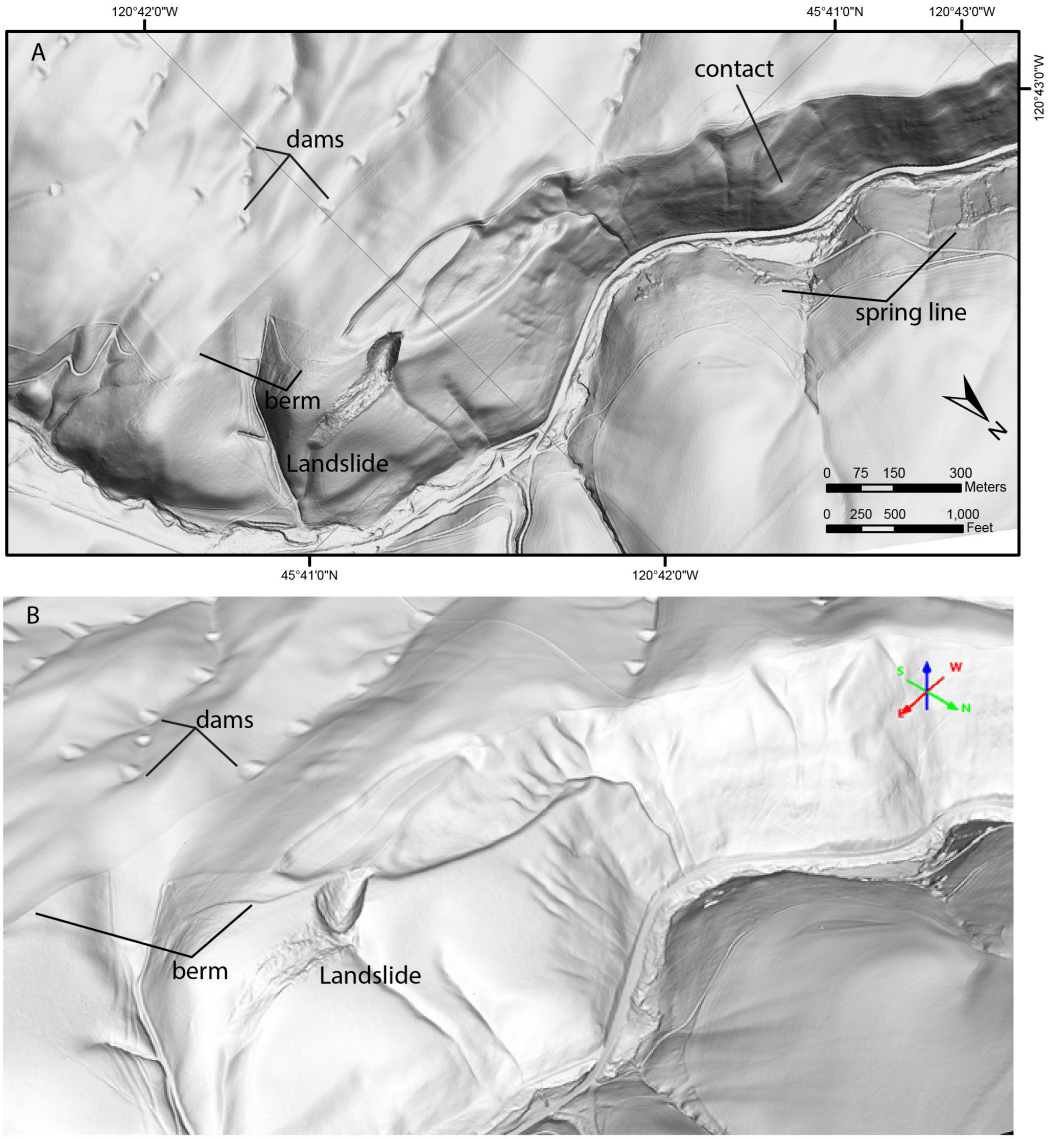

Qac **Columbia River alluvium (Holocene and Upper Pleistocene)**—Silt, sand, and gravel deposited in the channel and on the floodplain of the Columbia River**.** Much of the floodplain is now inundated by the waters of Lake Celilo and Lake Umatilla or buried by fill. The uphill limit of alluvium is poorly exposed and is largely mapped on the basis of a break in slope where the floodplain is buried by colluvium or Missoula Flood deposits. A few water wells penetrate the Columbia River alluvium near Rufus, and well logs report 10–20 m (33–66 ft) of silty sand, sand, and pebble, cobble and boulder gravel. The unit is assigned a late Pleistocene to Holocene age, because it postdates the Missoula floods.

Qe **eolian deposits (Holocene and Upper Pleistocene)**—Wind-blown sand deposited at Biggs Junction, Rufus, the mouth of the John Day River, and the mouth of Helm Canyon. The eolian deposits have been largely obscured by development or inundated by Lake Celilo. In 1899 G. K. Gilbert took photographs of sand dunes near the current location of Biggs Junction, some of which were typical barchan forms (**Figure 5-3**).

Figure 5-3. Photographs of dunes (Qe) taken by G. K. Gilbert of the U.S. Geological Survey in 1899 at Biggs Junction. Stars on map indicate approximate camera locations, and arrows show approximate field of view. Basemap is USGS National Map. (https://www.sciencebase.gov/catalog/item/51dc5d7ae4b097e4d3836a72)

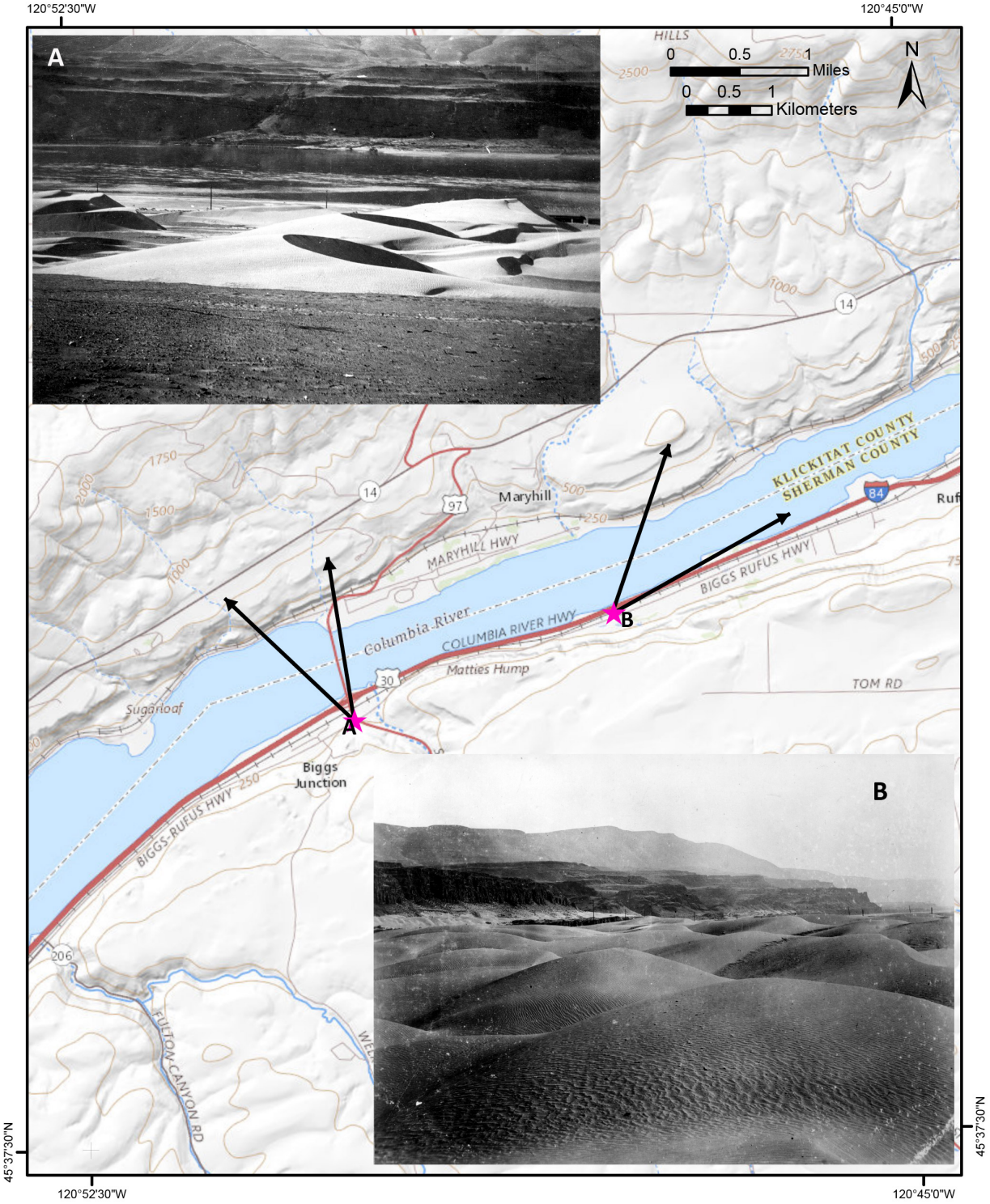

Qa **alluvium (Holocene and Upper Pleistocene)**—Unconsolidated gravel, sand, silt, and clay deposited in active stream channels and on adjoining floodplains and terraces of Fulton Canyon, Spanish Hollow, Gerking Canyon, Scott Canyon, Helm Canyon, and their tributaries (Plate 1). Gravel deposited as imbricated, massive to cross-stratified accumulations is the most common material in channels. In the steeper lower reaches of the canyons, floodplains are dominantly poorly bedded and floodplain deposits typically include poorly to well-bedded gravel, sand, and silt. In the less steep upper reaches, floodplain deposits are typically moderately to well-bedded white to grey sand and silt with some gravel layers and, locally, include a 10–20 cm thick layer of white sediment that may be volcanic ash. Ash from the ~7,627 kabp (Zdanowicz and others, 1999) eruption of Mount Mazama has been identified in the Petersburg quadrangle to the west (Jim O'Connor, personal communication, 2019). The thickness of alluvial deposits is poorly known. Cut banks expose up to ~5 m, and an engineering boring (SHER 50370) located just off the southern edge of the map area along Spanish Hollow penetrates 12 m (40 ft). Bedrock units may be locally exposed in the bases of stream channels within areas mapped as unit **Qa**. The extent of **Qa** was mapped on the basis of the edge of the floodplain interpreted from lidar imagery. The unit is assigned a Holocene and Late Pleistocene age on the basis of stratigraphic position. In areas below the level of inundation of the Missoula floods (~340 m [1,120 ft], **Figure 5-8**) most alluvium must be younger than the floods, but it may be substantially older above that level.

Figure 5-4. Quaternary alluvium (Qa) exposed along Frank Fulton Canyon in the southwest part of the map area (668325 E, - 5056308 N, view to west). Flow is from left to right (southeast to northwest) in the photograph. Highest vertical cut bank is approximately 5 m high.

Figure 5-5. Missoula flood inundation of the map area. Perspective view of the map area (heavy black line is map area boundary) showing extent of inundation by maximum flood levels of ~340 m (1,115 ft).

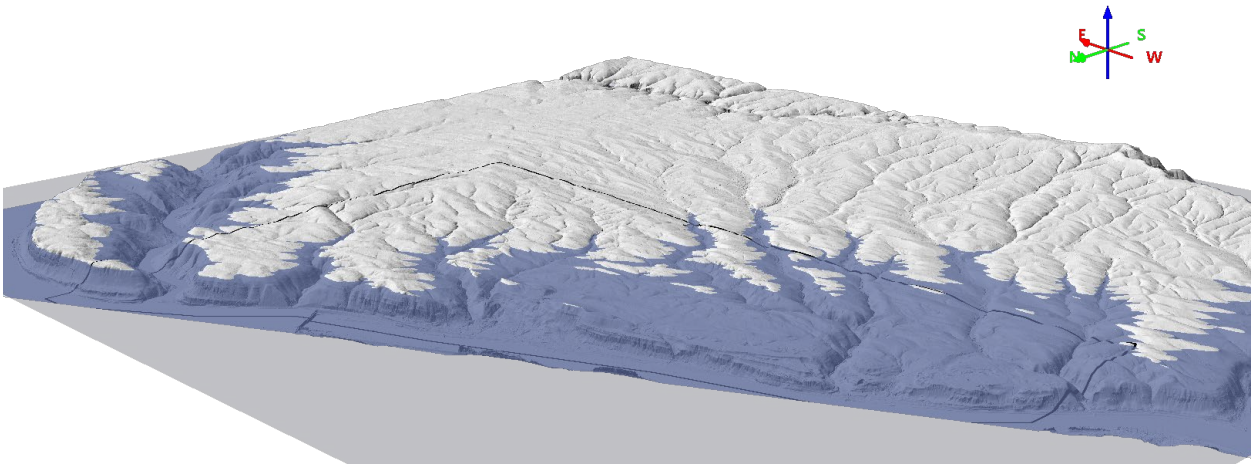

Qaf **fan deposits (Holocene and Upper Pleistocene)**—Unconsolidated deposits of boulders, cobbles, pebbles, granules, sand, silt, and clay, preserved in fan-shaped accumulations at the transition between low-gradient valley floodplains and steeper upland drainages (Plate 1). Alluvial fans occur in two distinct types. Dozens of small fans occur at the mouths of ephemeral stream channels tributary to larger streams with well-developed floodplains. There are also three large fans at the mouths of the major tributaries to the Columbia: at Scott and Gerking canyons (Rufus), Spanish Hollow Canyon (Biggs Junction), and Helm Canyon. The smaller fans are mapped solely on the basis of geomorphology visualized in lidar imagery. No exposures of fan deposits were seen. The sediment in the small fans originates in relatively gently sloping upland areas consisting of a few meters of loess or other fine sediment draped over weathered Columbia River Basalt flows. The deposits are probably a mix of silt, sand, clay, and gravel up to small boulders in size. The small fans are assigned a late Quaternary-Holocene age, based on their well-preserved shape and the fact that they all lie below the elevation of maximum Missoula flood inundation (~340 m [1,120 ft]), which probably removed pre-existing alluvial fan deposits. The larger fans form broad cones at the mouths of their respective canyons. At Scott and Gerking canyons and Spanish Hollow Canyon alluvial fan deposits have been covered by extensive artificial fill and eolian deposits and have been obscured by urban development or inundation by Lake Celilo. The fans are most apparent in the DEM made from the 1954 aerial photos, which shows the broad outlines of the fans prior to most of the development. No exposures of the deposits were observed. The log of one water well sited on the Rufus fan reports 4 m (15 ft) of "soil" over bedrock, and a second well, near the edge of the fan, reports 3.5 m (11 ft) of sand over basalt. On the Spanish Hollow Canyon fan, a single well located on the very edge of the fan penetrates 13 m (42 ft) of gravel over more than 11 m (38 ft) of sand gravel and cobbles. It is not clear how much of this well is in alluvial fan deposits or the underlying Missoula Flood deposits (**Qm**). The three large fans are assigned a late Quaternary-Holocene age because they are incised into Missoula flood deposits and there is evidence for historical deposition. In Biggs Junction a small lobe of fan material built out into Lake Celilo is visible on lidar, and in Rufus the storm and flood of 1964-1965 caused the creeks of Scott

and Gerking canyons to flow through Rufus, eroding the town's trailer park, depositing sediment and debris over much of the town, and covering the interstate highway with debris and mud for about a quarter mile (Waananen and others, 1971). In Biggs Junction the same flood washed out section of U.S. Route 97 in Spanish Hollow and the approaches to bridges on Interstate 84.

Qls **landslide deposits (Holocene and Upper Pleistocene)**—Unconsolidated, chaotically mixed masses of sediment, soil, and rock and soil deposited by landslides (e.g., slides, debris flows, rock avalanches; Plate 1). Landslide deposits are rare in the study area and fall into three types. Slump-earthflows originating in unit **Qlc** or **Tmdl** (**Figure 5-2**), rockfall deposits originating from bedrock cliffs, and slump-earthflows originating on colluvial fans. The widespread colluvial aprons along the cliffs bordering the Columbia River probably accumulated in part through rockfall from the cliffs and slumping and reworking of talus and colluvial deposits, but landslides are mapped only where there is clear morphology associated with a recent landslide. The landslides in the area are all very small; none exceed 1.8 ha (4.5 acres) in area. All are late Pleistocene or Holocene in age, as all occur in areas that were swept by the Missoula floods.

Qc **colluvium (Holocene and Upper Pleistocene)**—Unconsolidated mixtures of rock and soil deposited beneath cliffs and steep slopes (Plate 1). Along the cliffs making up the Oregon side of the Columbia River Gorge, large aprons of colluvium have developed, both at the base of the lowest cliff and locally on benches below successively higher cliffs. The thickness of colluvial deposits is highly varied, and no direct measurements are available. Approximations of the geometry of the immediate post-flood topography suggest that deposits are commonly 20–30 m thick at their apex and may reach as much as 60 m (200 ft). The unit is assigned a Holocene and Late Pleistocene age because it occurs predominantly on slopes that were scoured by the Missoula floods and therefore postdate the floods.

Qt **older alluvium (Holocene[?] and Upper Pleistocene[?])**—white, weakly stratified, sand, silt, and clay deposited along the margins of modern floodplains in the upper reaches of major canyons of the area. The terrace deposits have been eroded significantly and geomorphically appear as areas of lower slope situated 5–10 m (16–33 ft) above the modern floodplains. All of the observed outcrops are at or above the estimated maximum Missoula flood inundation level, which suggests that the deposits predate the floods and have been largely removed by flood scour below the inundation limit. The Pleistocene age is based on the degree of erosion of the terrace surfaces and the evidence for predating the Missoula floods.

Figure 5-6. Bedded sand and silt older alluvium deposits (Qt) exposed in stream bank at 681,635 E, 5,057,743 N. Cut is ~ 3 m (10 ft) high.

Qm **Missoula flood bars and terraces (Upper Pleistocene)**—Poorly consolidated moderately to well-bedded silt, sand and gravel deposited by catastrophic floods caused by the repeated failure of the glacial ice dam that impounded glacial Lake Missoula (Bretz and others, 1956; Baker and Nummedal, 1978; Waitt, 1985; Allen and others, 1986, Benito and O'Connor, 2003). The estimated peak discharges of 1–10 × 10^6 m^3/s (Benito and O'Connor, 2003) resulted in flood depths of nearly 300 m through the Columbia River gorge in the map area. These flows removed any unconsolidated surficial deposits in the gorge and for some distance up the tributary canyons, leaving a landscape of steep bedrock cliffs interspersed with bare bedrock benches formed on the scoured tops of lava flows. Waning flows during large floods or smaller floods later in the sequence deposited a thin layer of silt and sand on upland surfaces and thicker deposits of silt, sand, and gravel in bars at the mouths of tributary canyons and extending several kilometers up the tributaries (unit **Qm**). Benito and O'Connor (2003) reported two locations at 360 m (1,180 ft) elevation just east of the map area where the divide between the Columbia and John Day rivers was not crossed by the floods, an erratic at an elevation of 340 m (1,115 ft) just west of the map area, two areas of preserved loess and residual soils near Biggs Junction at 321 (1,052 ft) and 345 m (1,131 ft), and an erosional scarp at 323 m (1,059 ft) near the mouth of Frank Fulton Canyon. From these data points the assumed maximum flood inundation elevation for the study area is 340 m (1,115 ft). The thin upland deposit overlies pre-existing loess and may be overlain by or interbedded with younger loess and other eolian deposits; this deposit is not mapped as a separate unit, but a line on Plate 1 at the 340 m (1,115 ft) level indicates the extent of inundation and deposition. Unit **Qm** is composed of interbedded sand and pebble and cobble gravel, deposited in thick bars at the mouths of the John Day River and Helm, Scott, Gerking, and Spanish

Hollow canyons, and poorly stratified sand and silt valley fill extending back into those canyons (**Figure 5-7, Figure 5-8, Plate 1**). **Qm** is also mapped capping several of the scoured bedrock flow tops, where the deposit is thick enough to have obscured the scoured topography. Benito and O'Connor (2003) described at least 12 m (39 ft) of interbedded sand and gravel at Helm Canyon, and the bar deposits at Scott and Spanish Hollow canyons are about 20 m (65 ft) thick, on the basis of topography. The valley fill deposits are poorly exposed but are probably only 3–5 m (10–16 ft) thick. The deposits capping scoured flow tops are at least 5 m (16 ft) thick, in order to have obscured the typical relief on the scoured flow tops. The Missoula flood deposits were emplaced between about 19,000 and 15,000 years ago, on the basis of tephra and radiocarbon ages from outside the area (Benito and O'Connor, 2003, Waitt, 2016), and are assigned a Late Pleistocene age.

Figure 5-7. Missoula flood sand and gravel deposits (Qm) located at 677290 E, 5061775 N. View is to the west. Deposits are 190 m (620 ft) above modern river level.

Figure 5-8. Missoula flood sand and gravel beds in a construction excavation in Biggs Junction (668478 E, 5059316 N). View is to south. Orthomosaic projection of 3D model, full-resolution image in digital appendix.

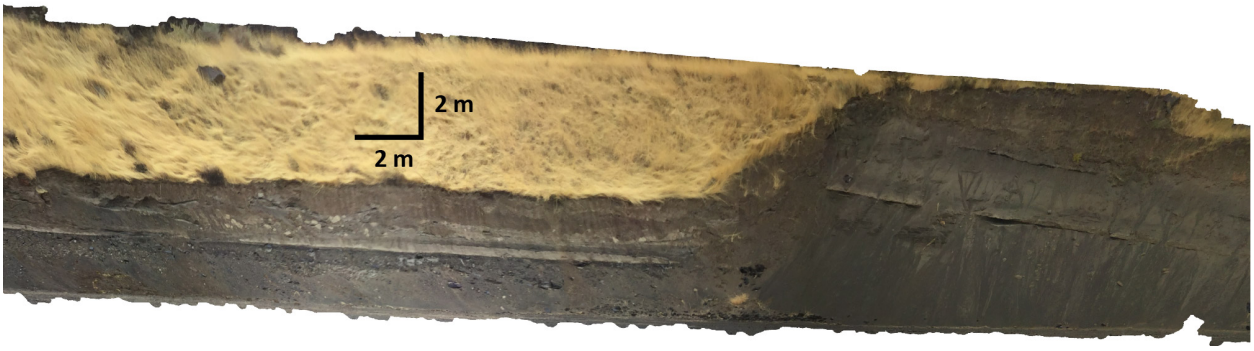

Qlc **cultivated loess (Holocene and Pleistocene[?])**—Pale yellowish brown micaceous, quartzo-feldspathic silt and minor amounts of very fine grained sand and clay mantling upland surfaces across much of the project area (Plate 1). One or more caliche horizons are commonly present in the thicker sections of loess exposed in roadcuts (**Figure 5-9**). Except where caliche horizons are present, loess typically forms a massive featureless deposit that has been extensively modified by dry-land agricultural practices over the past century. Commonly, the edges of wheat fields constructed in loess are characterized by steep 1- to 2-m-high (3.3 to 6.5 ft) embankments resulting from circular, annual tilling of large fields (**Figure 5-2**). This feature is readily apparent on lidar and orthoimagery and is the primary basis for the mapping of unit **Qlc**. Thickness of the unit ranges from thin veneers <1 m thick (3.3 ft) to as much as 6 m (20 ft) on the basis of information reported from well logs; local outcrops exposed by roadcuts may contain up to 3 to 5 m (9.8 to 16.4 ft) of loess in vertical section. The distribution of loess across this part of the Columbia Plateau indicates episodic deposition by southwesterly winds (McDonald and others, 2012). Loess deposits in the eastern Middle Columbia Basin are assigned a Late to Middle Pleistocene age on the basis of stratigraphic position and may be as old as ca. 600 ka. Medley (2012) interpreted loess deposits and Missoula flood deposits exposed along U.S. Highway 197 between Biggs Junction-Rufus and The Dalles to lie above a series of older paleosols that contain pumice correlated to the ca. 600 ka Dibekulewe tuff from Nevada (Cordero, 1997). Pluhar and others (2014a,b) reported paleomagnetically reversed paleosols at the base of U.S. Highway 197 section, so loess in this area may in some places be older than 0.78 Ma. The unit was identified as the Palouse Formation by Waters (1968).

Figure 5-9. Cultivated loess (Qlc) exposed in a roadcut across a dune crest located at 679812 E, 5056227 N, view to east. Dipping resistant layers and angular float are caliche, cut height is ~ 4 m (13 ft).

Unconformity

5.2.1 Dalles Formation

Tmdl **Dalles Formation (lower Pleistocene[?] and upper Miocene[?])**—Poorly exposed bedded fluvial sedimentary rocks overlying Columbia River Basalt units over most of the map area. The unit was not directly observed within the map area, but its presence is inferred from several lines of evidence. The most direct evidence comes from distant observation of tan and white bedded sedimentary rocks visible at the top of basalt cliffs between Rufus and the mouth of the John Day river (Figure **5-10**). Bands of light-colored soil that follow contours are also evident in the historical 1947 and 1964 orthomosaics and are interpreted as bedded sedimentary rocks. Newcomb (1966) mapped a fine-grained sedimentary facies of the Dalles Formation over much of the area (**Figure 5-11**), and the aggregate thickness of the section above the top of the Basalt of Sentinel Gap (**Twfs**) is locally much greater than can be accounted for by the Basalt of Roza (**Twr**), Basalt of Rosalia (**Twpr**), and cultivated loess (**Qlc**) (**Figure 5-12**). From these lines of evidence a fluvial sedimentary Dalles Formation is inferred throughout the map area with contacts based on geomorphology, rare patches of light-colored material visible in orthoimagery, and the estimated thickness of the underlying basalt units (Plate 1).

Several water wells in the uplands southwest of Rufus probably penetrate the Dalles Formation, and the logs describe a diverse assemblage of sedimentary material up to 15 m (50 ft) thick including gray, tan, black, and brown clay and claystone, grey sand, yellow and brown sandstone, conglomerate, and sand and gravel. Newcomb (1966) described the fine-grained facies of the Dalles Formation that he mapped in the area as tuff, silt, and sand with interbeds of pebble

to small boulder conglomerate containing lithologies characteristic of the Columbia River Basalt and John Day and Clarno Formations. Small exposures of similar conglomerate were observed ~4 km (2.4 mi) east of the northeast corner of map area on Phillipi Lane and ~ 9.5 km (5.7 mi) west of the northwest corner of the map area. From the modelled thickness of the section above the Basalt of Sentinel gap (**Twfs**) and the observed thickness of the Basalt of Roza (**Twr**), Basalt of Rosalia (**Twpr**), and cultivated loess (**Qlc**), the Dalles Formation is typically 20–30 m (66–99 ft) thick and as much as 50 m (165 ft) thick.

Figure 5-10. Google Earth™ view of the cliffs east of Rufus. Areas of white and yellow-tan sediment exposed above basalt (indicated by black arrows) are inferred to be bedded volcaniclastic sedimentary rocks of the Dalles Formation (Tmdl).

Figure 5-11. Mapping of Dalles Formation by Newcomb (1966).

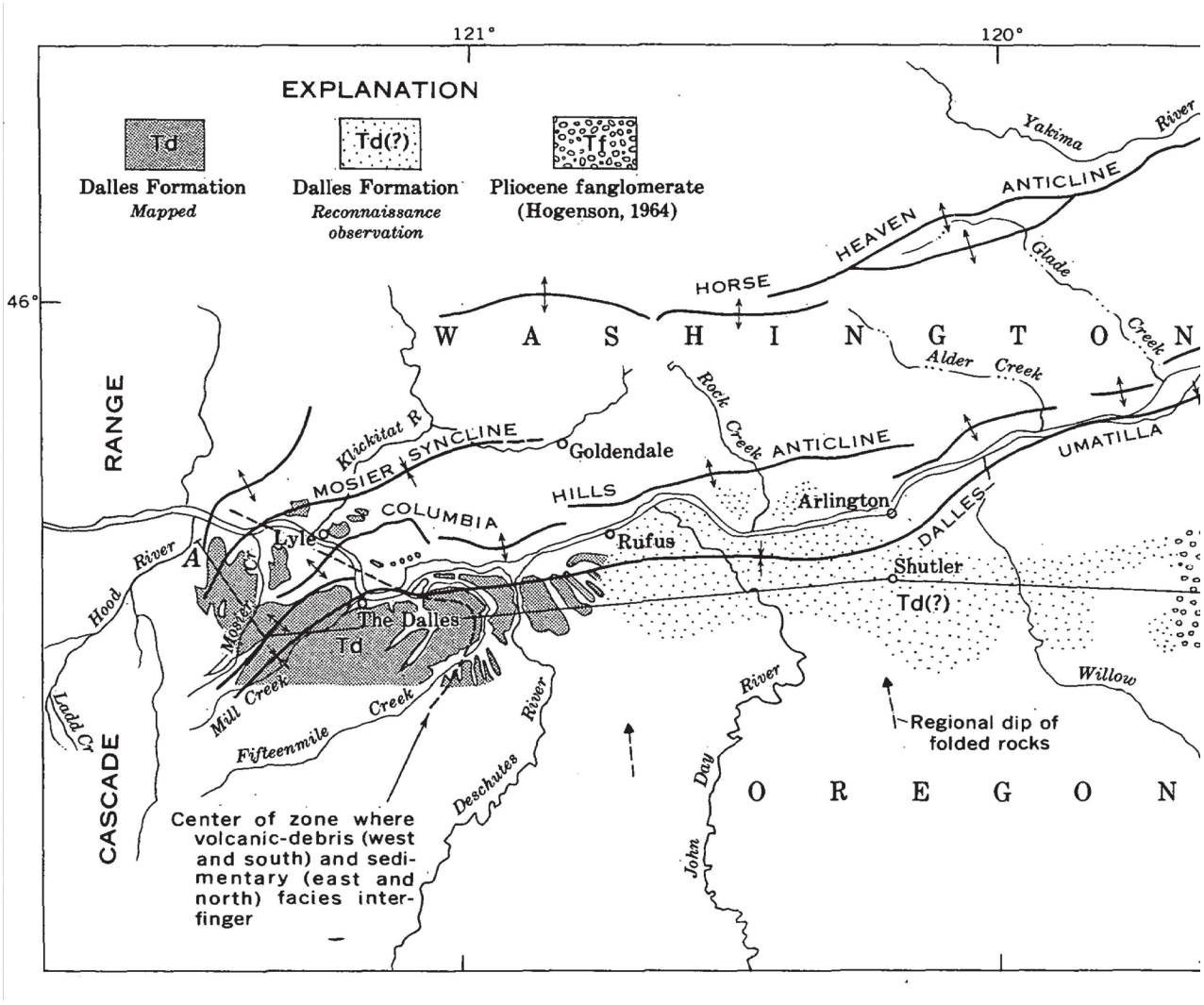

Figure 5-12. Thickness of section above the Basalt of Sentinel Gap (Twfs). Map of the difference between the topographic DEM and the modeled elevation of the top of the Basalt of Sentinel Gap (Twfs). The difference DEM comprises the combined thickness of the Basalt of Roza (Twr), Basalt of Rosalia (Twpr), Dalles Formation (Tmdl), and cultivated loess (Qlc). The heavy black line shows the mapped extent of the Basalt of Rosalia (Twpr) in the project area and adjacent quadrangles to the south. The southern edge of the Basalt of Rosalia (Twpr) corresponds with an alignment of drainage anomalies similar to that shown in the inset, where Frank Fulton Canyon takes an abrupt lateral step.

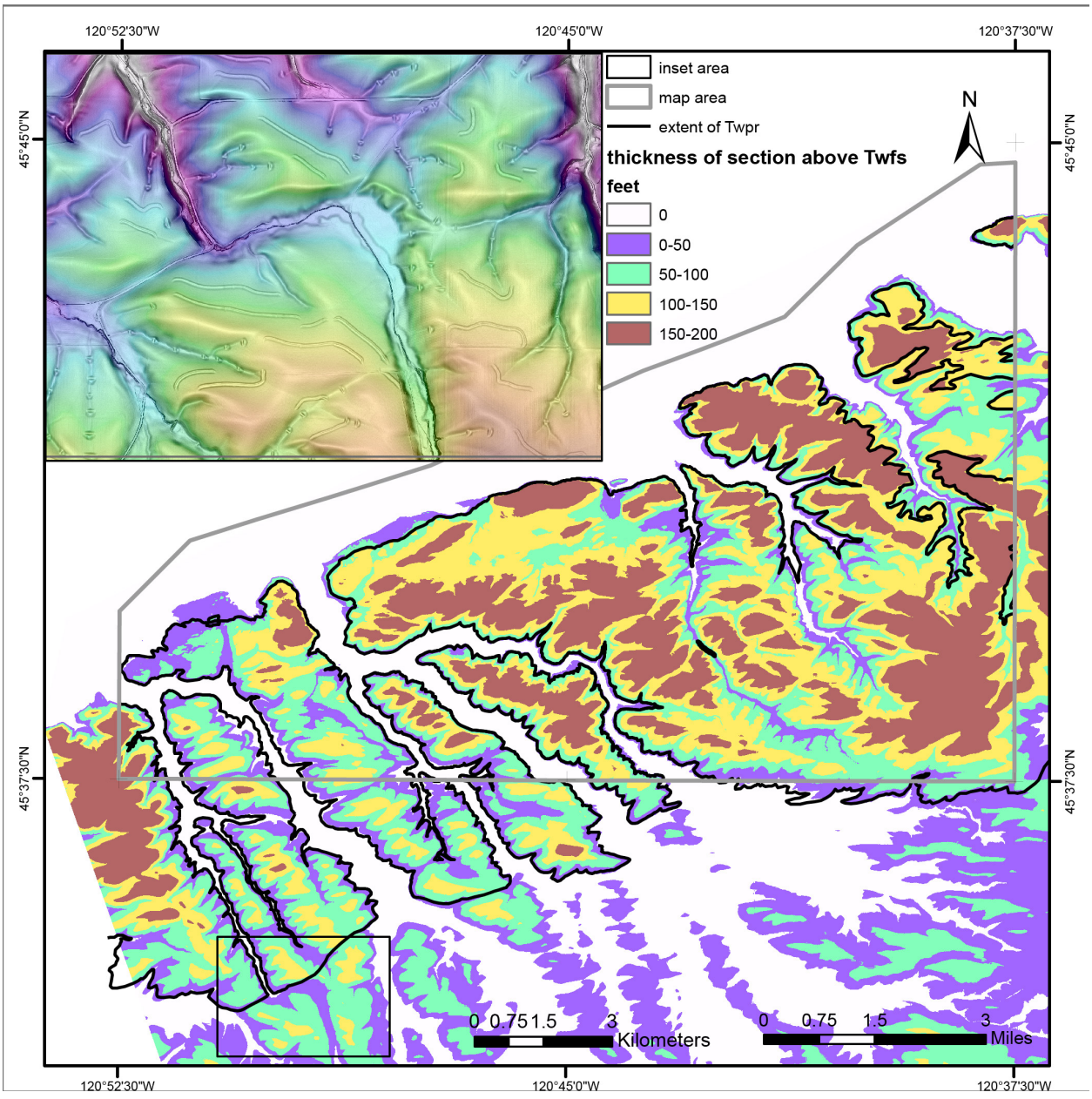

Angular unconformity to disconformity

5.2.2 Lower and Middle Miocene volcanic and sedimentary rocks

5.2.2.1 Columbia River Basalt Group

The Columbia River Basalt Group (CRBG) is an extensive succession of tholeiitic basalt and basaltic andesite lavas that cover more than 210,000 km^2 (130,000 mi^2) in parts of Washington, Oregon, and Idaho (**Figure 5-13**, **Figure 5-14, Figure 5-15**; Tolan and others, 1989; Reidel and others, 2013). Members of the CRBG exposed in the map area include flows of the Priest Rapids Member (**Twpr**), Roza Member (**Twr**), and parts of the Frenchman Springs Member (**Twfs**, **Twfh**, **Twfg**) of the Wanapum Basalt and Sentinel Bluffs Member (**Tgsb**) of the Grande Ronde Basalt (**Figure 5-14**; Plate 1). Older Grande Ronde flows are inferred to be present in the subsurface in the map area based in part on the log of a 234-m (767 ft) deep well located at the John Day dam (**Figure 5-16**) but are not shown on the map or cross sections. Generally thin (< 2 m [6.6 ft]) and discontinuous horizons of clastic sedimentary rock, tuff, or paleosols are locally found separating individual lava flows, and pillow lavas are present at some contacts. CRBG units commonly form distinctive bench and slope topography, resulting from differential erosion within and between flows. This is most apparent along the Columbia River Gorge, where flow bodies form prominent cliffs up to 120 m (400 ft) high interspersed with flat, flood-scoured benches that may be as wide as 500 m (1,600 ft) (**Figure 5-17**). Subtle bench and cliff topography is apparent in many of the tributary canyon walls and is very useful in tracing flow contacts.

Individual CRBG units can be difficult to identify with certainty in the field but can be distinguished on the basis of a multiple-criteria mapping approach using stratigraphic position and thickness, geochemistry, magnetic polarity, paleomagnetic analysis of oriented core samples, and petrography following the work of Swanson and others (1979a,b), Reidel and others (1989), Beeson and others (1985, 1989), Wells and others (1989, 2009), and Hooper (2000) (**Figure 5-18** and **Figure 5-19**). The primary uncertainties in accurately mapping these flows arise from 1) poor exposure and recognition of flow contacts, 2) intraflow chemical variation, and 3) the effect of weathering on chemical composition (Wells and others, 2009). Where flows are correlated chemically, the work of Wells and others (2009) was followed and FeO* <11 weight percent was as an indicator of weathered samples. In areas of isolated outcrops, or where additional analytical techniques could not be applied, a lithologic approach to mapping these units was used by comparing outcrop samples to hand sample "standards" obtained from locations where units had been confidently identified. Unit identification was aided by XRF geochemical analyses of 18 samples collected in the map area and adjacent quadrangles, and another 15 samples from two detailed sections from adjacent quadrangles located at Gordon Ridge on the Locust Grove quadrangle and Fulton Canyon on the Wishram quadrangles (**Figure 5-20**, **Figure 5-21**, **Table 5-1**). The entire CRBG section is visible in the Missoula flood-scoured cliffs above Biggs Junction, providing a clear view of large-scale flow characteristics (**Figure 5-17**).

Figure 5-13. Sketch map showing the outcrop distribution of the CRBG (yellow). Extent of flows includes areas from which the lavas have been eroded in addition to areas where lavas are concealed by younger units. Modified from Reidel and others (2013) and Ferns and McClaughry (2013).

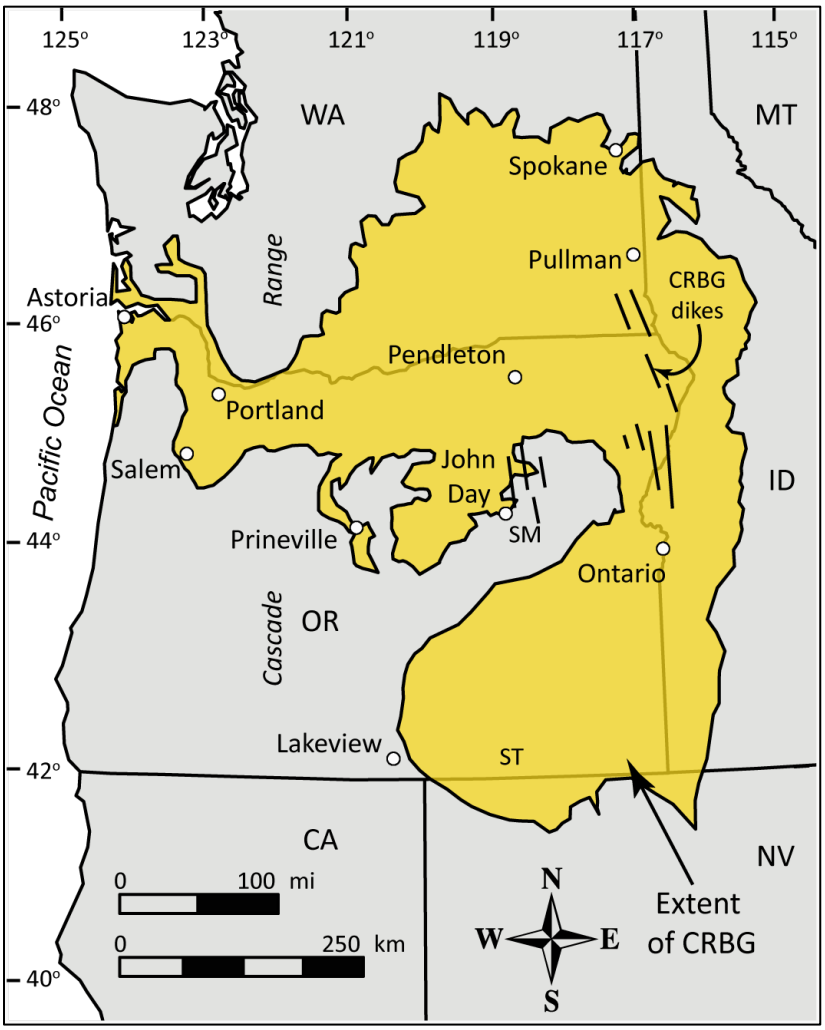

Figure 5-14. Chart showing stratigraphy and nomenclature for the Columbia River Basalt Group. Modified from Reidel and others (2002), with updated stratigraphy from Reidel and others (2013) and Reidel and Tolan (2013) and updated ages from Kasbohm and Schoene (2018). Units in this map area are shown in boldface.

Series	Group	Formation	Member	Age (Ma)	Magnetic Polarity
Miocene, Upper	Columbia River Basalt Group	Saddle Mountains Basalt	Lower Monumental Member	6	N
			Ice Harbor Member	8.5	
			Basalt of Goose Island		N
			Basalt of Martindale		R
			Basalt of Basin City		N
			Buford Member		R
			Elephant Mountain Member	10.5	R,T
Miocene, Middle			Craigmont Member		T
			Swamp Creek Member		T
			Feary Creek Member		T
			Pomona Member	12	R
			Esquatzel Member		N
			Grangeville Member		
			Basalt of Eden		R
			Weissnefels Ridge Member		
			Basalt of Slippery Rock		N
			Basalt of Tenmile Creek		N
			Basalt of Lewiston Orchards		N
			Basalt of Cloverland		N
			Asotin Member	13	
			Basalt of Huntzinger		N
			Basalt of Lapwai		N
			Wilber Creek Member		
			Basalt of Wahluke		N
			Umatilla Member	13.5	
			Basalt of Sillusi		N
			Basalt of Umatilla Member		N
		Wanapum Basalt	Priest Rapids Member		
			Basalt of Lolo	15.895	R
			Basalt of Rosalia		R
			Roza Member		T,R
			Shumaker Creek Member		N
			Frenchman Springs Member		
			Basalt of Sentinel Gap		N
			Basalt of Sand Hollow		N
			Basalt of Silver Falls		N,E
			Basalt of Ginkgo		E
			Basalt of Palouse Falls		E
			Lookingglass Member		N
			Eckler Mountain Member		
			Basalt of Dodge		N
			Basalt of Robinette Mountain		N
			Vantage horizon	16.066	
Miocene, Middle		Grande Ronde Basalt (Prineville Basalt)	**Sentinel Bluffs Member**		N_2
			Winter Water Member		
			Field Springs Member		
			Indian Ridge Member		
			Ortley member		
			Armstrong Canyon member		
			Buttermilk Canyon member		
			Slack Canyon Member		
			Meyer Ridge Member	16.21	R_2
			Grouse Creek member		
			Wapshilla Ridge Member	16.254	
			Mt. Horrible member		
Miocene, Lower		Grande Ronde Basalt (Picture Gorge Basalt)	Cold Spring Ridge Member		N_1
			Hoskin Gulch Member		
			China Creek Member		
			Frye Point member		
			Downey Gulch Member		
			Brady Gulch member		?
			Kendrick Grade member		R_1
			Center Creek member		
			Skeleton Creek member		
			Rogersburg member		
			Teepee Butte Member		
			Birch Creek member		
			Buckhorn Springs Member		
		Imnaha Basalt		16.572	R_1
					T
					N_0
					R_0

Figure 5-15. FeO*/MgO versus SiO_2 diagram showing tholeiitic composition for lavas in the Columbia River Basalt Group, wherein the FeO*/MgO ratio increases as SiO_2 increases. Tholeiitic and calc-alkaline dividing line is from Miyashiro (1974). Data shown include 366 CRBG analyses from the Middle Columbia Basin reported by McClaughry and others (2012) and unpublished data collected by J. D. McClaughry (2014–2017). Note flows of the Saddle Mountains Basalt included here are not exposed in the map area.

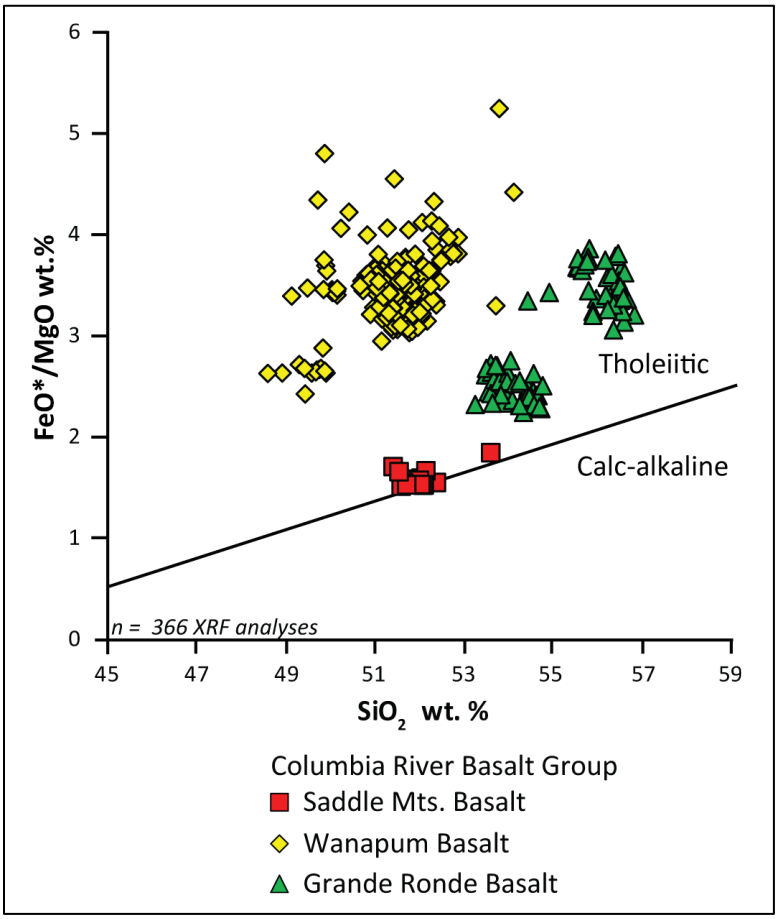

Figure 5-16. Detailed stratigraphic section of part of the Grande Ronde Basalt in the Rufus area constructed from drill logging and sampling of the John Day water well located at the Oregon abutment of the John Day dam. (https://or.water.usgs.gov/projs_dir/crbg/data/wells/john___day/index.html).

Geologic Log For Site JOHN DAY

NWIS Site ID: 454241120411801
OWRD Log ID: JOHN DAY
Well location: 03N/17E-28DDB
Depth drilled, in feet below land surface: 767
Land surface altitude, in feet above Nation Geodetic Vertical Datum of 1929: 190

Logged by: M. H. Beeson and T. L. Tolan
Date drilled: 1961

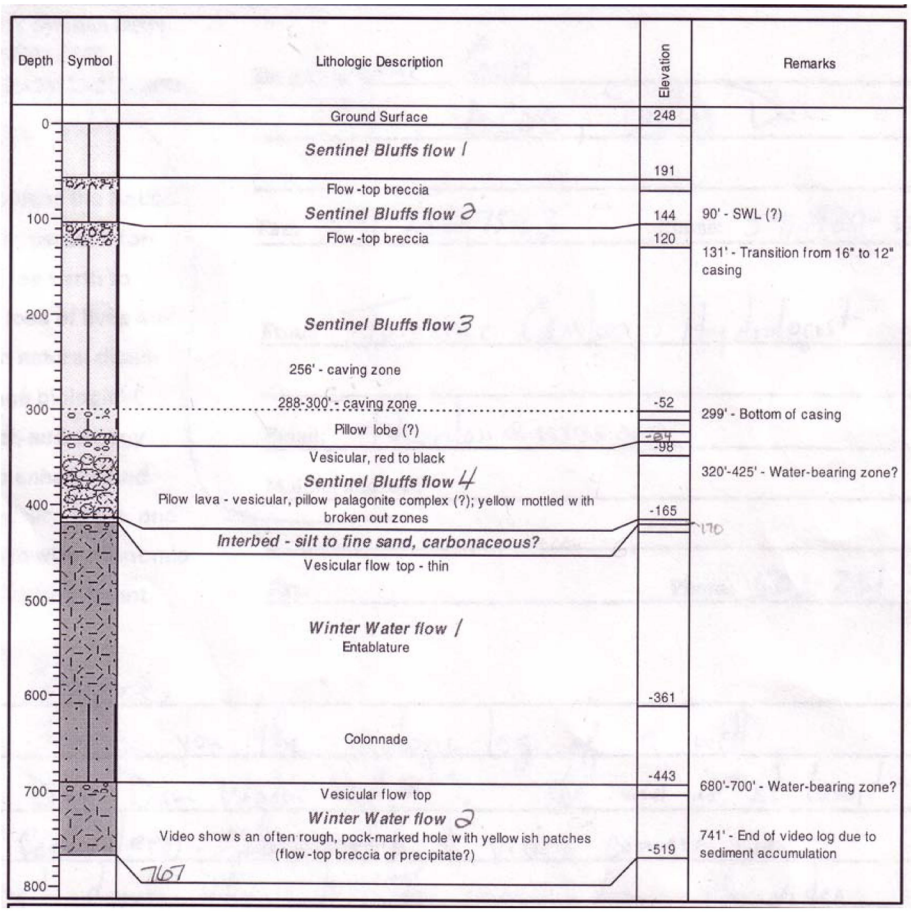

Figure 5-17. (A) Simplified bedrock geology map and (B) perspective view of the cliffs east of Biggs Junction. Missoula flood scour has clearly delineated the edges and tops of the flows of the Basalt of Sand Hollow (Twfh), Sentinel Gap (Twfs), Roza (Twr), and Rosalia (Twpr). Flows of the Basalt of Ginkgo (Twfg) and Sentinel Bluffs (Tgsb) are also visible in the image but do not form prominent benches and are not labeled.

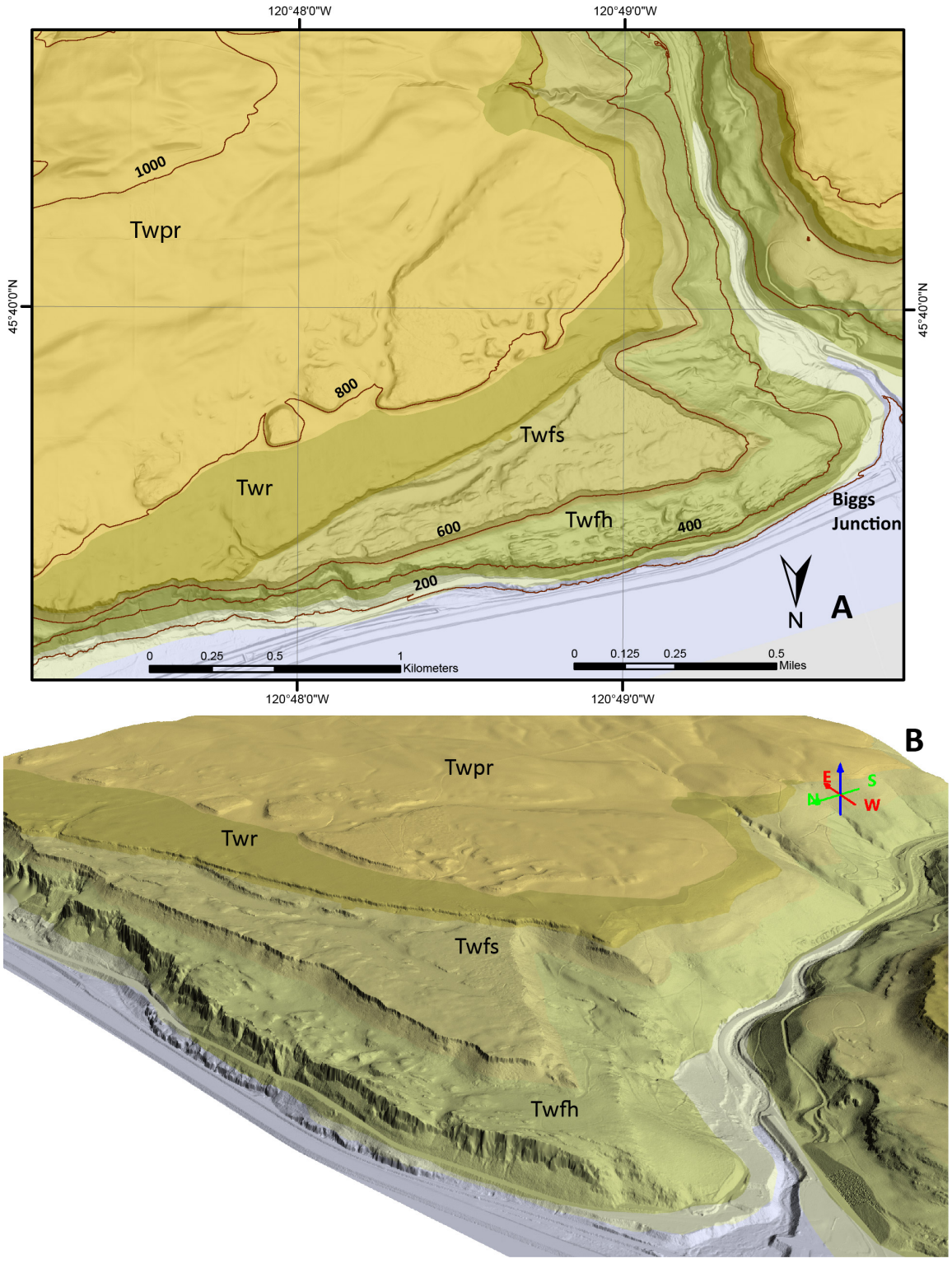

Figure 5-18. Total alkalis ($Na_2O + K_2O$) vs. silica (SiO_2) (TAS) classification of Columbia River Basalt Group lavas from whole-rock XRF analyses (normalized to 100 percent anhydrous). Fields and rock names are from Le Bas and others (1986) and Le Maitre and others (1989). Red-dashed line is the dividing line between alkaline, subalkaline/tholeiitic fields after Cox and others (1979). Data shown include 366 CRBG analyses from the Middle Columbia Basin reported by McClaughry and others (2012) and unpublished data collected by J. D. McClaughry (2014–2017). Flows of the Saddle Mountains Basalt and Basalt of Lolo flows of the Priest Rapids Member of the Wanapum Basalt included here are not exposed in the map area.

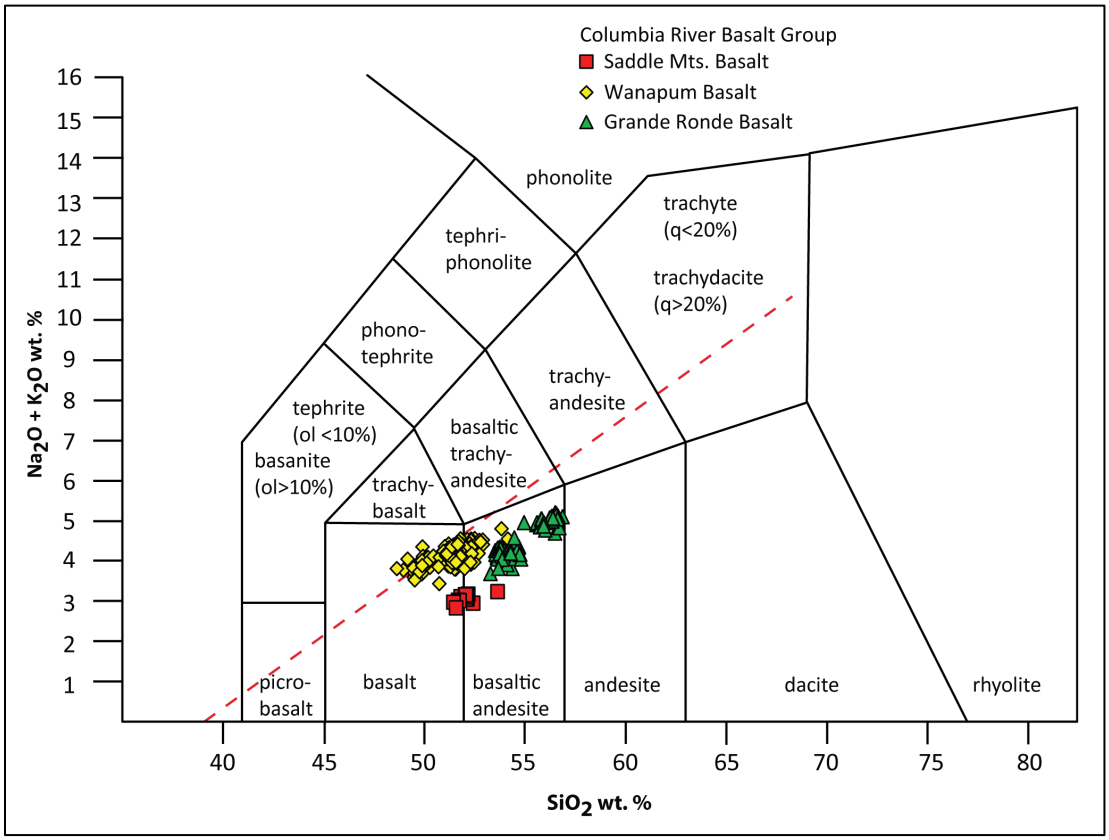

Figure 5-19. Chemical variation diagrams showing geochemical groupings for the Columbia River Basalt Group. (A) Weight percent P_2O_5 versus TiO_2 chemical discrimination plot for Grande Ronde and Wanapum Basalts, illustrating the chemical differences between the two formations. "Ti gap" after Seims and others (1974). (B) TiO_2 versus Cr. (C) Cr versus Ti/Zr. (D) P_2O_5 versus Ti/Zr. Data shown include 366 CRBG analyses from the Middle Columbia Basin reported by McClaughry and others (2012) and unpublished data collected by J.D. McClaughry (2014–2017). Flows of the Saddle Mountains Basalt and Basalt of Lolo flows of the Priest Rapids Member of the Wanapum Basalt included here are not exposed in the map area.

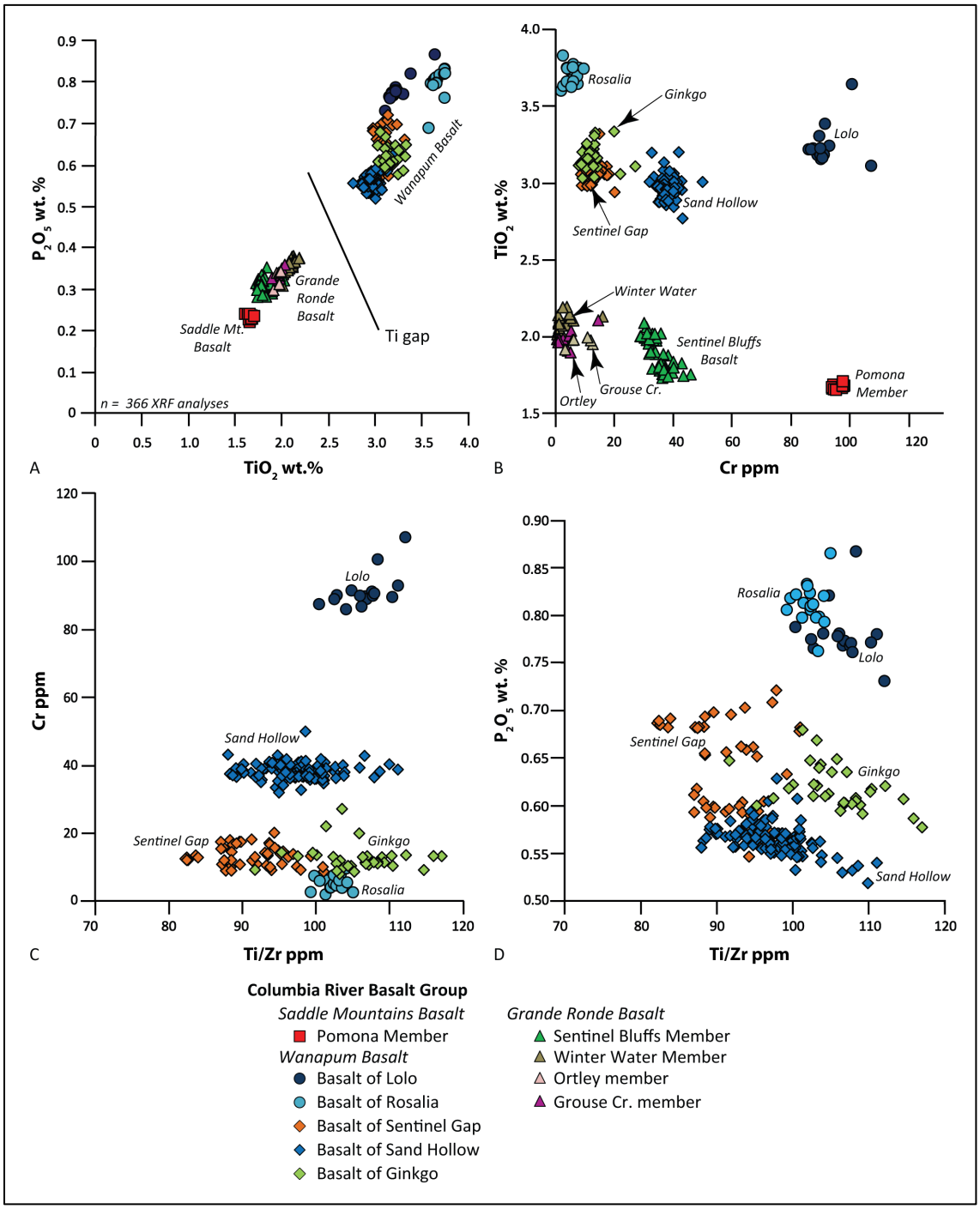

Figure 5-20. Location map for samples analyzed by XRF for whole-rock and trace element geochemistry. Fulton Canyon and Gordon Ridge sections detailed in Figure 5-21.

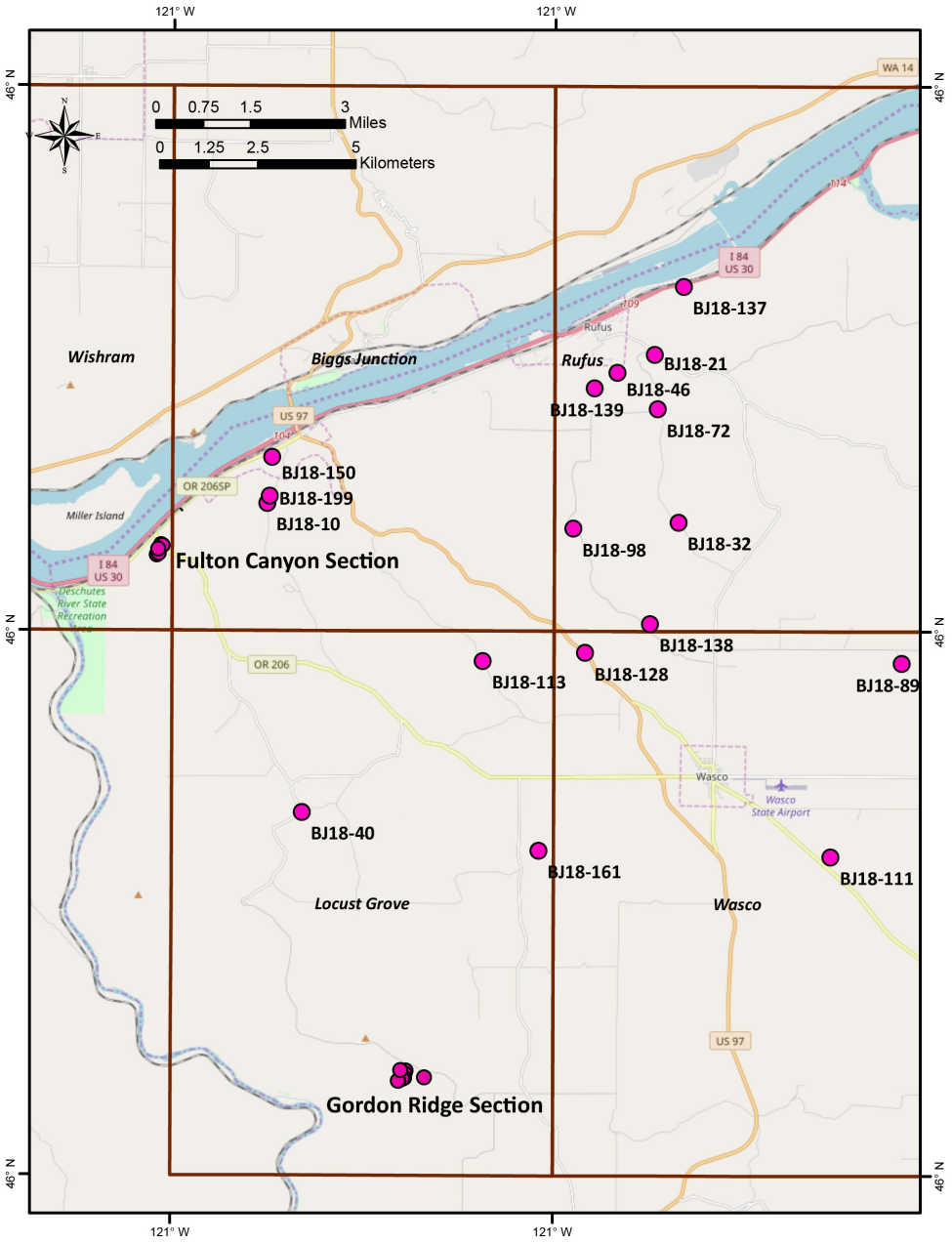

Figure 5-21. Sample locations and unit thicknesses for Columbia River Basalt Group sequence in (top) Fulton Canyon (Wishram quadrangle, not in this report) and (bottom) Gordon Ridge (Locust Grove quadrangle, not in this report) sections. Twpr is Basalt of Rosalia; Twfs is Basalt of Sentinel Gap; Twfh is Basalt of Sand Hollow; Twfg is Basalt of Ginkgo; Tgsb is Sentinel Bluffs Member; Tgww is Winter Water Member.

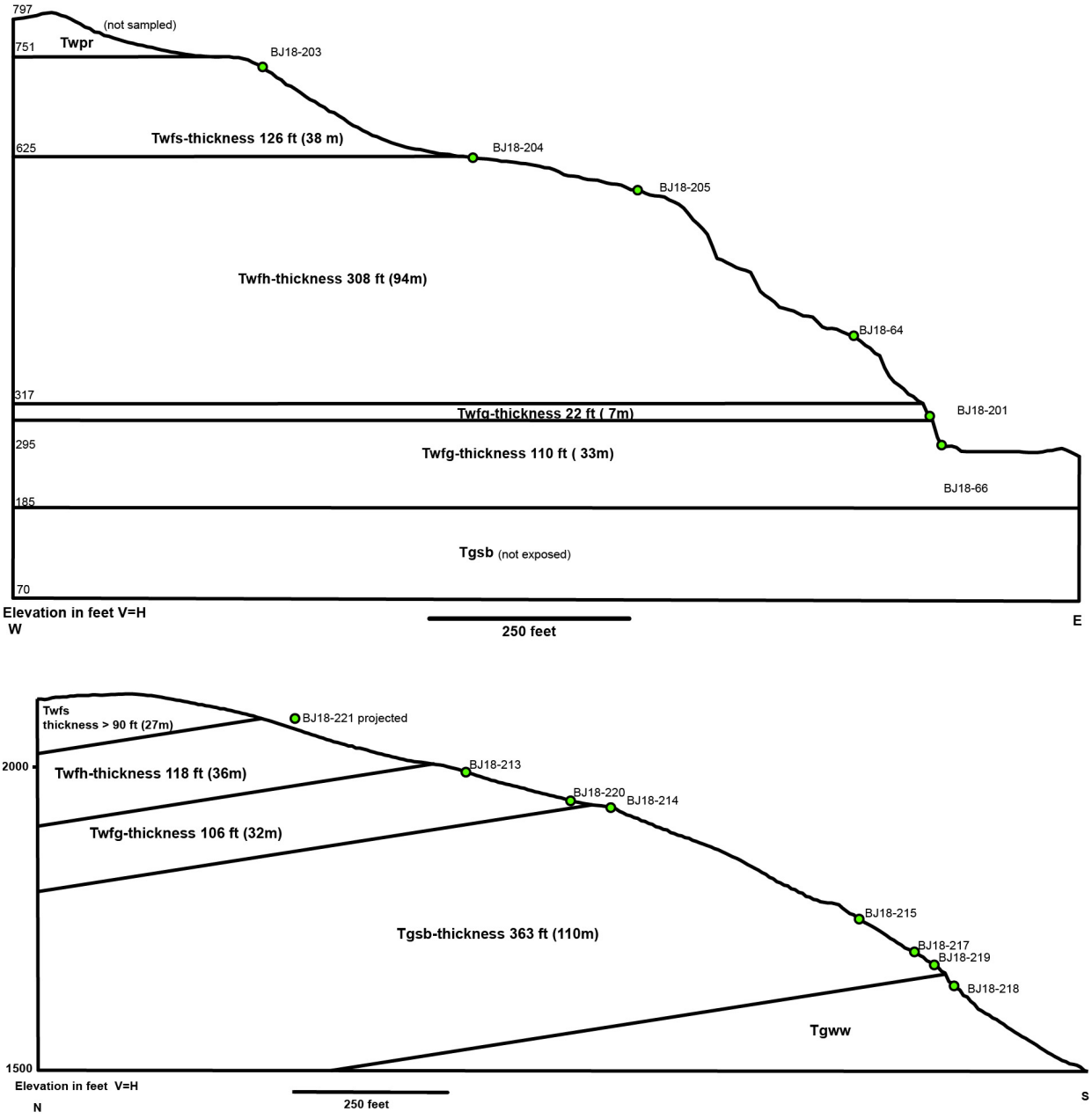

Table 5-1. Representative XRF analyses for early Miocene Columbia River Basalt Group (CRBG) flows sampled from the Biggs Junction, Rufus, Locust Grove, and Wasco 7.5' quadrangles. Regional mean values from 366 CRBG analyses from the Middle Columbia Basin reported by McClaughry and others (2012) and unpublished data collected by J. D. McClaughry (2014–2017).

Sample no.	BJ18-218A	Regional mean *n* = 23	BJ18-219	Regional mean *n* = 25	BJ18-217	BJ18-215	BJ18-214	Regional mean *n* = 19	BJ18-66	BJ18-137	BJ18-220	BJ18-213	BJ18-201A	Regional mean *n* = 52
Formation	Grande Ronde	Grande Ronde	Grande Ronde	Grande Ronde	Grande Ronde	Grande Ronde	Grande Ronde	Grande Ronde	Wanapum	Wanapum	Wanapum	Wanapum	Wanapum	Wanapum
Member	Winter Water	Winter Water	Sentinel Bluffs	Sentinel Bluffs	Sentinel Bluffs	Sentinel Bluffs	Sentinel Bluffs	Sentinel Bluffs	Frenchman Springs	Frenchman Springs	Frenchman Springs	Frenchman Springs	Frenchman Springs	Frenchman Springs
Map Unit Name	Winter Water	Winter Water	McCoy Canyon?	McCoy Canyon	Sentinel Bluffs	Sentinel Bluffs	Sentinel Bluffs	Sentinel Bluffs	Ginkgo	Ginkgo	Ginkgo	Ginkgo	Ginkgo	Ginkgo
Map Unit Label	Tgww	Tgww	Tgsb	Tgsb	Tgsb	Tgsb	Tgsb	Tgsb	Twfg	Twfg	Twfg	Twfg	Twfg	Twfg
UTM_E (NAD 83)	671785		671775		671882	671927	671941		665304	678436	671819	671959	665350	
UTM_N (NAD 83)	5043257		5043256		5043315	5043340	5043453		5056748	5063724	5043529	5043524	5056725	
Map_No.										G12				
Normalized major elements, weight percent														
SiO_2	56.25	55.96	54.00	53.83	54.47	54.12	54.82	54.41	51.52	51.94	51.95	51.37	52.37	51.31
TiO_2	2.08	2.09	1.99	1.98	1.93	1.90	1.82	1.79	3.12	3.13	3.20	3.27	3.17	3.18
Al_2O_3	13.69	13.58	13.92	13.98	14.01	14.15	14.46	14.34	13.21	13.28	13.55	13.69	13.83	13.38
FeO*	11.97	12.22	12.23	12.17	11.79	11.62	11.12	11.39	14.82	14.19	14.07	14.23	13.31	14.64
MnO	0.20	0.21	0.21	0.21	0.19	0.20	0.19	0.19	0.23	0.23	0.23	0.21	0.22	0.21
MgO	3.50	3.47	4.74	4.74	4.84	4.85	4.75	4.75	4.09	4.24	3.90	4.05	3.70	4.13
CaO	7.27	7.21	8.61	8.62	8.58	9.00	8.62	8.63	8.22	8.24	8.48	8.82	8.76	8.38
Na_2O	2.89	3.13	2.81	2.99	2.88	2.75	2.65	2.99	2.77	2.71	2.70	2.56	2.71	2.92
K_2O	1.81	1.79	1.16	1.15	1.03	1.12	1.26	1.19	1.33	1.44	1.31	1.23	1.24	1.22
P_2O_5	0.34	0.36	0.33	0.32	0.29	0.29	0.32	0.32	0.68	0.61	0.61	0.57	0.68	0.62
Total_I	100.00		100.00		100.00	100.00	100.00		100.00	100.00	100.00	100.00	100.00	
Unnormalized trace elements, parts per million														
Ni	2	7	13	15	11	15	14	15	10	14	14	15	11	16
Cr	2	5	36	32	32	34	37	38	10	12	11	13	10	13
Sc	34	33	39	37	37	37	37	36	37	37	37	38	38	37
V	337	342	320	321	318	324	308	309	377	439	425	431	389	424
Ba	615	635	494	488	472	452	511	530	580	608	567	500	817	558
Rb	46	48	28	27	24	24	29	29	34	34	33	26	32	30
Sr	317	321	311	314	304	315	314	320	324	311	324	332	379	325
Zr	183	183	159	161	156	152	155	160	182	196	183	170	181	180
Y	37	38	35	35	34	33	38	34	41	44	42	38	42	41
Nb	13.0	13	11.9	11	11.0	11.1	11.1	11	14.1	15.1	14.2	13.1	14.3	14
Ga	22	22	21	20	21	20	20	20	23	22	23	22	22	21
Cu	8	11	29	30	30	29	27	27	22	26	25	24	23	25
Zn	127	132	120	122	116	115	120	115	141	150	143	137	144	145
Pb	7	8	7	5	6	6	7	6	8	8	7	7	7	6
La	26	25	23	19	21	17	22	20	26	29	25	24	25	25
Ce	53	55	43	44	47	42	47	45	61	61	60	47	58	56
Th	7	6	4	3	3	3	4	4	4	5	5	4	5	4
Nd	26	29	24	24	25	23	27	24	33	34	33	28	32	31
U	3	2	2	2	1	2	3	1	2	4	3	2	4	2

Major element determinations have been normalized to a 100-percent total on a volatile-free basis and recalculated with total iron expressed as FeO*; na - not applicable or no information.

Table 5-2. Representative XRF analyses for early Miocene Columbia River Basalt Group (CRBG) flows sampled from the Biggs Junction, Rufus, Locust Grove and Wasco 7.5′ quadrangles.Regional mean values from 366 CRBG analyses from the Middle Columbia Basin reported by McClaughry and others (2012) and unpublished data collected by J. D. McClaughry (2014–2017).

Sample no.	BJ18-57	BJ18-64	BJ18-150B	BJ18-150C	BJ18-164	BJ18-205	BJ18-204	BJ18-221	Regional mean *n* = 112	BJ18-46	BJ18-203	BJ18-40	BJ18-89	BJ18-98	BJ18-111	BJ18-113	BJ18-128	BJ18-138	BJ18-161	Regional mean *n* = 41
Formation	Wanapum	Wanapum	Wanapum	Wanapum	Wanapum	Wanapum	Wanapum	Wanapum	Wanapum	Wanapum	Wanapum	Wanapum	Wanapum	Wanapum	Wanapum	Wanapum	Wanapum	Wanapum	Wanapum	Wanapum
Member	Frenchman Springs	Frenchman Springs	Frenchman Springs	Frenchman Springs	Frenchman Springs	Frenchman Springs	Frenchman Springs	Frenchman Springs	Frenchman Springs	Frenchman Springs	Frenchman Springs	Frenchman Springs	Frenchman Springs	Frenchman Springs	Frenchman Springs	Frenchman Springs	Frenchman Springs	Frenchman Springs	Frenchman Springs	Frenchman Springs
Map Unit Name	Sand Hollow	Sand Hollow	Sand Hollow	Sand Hollow	Sand Hollow	Sand Hollow	Sand Hollow	Sand Hollow	Sand Hollow	Sentinel Gap	Sentinel Gap	Sentinel Gap	Sentinel Gap	Sentinel Gap	Sentinel Gap	Sentinel Gap	Sentinel Gap	Sentinel Gap	Sentinel Gap	Sentinel Gap
Map Unit Label	Twfh	Twfh	Twfh	Twfh	Twfh	Twfh	Twfh	Twfh	Twfh	Twfs	Twfs	Twfs	Twfs	Twfs	Twfs	Twfs	Twfs	Twfs	Twfs	Twfs
UTM_E (NAD 83)	685485	665288	668076	668076	675226	665237	665257	672438		676814	665202	669114	684287	675815	682634	673605	676210	677845	675170	
UTM_N (NAD 83)	5046218	5056674	5059058	5059058	5034104	5056630	5056519	5043366		5061479	5056484	5050034	5054278	5057471	5049296	5054026	5054311	5055099	5049236	
Map_No.			G6	G7						G10				G2				G1		
Normalized major elements, weight percent																				
SiO_2	51.71	51.71	51.61	52.21	51.79	51.31	51.48	51.78	51.67	51.76	51.61	52.33	51.99	51.76	52.08	51.93	51.58	51.83	51.84	52.04
TiO_2	2.97	2.99	3.00	3.00	2.88	3.02	3.01	2.91	2.97	3.13	3.14	3.10	3.10	3.12	3.09	3.11	3.07	3.09	3.09	3.07
Al_2O_3	13.33	13.33	13.34	13.39	13.44	13.33	13.41	13.32	13.44	13.18	13.16	13.24	13.21	13.43	13.25	13.19	13.16	13.18	13.17	13.21
FeO*	14.48	14.31	14.32	13.98	14.26	14.60	14.12	14.33	14.16	14.40	14.79	14.31	14.61	14.42	14.57	14.79	15.02	14.81	14.77	14.31
MnO	0.21	0.22	0.23	0.21	0.21	0.22	0.24	0.23	0.22	0.23	0.22	0.22	0.23	0.22	0.22	0.21	0.22	0.22	0.22	0.23
MgO	4.60	4.50	4.47	4.30	4.60	4.50	4.21	4.51	4.35	4.25	4.18	4.16	3.95	4.14	4.16	4.07	4.27	4.17	4.28	4.01
CaO	8.10	8.40	8.40	8.27	8.23	8.57	9.00	8.38	8.46	8.28	8.38	7.94	8.10	8.31	8.12	7.92	8.09	7.92	8.03	8.14
Na_2O	2.79	2.77	2.72	2.82	2.80	2.59	2.67	2.71	2.87	2.63	2.67	2.71	2.66	2.70	2.67	2.82	2.79	2.85	2.70	2.93
K_2O	1.27	1.23	1.36	1.26	1.25	1.31	1.30	1.28	1.27	1.51	1.26	1.41	1.58	1.33	1.28	1.36	1.19	1.35	1.33	1.43
P_2O_5	0.54	0.55	0.56	0.56	0.54	0.54	0.56	0.55	0.56	0.62	0.60	0.58	0.57	0.57	0.57	0.60	0.59	0.58	0.56	0.63
Total_I	100.00	100.00	100.00	100.00	100.00	100.00	100.00	100.00		100.00	100.00	100.00	100.00	100.00	100.00	100.00	100.00	100.00	100.00	
Unnormalized trace elements, parts per million																				
Ni	16	16	16	15	18	16	16	16	19	13	13	12	12	13	13	14	11	11	13	16
Cr	36	38	39	37	41	37	37	37	38	13	16	14	14	16	14	15	12	15	15	14
Sc	36	37	37	37	37	38	37	37	37	37	38	37	36	37	36	37	38	36	36	37
V	411	419	423	423	405	427	417	410	415	439	434	419	428	438	430	432	424	433	433	422
Ba	560	558	561	568	557	520	541	551	569	589	573	586	622	567	601	592	596	589	559	630
Rb	33	30	33	34	32	31	31	29	31	35	28	36	35	32	29	35	24	36	36	36
Sr	302	313	318	310	306	317	311	314	321	312	311	298	310	319	309	300	310	303	300	314
Zr	184	182	183	182	181	175	180	183	183	194	192	203	202	195	199	197	195	199	197	204
Y	41	42	41	41	40	40	39	41	41	43	43	44	44	43	44	43	43	43	43	45
Nb	14.7	13.3	14.5	14.4	14.6	13.4	14.0	14.7	14	14.3	15.0	15.8	15.8	16.0	14.9	14.9	16.0	15.8	16.1	16
Ga	21	22	22	20	21	21	21	21	21	22	21	21	22	22	23	21	21	21	21	21
Cu	29	29	29	27	27	28	27	28	28	24	24	27	24	23	24	24	23	24	24	25
Zn	138	139	140	139	138	137	134	139	141	147	143	143	142	147	142	145	141	143	143	149
Pb	7	8	7	7	9	7	8	8	6	6	7	8	8	9	8	8	8	8	7	7
La	28	25	25	27	26	23	26	27	25	27	25	26	29	24	27	26	27	26	25	27
Ce	56	54	56	58	56	52	51	56	55	59	58	58	61	59	62	59	60	60	56	62
Th	4	4	5	4	4	4	4	4	4	5	4	4	5	5	4	4	5	5	5	4
Nd	29	32	32	32	31	29	30	31	31	35	32	35	34	34	33	36	33	34	30	35
U	3	0	2	3	2	2	2	3	2	1	2	2	2	3	2	3	3	3	2	2

Major element determinations have been normalized to a 100-percent total on a volatile-free basis and recalculated with total iron expressed as FeO*; na - not applicable or no information.

Table 5-3. Representative XRF analyses for early Miocene Columbia River Basalt Group (CRBG) flows sampled from the Biggs Junction, Rufus, Locust Grove, and Wasco 7.5' quadrangles. Regional mean values from 366 CRBG analyses from the Middle Columbia Basin reported by McClaughry and others (2012) and unpublished data collected by J. D. McClaughry (2014–2017).

Sample no.	MAD BJ18-72	MAD BJ18-139	MAD BJ18-199	MAD BJ18-10	MAD BJ18-32B	Regional mean *n* = 17	BJ18-21
Formation	Wanapum	Wanapum	Wanapum	Wanapum	Wanapum	Wanapum	Wanapum
Member	Roza	Priest Rapids	Priest Rapids	Priest Rapids	Priest Rapids	Priest Rapids	Wanapum?
Map Unit Name	Roza	Rosalia	Rosalia	Rosalia	Rosalia	Rosalia	Tfsh?
Map Unit Label	Twr	Twpr	Twpr	Twpr	Twpr	Twpr	
UTM_E (NAD 83)	677864	676241	668043	667989	678496		677749
UTM_N (NAD 83)	5060581	5061059	5058078	5057886	5057710		5061963
Map_No.	G8	G9	G5	G4	G3		G11
Normalized major elements, weight percent							
SiO_2	50.80	50.10	50.68	52.02	51.04	50.24	52.66
TiO_2	3.19	3.61	3.70	4.00	3.75	3.70	3.71
Al_2O_3	13.56	12.82	12.93	14.11	13.43	13.09	12.32
FeO*	14.33	15.60	14.69	12.69	13.26	14.98	14.86
MnO	0.23	0.25	0.24	0.22	0.25	0.25	0.25
MgO	4.68	4.64	4.45	3.08	3.20	4.07	3.36
CaO	8.77	8.29	8.65	9.29	10.39	8.70	7.77
Na_2O	2.60	2.69	2.56	2.55	2.64	2.67	2.74
K_2O	1.19	1.24	1.32	1.18	1.24	1.29	1.64
P_2O_5	0.65	0.77	0.79	0.86	0.79	0.81	0.69
Total_I	100.00	100.00	100.00	100.00	100.00		100.00
Unnormalized trace elements, parts per million							
Ni	21	16	15	12	18	19	6
Cr	29	5	5	5	7	5	0
Sc	39	39	40	41	26	39	40
V	415	420	421	437	419	424	418
Ba	534	575	569	756	1089	584	691
Rb	28	31	32	28	32	31	42
Sr	307	286	294	322	342	297	295
Zr	184	218	220	231	222	218	228
Y	42	51	51	54	51	51	50
Nb	14.8	18.8	18.0	19.1	17.8	18	17.8
Ga	22	21	23	23	22	22	23
Cu	30	22	21	25	23	24	34
Zn	138	152	155	168	156	159	158
Pb	7	8	8	7	8	6	9
La	28	32	29	31	35	29	29
Ce	59	71	67	70	39	69	70
Th	5	4	4	4	3	4	6
Nd	34	39	41	42	26	40	39
U	2	2	2	2	2	2	2

Major element determinations have been normalized to a 100-percent total on a volatile-free basis and recalculated with total iron expressed as FeO*; na - not applicable or no information.

5.2.2.2 Wanapum Basalt

The Wanapum Basalt in the Biggs Junction-Rufus area consists of lavas assigned to the Frenchman Springs, Roza, and Priest Rapids Members.

5.2.2.2.1 Priest Rapids Member

The Priest Rapids Member forms the upper part of the Wanapum Basalt, unconformably overlying the Frenchman Springs and Roza Members (**Figure 5-14**, Plate 1). The member consists of two flows assigned to the Lolo and Rosalia chemical types, which are differentiated on the basis of lithology and geochemistry (**Figure 5-19**; Wright and others, 1973; Camp, 1981; Anderson, 1987; Anderson and Vogt, 1987). Priest

Rapids lavas are distinguished from other CRBG units by their relatively high concentrations of MgO, TiO_2 (>3.50 weight percent), FeO*, and P_2O_5 (**Figure 5-19**; **Table 5-3**; appendix). Lavas in the Priest Rapids Member also have reversed magnetic polarity, which serves to distinguish these flows from adjacent units (Swanson and others 1979b). The Priest Rapids Member was erupted around 15.895 ± 0.019 Ma (Kasbohm and Schoene, 2018). Lavas of the Priest Rapids Member were erupted from linear dike systems in the Clearwater Embayment of western Idaho and flowed westward (Camp, 1981), covering most of the north and central parts of the Columbia Plateau. These flows were largely confined as intracanyon flows as they traversed the area of the present-day Cascade Range (Anderson and Vogt, 1987). Effusion of the Priest Rapids Member produced over 2,800 km^3 (672 mi^3) of lava that covered an area exceeding 57,300 km^2 (22,123 mi^2) (Swanson and others, 1979b, Camp, 1981; Tolan and others, 1989). The maximum thickness of the Priest Rapids Member in the Biggs Junction-Rufus area is ~75 m (245 ft) (**Figure 5-12**).

Twpr **Basalt of Rosalia (middle Miocene)**—One or more flows of dark gray, aphyric to sparsely plagioclase-phyric basalt covering most of the uplands in the map area (**Figure 5-17**, Plate 1). The Basalt of Rosalia is rarely exposed, with the exception of cliffs between Rufus and Biggs and scattered roadcuts and quarries. The Basalt of Rosalia appears to have been deposited in a broad shallow channel, the axis of which was near or north of the current Columbia River channel. There are several lines of evidence to suggest this. First, the unit thins to the south and west and pinches out just south of the map area. The location of the pinchout is not well constrained by well or exposure data, but a map of the total thickness of section above the top of the underlying Basalt of Sentinel Gap (**Twfs**) (**Figure 5-12**) shows a fairly abrupt change in thickness interpreted to be the southern edge of the Basalt of Rosalia. There is also an alignment of anomalous drainages, where streams flowing NNW, down the regional dip, turn abruptly to a WSW trend (**Figure 5-12**). The alignment of diverted drainages roughly coincides with the rapid thinning of the section above the Basalt of Sentinel Gap. The emplacement of the Basalt of Rosalia in a broad channel may have blocked the developing NNW trending drainage network and caused the streams to divert along the edge of the newly emplaced flow. Finally, there is a subtle change in the aeromagnetic map (**Figure 4-2**) with generally lower intensity north of the line of anomalous drainages, which may reflect the presence of reversely polarized Basalt of Rosalia on top of an otherwise normally polarized section. The Basalt of Rosalia is 25–30 m (80–100 ft) thick at the northern edge of the area and thins to the south.

In a quarry exposure near Rufus (**Figure 5-22**) the basalt forms 1.5- to 2-m diameter columns with incipient blocky or platy jointing. Several roadcut exposures have pillow jointing with glassy pillow rinds, and a quarry just south of the map area contains exposures of pillows in a palagonite matrix, overlying a thin tuff and sandstone interbed (**Figure 5-23**). The basal contact of the Basalt of Rosalia is locally separated from the underlying CRBG flows by sedimentary interbeds and a tuff. Sand, gravel, and silt are described in well logs, and diatomite at least 2 m thick (**Figure 5-24**) is exposed in one location. At several sites, air fall tuff (**Figure 5-25**) was observed separating the Basalt of Rosalia from the underlying Basalt of Roza or Basalt of Sentinel Gap.

Typical hand samples are generally aphyric, but Anderson (1987) reported that yellow-colored plagioclase phenocrysts and glomerocrysts 3 mm to 1 cm across (0.1 to 0.4 in) are sparsely distributed throughout the unit elsewhere. The groundmass is fine to medium grained with equant to acicular plagioclase and equant olivine microphenocrysts (**Figure 5-26**). Samples from the Basalt of Rosalia analyzed for this study have a basaltic chemical composition with 50.1 to 52.02 weight percent SiO_2, 3.61 to 4.00 weight percent TiO_2, 3.08 to 4.64 weight percent MgO,

0.77 to 0.86 weight percent P_2O_5, and 5 to 7 ppm Cr (**Table 3-1**; appendix). The Basalt of Rosalia is distinguished from the rest of the CRBG by relatively higher concentrations of MgO, TiO_2, and P_2O_5, and lesser amounts of Cr (**Figure 5-19**; **Table 3-1**; Anderson and Vogt, 1987).

Outcrops of the Basalt of Rosalia measured in the field area have reversed magnetic polarity, although two sites of pillow lava showed anomalous normal polarity. The unit is assigned a middle Miocene age on the basis of U/Pb dating of an ash between the Basalt of Rosalia and the Basalt of Lolo, which gives an age of 15.895 ± 0.019 Ma (Kasbohm and Schoene, 2018). Equivalent to the Rosalia chemical type of Wright and others (1973).

Figure 5-22. Basalt of Rosalia exposed in quarry face located at 676,241 E, 5,061,059 N, view to south. Orthomosaic projection of 3D model, full-resolution image in digital appendix.

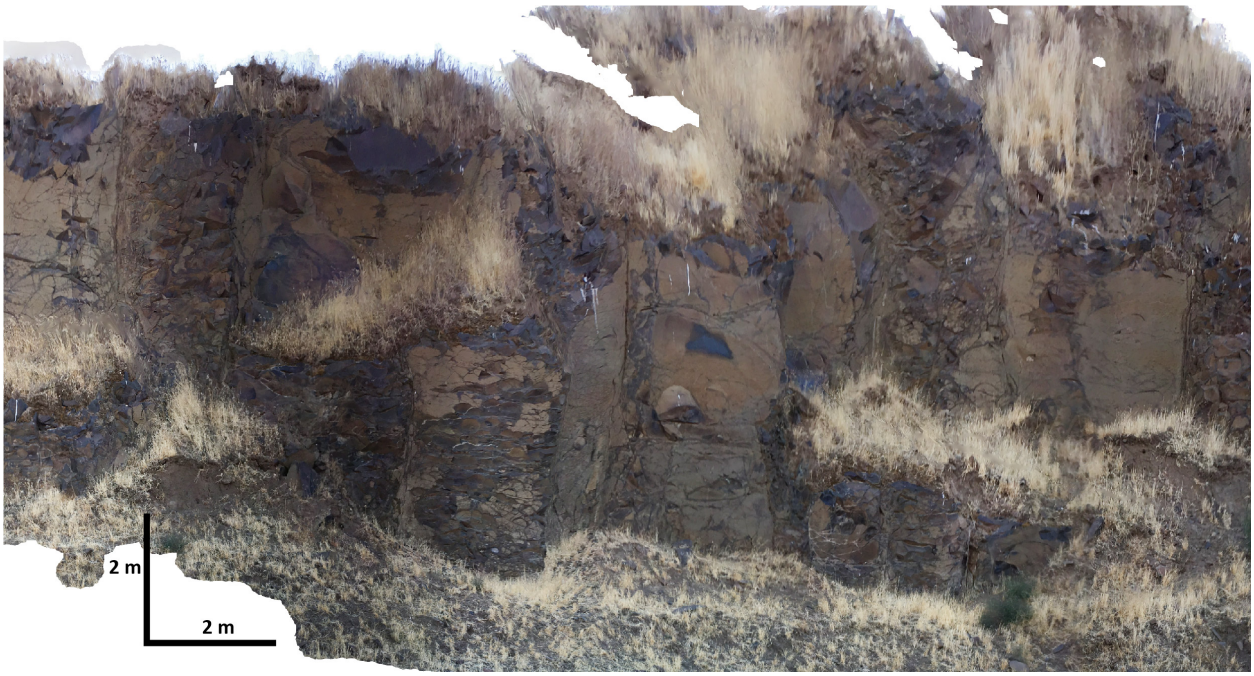

Figure 5-23. Basalt of Rosalia pillows in small quarry face. Location is 669338 E, 5053773 N, ~900 m (3,000 ft) south of the map area along the Celilo-Wasco Highway (Oregon Route 206). View to south.

Figure 5-24. Diatomite interbed between the Basalt of Roza (Twr) and Basalt of Rosalia (Twpr). (A) Outcrop photo of diatomite exposure, (B) hand sample, (C) photomicrograph showing unidentified diatom species. Location 668006 E, 5057022 N.

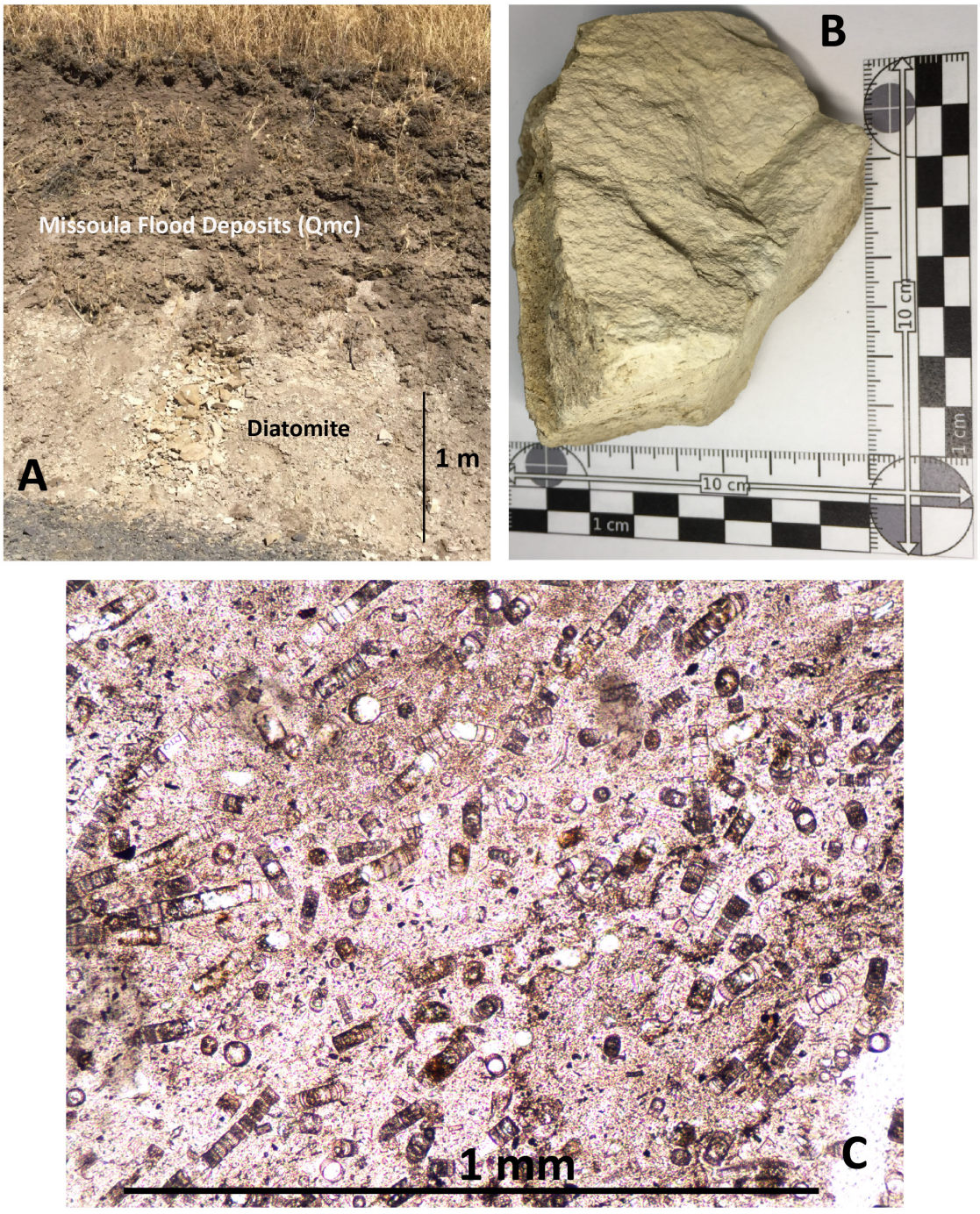

Figure 5-25. Tuff interbed beneath Basalt of Rosalia. (A) Outcrop photo of white tuff exposed between the Basalt of Sentinel Gap (below and to left) and overlying Basalt of Rosalia (678496 E, 5057710 N, view to northeast). (B) Hand sample of tuff. Sample BJ18-32.

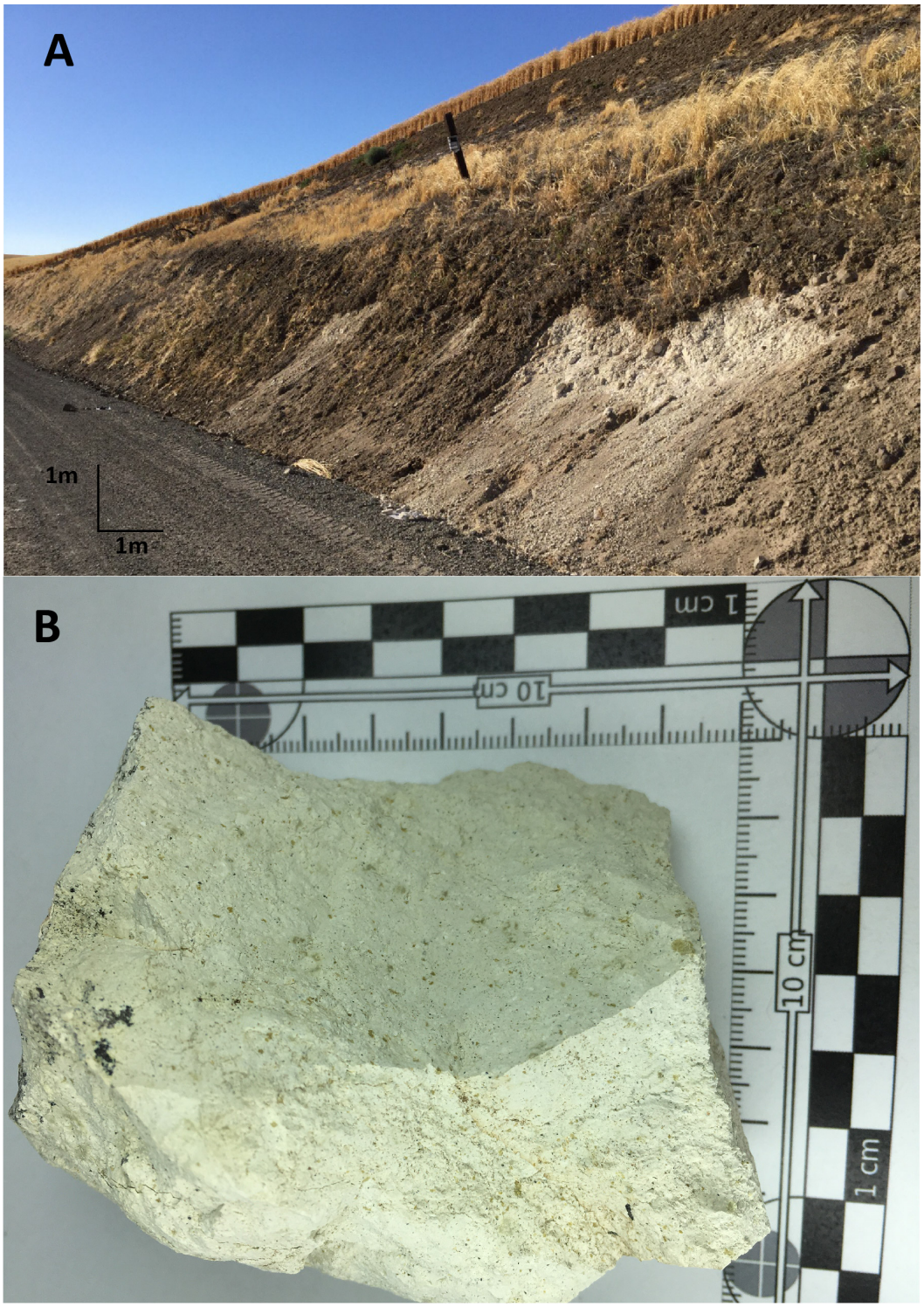

Figure 5-26. Hand sample of Basalt of Rosalia. Sample BJ18-199.

5.2.2.2.2 Roza Member

The Roza Member is one of the most distinctive units in the CRBG because of the abundance of plagioclase phenocrysts. The unit covers ~ 40,000 km^2 in Oregon and Washington and consists of one to four flows that are divided into six chemical subtypes (Martin, 1989). The Roza Member flows originated from vents along an arc stretching from Troy, Oregon, to Colfax, Washington; most of the flows were largely restricted to the vent area, with only two flows extending as far as the Mid-Columbia Basin (Martin, 1989). Only one of these two flows was observed in the map area.

Twr **Basalt of Roza (lower Miocene)**—A single flow of dark grey, plagioclase-phyric basalt stratigraphically between the Basalt of Sentinel Gap and the Basalt of Rosalia. The Basalt of Roza is exposed as a nearly continuous cliff near the top of the Columbia River Gorge between Biggs Junction and the mouth of the John Day river and in a few roadcuts and stream channels (**Figure 5-17**, Plate 1). It forms a prominent bench and cliff at Biggs Junction where the CRBG section has been scoured by Missoula Floods (**Figure 5-17**). The flow is ~20 m (70 ft) thick in the cliff exposure and pinches out to the south and west.

A well-developed colonnade is visible in the cliff exposures and at several roadcut exposures, and the basalt is easily recognized by the abundance of plagioclase phenocrysts (2,000–5,000 per square meter) visible on weathered surfaces (**Figure 5-27**). The basal contact with the underlying Basalt of Sentinel Gap is well exposed at the intersection of Scott Canyon Road and Herin Road, where the vesicular top of the Basalt of Sentinel Gap is overlain by ~1 m (3 ft) of light yellowish-orange coarse sandstone. The basal ~1 m (3 ft) of the Basalt of Roza overlying the sandstone has strongly developed horizontal platy jointing, while the remainder of the exposed flow has well-developed columns 0.25–0.75 m (10–30 in) in diameter (**Figure 5-28**).

Typical hand samples are dark grey fine-grained porphyritic basalt with abundant lath shaped plagioclase microphenocrysts 0.5–1 mm long and abundant clear to light yellow, lath-shaped, prismatic or blocky plagioclase phenocrysts 1.5–10 mm long (**Figure 5-26**).

The sample of the Basalt of Roza analyzed for this study has a basaltic chemical composition with 50.8 weight percent SiO_2, 3.19 weight percent TiO_2, 4.68 weight percent MgO, 0.65 weight percent P_2O_5, and 29 ppm Cr (**Table 5-3**; appendix). From the location and chemistry, the Basalt of Roza in the map area is part of the IIA chemical subtype of Martin (1989). The Basalt of Roza is distinguished from the rest of the CRBG by stratigraphic position near the top of the Wanapum Basalt and the abundance of plagioclase phenocrysts. The Basalt of Gingko, which also can have abundant plagioclase phenocrysts, has lower MgO and Cr and occurs at the bottom of the Wanapum Basalt.

Samples of the Basalt of Roza measured in this study had normal magnetic polarity. The unit is assigned an early Miocene age and is bracketed by U/Pb dates of 15.895 ± 0.019 Ma for ash between the Basalt of Rosalia and Basalt of Lolo and 16.066 ± 0.04 Ma for ash between the Basalt of Ginkgo and the Sentinel Bluffs Member (Kasbohm and Schoene, 2018).

Figure 5-27. Basalt of Roza. (A) Roadcut outcrop of columnar-jointed Basalt of Roza on China Hollow Road (677864 E,5060581 N, view to north), orthomosaic projection of 3D model, full-resolution image in digital appendix. (B) detail of outcrop showing abundance of plagioclase phenocrysts. Inside dimension of wooden frame is 30 cm (10 inches). Sample BJ18-72.

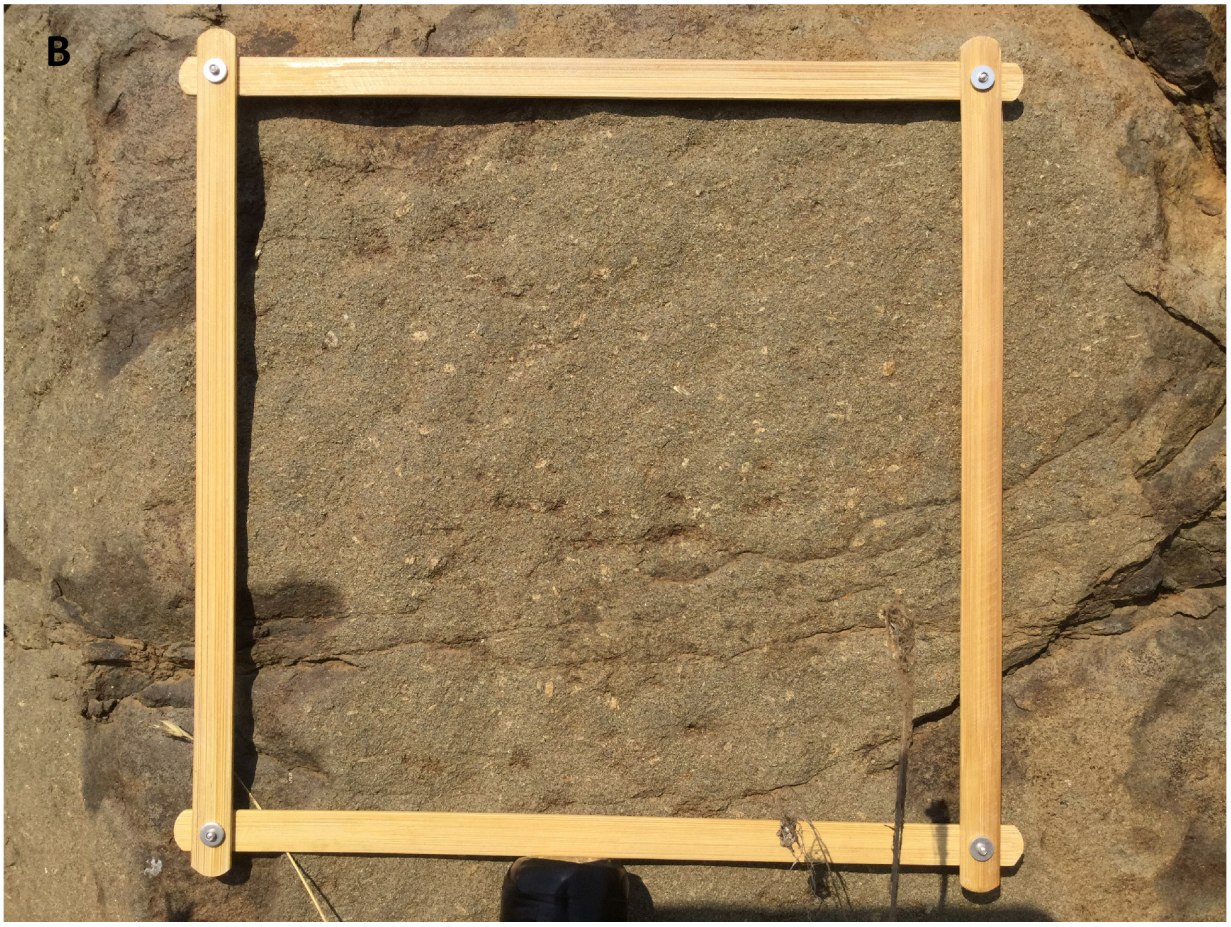

Figure 5-28. Contact between Basalt of Sentinel Gap and overlying Basalt of Roza at intersection of Scott Canyon Road and Herin Road (680124 E, 5060838 N, view to north). Approximately 1 m (3 ft) of tan-orange coarse sandstone separates the Basalt of Roza (Twr) from the underlying Basalt of Sentinel Gap (Twfs), and the basal meter of the Basalt of Roza has strongly developed horizontal platy jointing. Hammer is 85 cm long. Sample BJ18-25 is from this outcrop.

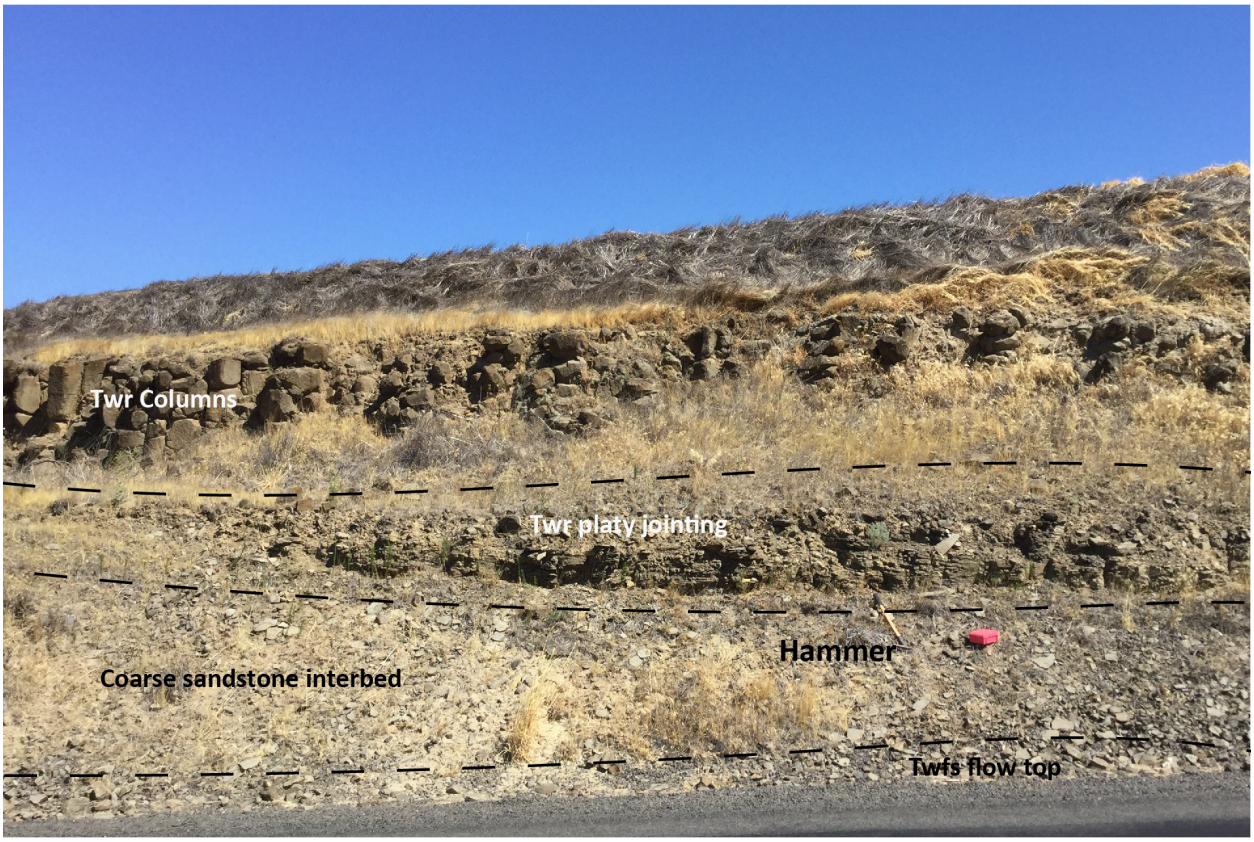

Figure 5-29. Hand sample of Basalt of Roza. Sample BJ18-25A.

5.2.2.2.3 Frenchman Springs Member

The Frenchman Springs Member forms the lower part of the Wanapum Basalt and in this area consists of four or five individual flows. On the basis of lithology, phenocryst distribution, and geochemistry, these lavas are divided from oldest to youngest into the Basalt of Ginkgo (**Twfg**), Basalt of Sand Hollow (**Twfh**), and Basalt of Sentinel Gap (**Twfs**) (**Figure 5-14** and **Figure 5-19**; Beeson and others, 1985; Martin and others, 2013). Frenchman Springs lavas are distinguished from other CRBG units by large, widely scattered to locally abundant plagioclase phenocrysts and high TiO_2 contents (~2.9 to 3.06 weight percent) (Beeson and others, 1985, 1989; **Figure 5-19a-b**; **Table 5-1, Table 5-2**; appendix). Upper lavas (**Twfs**, **Twfh**) in the Frenchman Springs Member have normal magnetic polarity, while those in the lower part of the member (**Twfg**) have excursional polarity (Beeson and others, 1985; Martin and others, 2013) (**Figure 5-14**). These lavas overlie lavas of the Sentinel Bluffs Member (**Tgsb**) at the top of the Grande Ronde Basalt and, in turn, are overlain by the transitional polarity Roza Member, present only in the northeast portion of the map area, or the reversed-polarity lavas of the Priest Rapids Member, forming the upper part of the Wanapum Basalt (**Figure 5-14;** Plate 1). The age of the Frenchman Springs Member is bracketed by U/Pb dates of 15.895 ± 0.019 Ma for ash between the Basalt of Rosalia and Basalt of Lolo

and 16.066 ± 0.04 Ma for ash between the Basalt of Ginkgo and the Sentinel Bluffs Member (Kasbohm and Schoene, 2018). Lavas of the Frenchman Springs Member were erupted from a northerly trending vent system in eastern Washington and northern Oregon (Kuehn, 1995) and flowed west down an ancestral paleoslope (**Figure 5-13**). Eruption of Frenchman Springs Member material produced over 7,628 km^3 (1,830 mi^3) of lava that covered an area exceeding 72,595 km^2 (28,029 mi^2) (Martin and others, 2013). The composite thickness of the Frenchman Springs Member in the Rufus-Biggs Junction area is ~167 m (550 ft) at the mouth of the John Day, ~190 m (620 ft) at Rufus, ~140 m (460 ft) at Biggs Junction, and ~150 m (500 ft) at Fulton Canyon(**Figure 5-16**; Plate 1).

The Frenchman Springs Member is subdivided in the map area into:

Twfs **Basalt of Sentinel Gap (lower Miocene)**—One or two flows of aphyric to sparsely plagioclase-phyric basalt lying stratigraphically above the Basalt of Sand Hollow (**Twfh**) and extending throughout the map area (**Figure 5-14, Figure 5-21**; Plate 1). Good exposures are common along the cliffs of the Columbia River Gorge and in the lower reaches of the tributary canyons, and in flood-scoured areas of the uplands (**Figure 5-17**). Elsewhere in the uplands, exposures are typically restricted to small roadcuts, low outcrops on uncultivated slopes, and the bottoms of stream drainages. South and east of Biggs Junction, only one flow is present, but two are present along the western edge of the map area and at Frank Fulton Canyon. Thickness of the unit in the map area ranges between 36 and 46 m (120–150 ft) (**Figure 5-21**; Plate 1).

Good outcrops are typically characterized by a well-defined colonnade with columns 1-2 m (3–6 ft) in diameter and/or platy jointing (**Figure 5-30, Figure 5-31**). Spheroidal weathering is common in more weathered exposures. The base of the Basalt of Sentinel Gap is commonly separated from the underlying Basalt of Sand Hollow **(Twfh)** by a sedimentary interbed. The interbed was rarely observed in outcrop (**Figure 5-30**) but was commonly reported in well logs as sand, clay, or gravel typically 3–5 m (10–16 ft) thick and locally up to 11 m. Well logs also commonly report agate or opal from this interval, the result of extensive hydrothermal alteration discussed in detail in the following section describing the Basalt of Sand Hollow **(Twfh)**. The contact between the two flows is commonly marked by a prominent line of springs supporting lush vegetation on otherwise arid slopes (**Figure 5-2**).

Typical hand samples of the basalt are medium dark gray (N4) to dark gray (N2) and aphyric to very sparsely porphyritic (one phenocryst per square meter) and microporphyritic (**Figure 5-32**). The basalt contains <<1 percent euhedral to subhedral, prismatic- to lath-shaped and blocky, clear to yellow-amber colored plagioclase phenocrysts up to 7 mm (0.3 in) in length and common blocky to lath-shaped plagioclase microphenocrysts enclosed within a fine-grained crystalline to glassy groundmass. Consistent with regional averages, samples obtained from this unit have a high-TiO_2 basaltic to basaltic andesite chemical composition with 51. 58 to 52.33 weight percent SiO_2, 3.07 to 3.14 weight percent TiO_2, 3.95 to 4.28 weight percent MgO, 0.56 to 0.62 weight percent P_2O_5, and 12 to 16 ppm Cr (**Figure 5-18** and **Figure 5-19**; **Table 5-2**; appendix). These lavas are distinguished from the underlying Basalt of Sand Hollow **(Twfh)** on the basis of relatively higher amounts of TiO_2 and P_2O_5 and lesser amounts of Cr (**Figure 5-19**; **Table 5-2**; appendix). Sentinel Gap flows are distinguished from the overlying Roza Member **(Twr)** on the basis of phenocryst abundance, lower TiO_2 and P_2O_5, and higher Cr. Sentinel Gap flows are distinguished from the overlying Priest Rapids Member **(Twpr)** on the basis of magnetic polarity, lower TiO_2 and P_2O_5, and higher Cr.

The Basalt of Sentinel Gap has normal magnetic polarity and an early Miocene age bracketed by U/Pb dates of 15.895 ± 0.019 Ma for ash between the Basalt of Rosalia **(Twpr)** and Basalt of Lolo, and 16.066 ± 0.04 Ma for ash between the Basalt of Ginkgo **(Twfg)** and the Sentinel Bluffs Member **(Tgsb)** (Kasbohm and Schoene, 2018). (**Figure 5-14**; appendix). Equivalent to the Sentinel Gap flows of Mackin (1961) and Beeson and others (1985), and flows of Union Gap of Powell (1982).

Figure 5-30. Basal contact of Basalt of Sentinel Gap. Colonnade of Basalt of Sentinel Gap rests directly on ~1 m of hydrothermally altered sediment and flowtop of Basalt of Sand Hollow (Twfh). Hilderbrand China Hollow jasper mine, 672985 E, 5057966 N, view to east. Orthomosaic projection of 3D model, full-resolution image in digital appendix.

Figure 5-31. Roadcut exposure of columnar-jointed Basalt of Sentinel Gap, Mud Hollow Road, 671473 E, 5055795 N, view to southwest.

Figure 5-32. Hand sample of Basalt of Sentinel Gap. Sample BJ18-143, 679442E, 5061581N.

Twfh **Basalt of Sand Hollow (lower Miocene)**—A single flow of aphyric to sparsely plagioclase-phyric basalt lying stratigraphically beneath the Basalt of Sentinel Gap **(Twfs)** and above the Basalt of Gingko **(Twfg)** throughout the map area (**Figure 5-14**, **Figure 5-21**, Plate 1). Good exposures are common along the cliffs of the Columbia River Gorge and in the lower reaches of the tributary canyons, and in flood-scoured areas of the uplands (**Figure 5-17**). Elsewhere in the uplands, exposures are typically restricted to small roadcuts, low outcrops on uncultivated slopes, and the bottoms of stream drainages. The thickness of the Basalt of Sand Hollow is consistent throughout the map area, ranging from ~103 m (340 ft) at the mouth of the John Day River to ~94 m (304 ft) at Frank Fulton Canyon, just west of the northwest edge of the map area (Plate 1; **Figure 5-17** **Figure 5-21**).

Outcrops of the Basalt of Sand Hollow display a wide variety of jointing patterns beyond the basic colonnade-entablature pattern characteristic of flows of the CRBG. In the cliffs between Rufus and the John Day Dam, there is a colonnade with well-developed columns 1.5–2 m in diameter that have cross joints inclined to the column axis, giving the columns a spiral appearance. These columns are also unusually long, with some continuous for ~44 m (**Figure 5-33**). An abrupt change in column size is exposed in a roadcut on U.S. Route 97 southeast of Biggs Junction, with a zone of intense platy jointing ~ 5–25 cm thick separating the different jointing

styles (**Figure 5-34**). Complex and chaotic jointing is exposed in another long roadcut along U.S. Route 97 southeast of Biggs Junction (**Figure 5-35**). At this site, areas of regular columns abruptly change to variously oriented platy and prismatic joints and small lava tubes occur. Entablature jointing in the upper 35 m (115 ft) of the flow is well-exposed in the quarry above Biggs Junction (**Figure 5-36**). Prismatic jointing is commonly observed in exposures away from the cliffs along the Columbia River Gorge (**Figure 5-37**).

The contact between the Basalt of Sand Hollow and the underlying Basalt of Ginkgo (**Twfg**) was observed in several locations. It is typically sharp, with massive lava resting directly on the underlying vesicular flow top, and locally marked by a distinctive colonnade (**Figure 5-38, Figure 37, Figure 5-40**) with regular columns 1 m in diameter composed of unusually dark grey, aphyric, and dense basalt that is phonolitic and breaks with conchoidal fracture (**Figure 5-38**). The colonnade transitions abruptly upward into closely spaced horizontal jointing or platy-prismatic jointing.

The Basalt of Sand Hollow commonly shows effects of hydrothermal alteration and deposition, particularly at or near the top of the flow. In several exposures, extensive alteration of basalt to a mixture of iron oxide and clay was evident along joints, in many instances associated with deposits of opal or agate deposited in voids or along joints (**Figure 5-41, Figure 5-42, Figure 5-43**). Siliceous sinter and silicified sediments were observed at several locations, most notably at the Hilderbrand China Hollow jasper mine (**Figure 5-30, Figure 5-44**), and opal, agate, or "wascoite" (local name for silicified laminated fine-grained sediment) are commonly reported along with sand, clay, and gravel in driller logs of wells that penetrate the upper contact of the Basalt of Sand Hollow.

Typical hand samples of the Basalt of Sand Hollow are pale blue (5B 6/2) to medium dark gray (N4) and aphyric to very sparsely porphyritic (~1 phenocryst/m^2) and microporphyritic. The basalt contains <1 percent euhedral to subhedral, prismatic- to lath-shaped and blocky, clear to yellow-amber-colored plagioclase phenocrysts up to 20 mm in length and abundant lath-shaped plagioclase microphenocrysts up to 2 mm long enclosed within a fine-grained crystalline to glassy groundmass (**Figure 5-45**).

Samples obtained from the Basalt of Sand Hollow have a basaltic to basaltic andesite chemical composition with 51.31 to 52.21 weight percent SiO_2, 2.88 to 3.02 weight percent TiO_2, 4.21 to 4.60 weight percent MgO, 0.54 to 0.56 weight percent P_2O_5, and 36 to 41 ppm Cr (Table 5-2; appendix). These lavas are distinguished from other Frenchman Springs units on the basis of sparsely distributed plagioclase phenocrysts and relatively lower amounts of TiO_2, P_2O_5 and higher amounts of Cr (**Figure 5-19**; **Table 5-2**; appendix).

A small outcrop of lithologically and chemically anomalous basalt occurs within the Basalt of Sand Hollow flow at the intersection of Scott Canyon and Gerking Canyon roads (**Figure 5-46, Figure 5-47**). The outcrop has well-formed columns and is unusually coarse grained, with abundant lath-shaped plagioclase microphenocrysts and phenocrysts ranging up to 1 cm in length, abundant irregular clinopyroxene phenocrysts 2–6 mm in diameter, and abundant needles of opaque oxides up to 10 mm long. The distinctive lithology does not resemble any other flows in the map area and is known from only the one outcrop. Chemically, the lava is a basaltic andesite with 52.66 weight percent SiO_2, 3.71 weight percent TiO_2, 3.36 weight percent MgO, 0.69 weight percent P_2O_5, 1.74 weight percent K_2O, and 0 ppm Cr. Chemically, the basalt most closely resembles the Basalt of Rosalia (**Twpr**), but it occurs 105 m (345 ft) stratigraphically below the base of that unit. This basalt resembles "pegmatoid" variants that have been observed in the

Basalt of Sand Hollow and Priest Rapids Member elsewhere (Steve Reidel, personal communication, 2019; Barnett and others, 2007), which are attributed to accumulations of volatiles within cooling flows.

Outcrops of the Basalt of Sand Hollow measured in this study have normal magnetic polarity and the unit is assigned an early Miocene age bracketed by U/Pb dates of 15.895 ± 0.019 Ma for ash between the Basalt of Rosalia and Basalt of Lolo and 16.066 ± 0.04 Ma for ash between the Basalt of Ginkgo and the Sentinel Bluffs Member (Kasbohm and Schoene, 2018) (**Figure 5-14**). Equivalent to the Sand Hollow flows of Mackin (1961) and Beeson and others (1985) and the Kelly Hollow flow of Powell (1982).

Figure 5-33. Colonnade of the Basalt of Sand Hollow in cliffs between Rufus and the John Day River. Individual columns are as long as 44 m. Orthomosaic projection from 3D model, white areas are gaps in model.

Figure 5-34. Abrupt transition of column size within the Basalt of Sand Hollow flow exposed in roadcut on Highway 37 southeast of Biggs Junction (671274 E, 5057277 N view to northeast). Orthomosaic projection from 3D model, full-resolution image in digital appendix.

Figure 5-35. Complex and variable columnar, platy, and prismatic jointing in hydrothermally altered Basalt of Sand Hollow in a roadcut on U.S. Route 97 southeast of Biggs Junction (669842 N, 5058623 N view to east). Right-hand edge of each image overlaps left-hand edge of image below it. Orthomosaic projection from 3D model, white areas are gaps in model in areas not visible from the road. Full-resolution image in digital appendix.

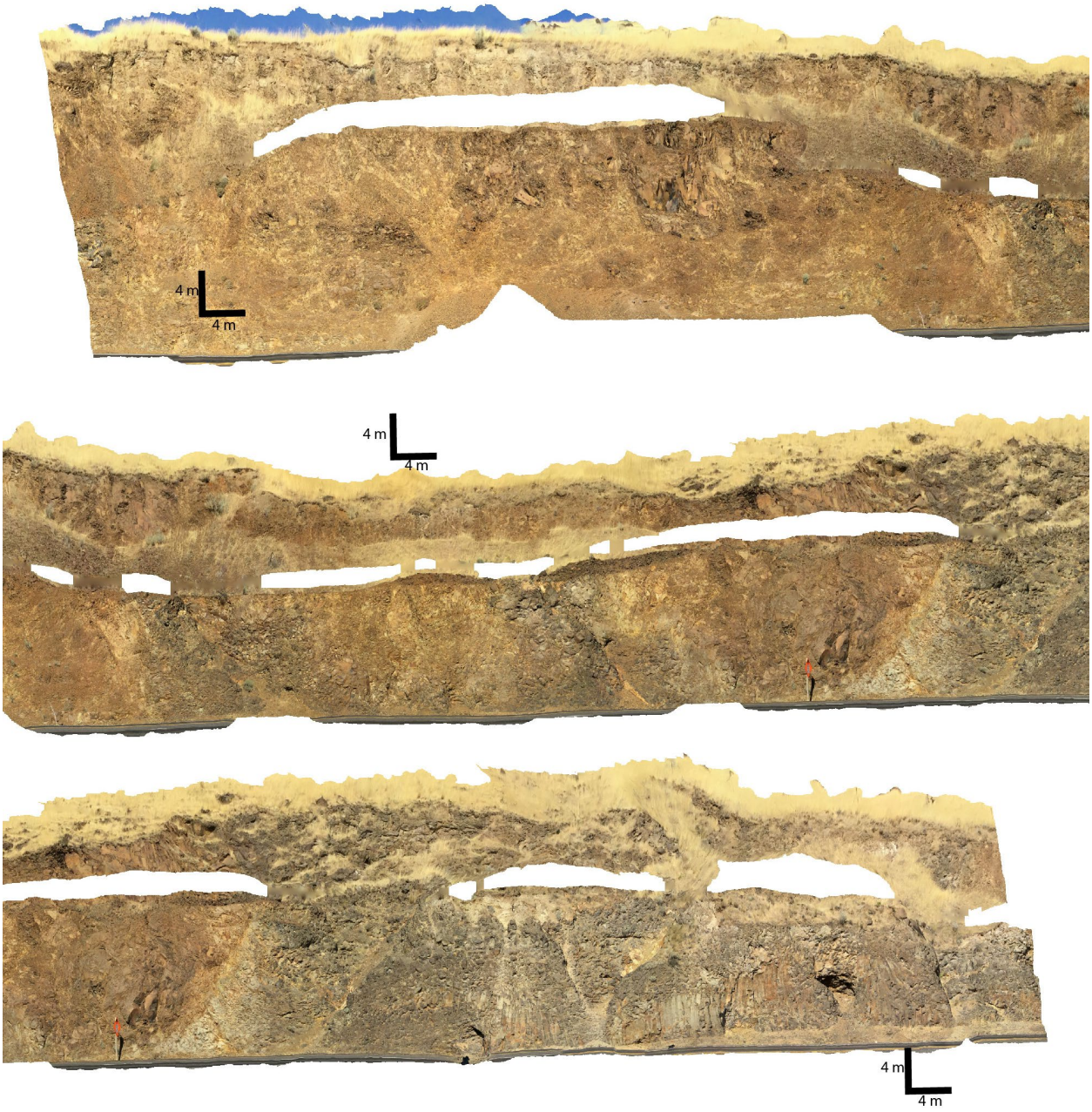

Figure 5-36. Entablature jointing of the Basalt of Sand Hollow exposed in highwall of quarry above Biggs Junction (668755 E, 5059318 N, view to west). Orthomosaic projection from 3D model, full-resolution image in digital appendix.

Figure 5-37. Prismatic jointing in the Basalt of Sand Hollow exposed in a quarry face just west of the northwest corner of the map area (665365 E, 5056919 E, view to south).

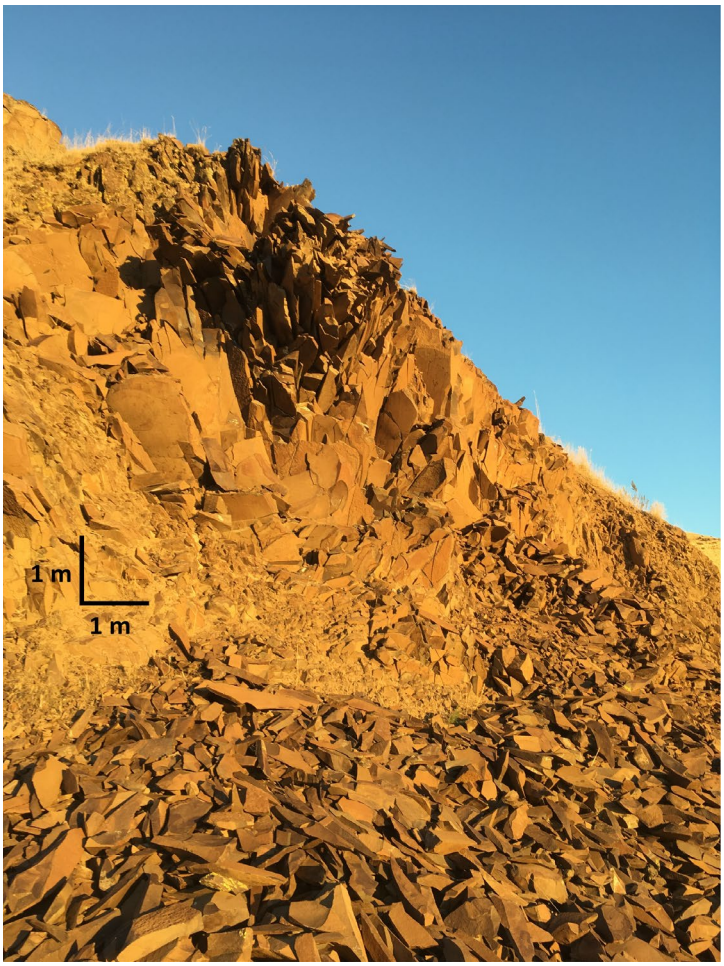

Figure 5-38. (A) Basal colonnade of Basalt of Sand Hollow overlying vesicular flow top of basalt of Ginkgo in a quarry face in Biggs Junction (668076 E, 5059058 N view to southeast). (B) Example of conchoidal fracture of basal colonnade columns, width of image ~0.5 m.

Figure 5-39. Quarry highwall at the mouth of Fulton Canyon, just west of the northwestern edge of the map area (665183 E, 5056856 N, view to west) showing the contact between the lower and upper flows of the Basalt of Ginkgo (Twfg) and the overlying Basalt of Sand Hollow (Twfh). The upper flow of the Basalt of Ginkgo is about 7 m (23 ft) thick; 13 m (42 ft) of the lower flow are exposed, the lower half of which has colonnade jointing while the upper half has entablature jointing. See Figure 5-21 for details of stratigraphy at this site.

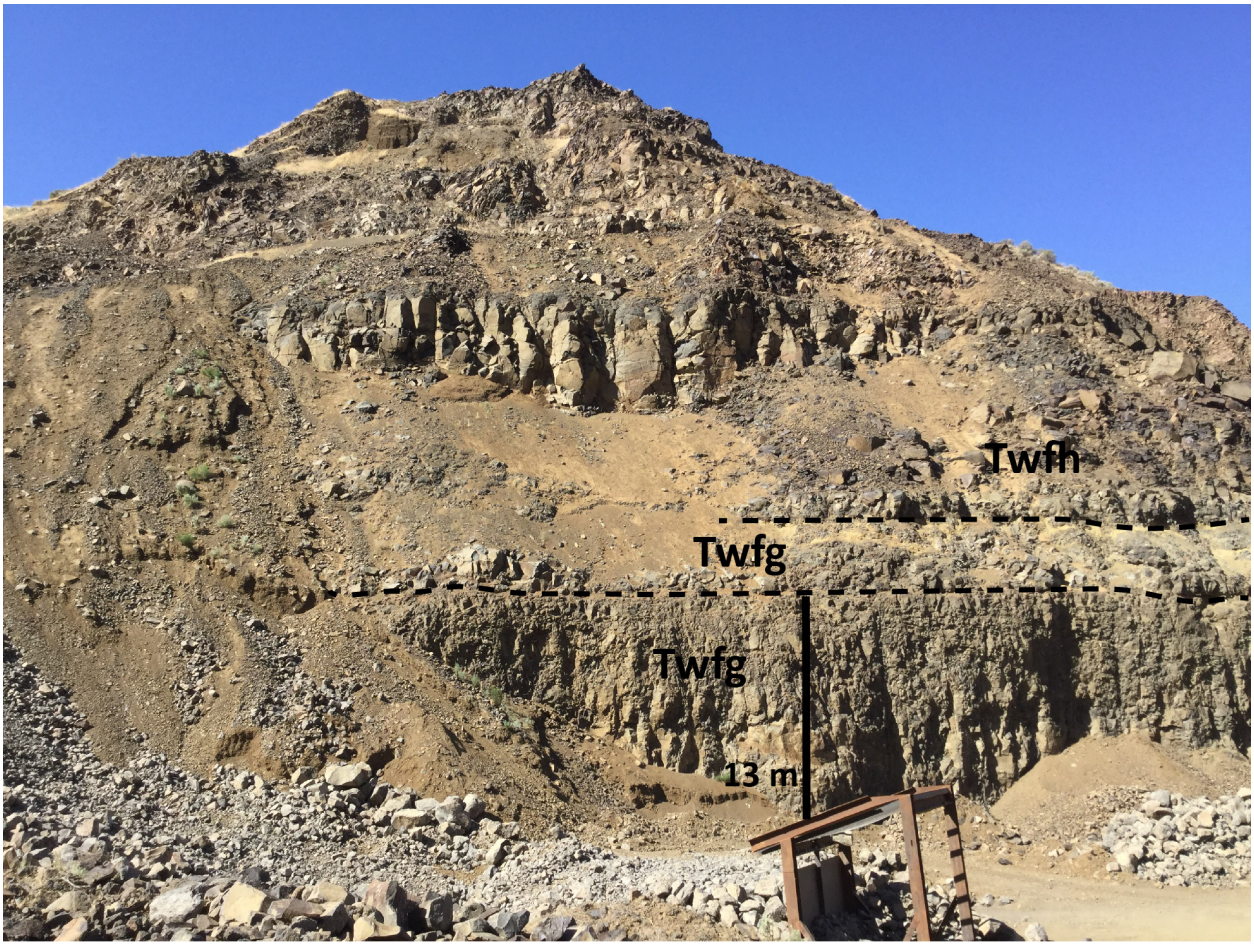

Figure 5-40. Basal contact of Basalt of Sand Hollow (Twfh) with the Basalt of Ginkgo (Twfg) along U.S. Route 97 southeast of Biggs Junction. Traffic cones in image are approximately 1 m high. Location 669662 E, 5059087N, view to northeast.

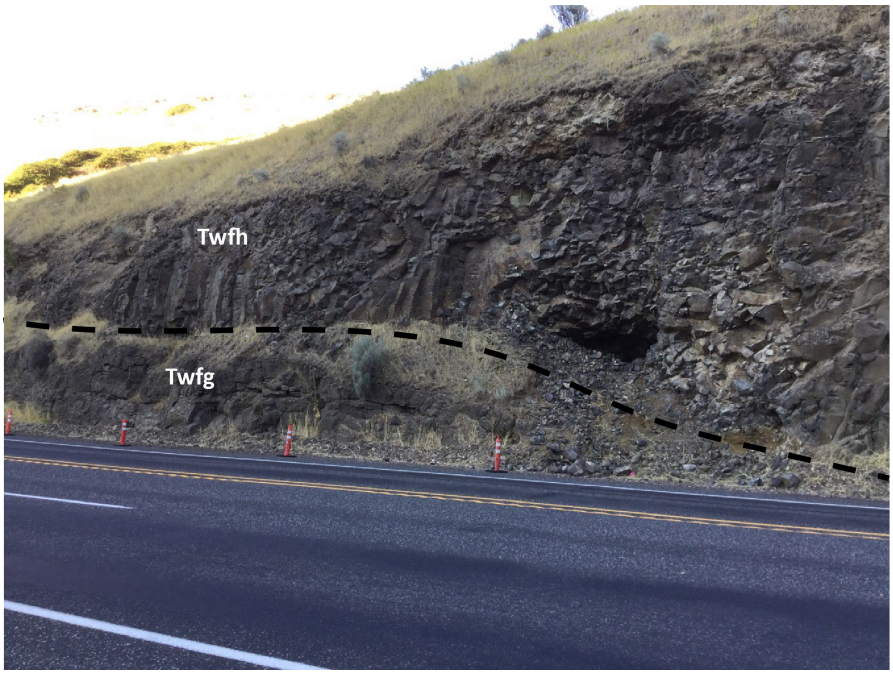

Figure 5-41. Hydrothermal alteration of the Basalt of Sand Hollow along U.S. Route 97 southeast of Biggs Junction. Red and yellow mixture of iron oxide and clays deposited along joints. Location 678472 E, 5061598 N, view to west.

Figure 5-42. Hydrothermal deposits in large void in the Basalt of Sand Hollow along U.S. Route 97 southeast of Biggs Junction. Multi colored mixture of iron oxide and clays deposited with resistant bodies of red, black, white, grey and yellow siliceous sinter. (A) overview, (B) close-up of void, (C) detail of deposits; note location of (C) shown on (B) shown by white rectangle. Location 678472 E, 5061598 N, view to west.

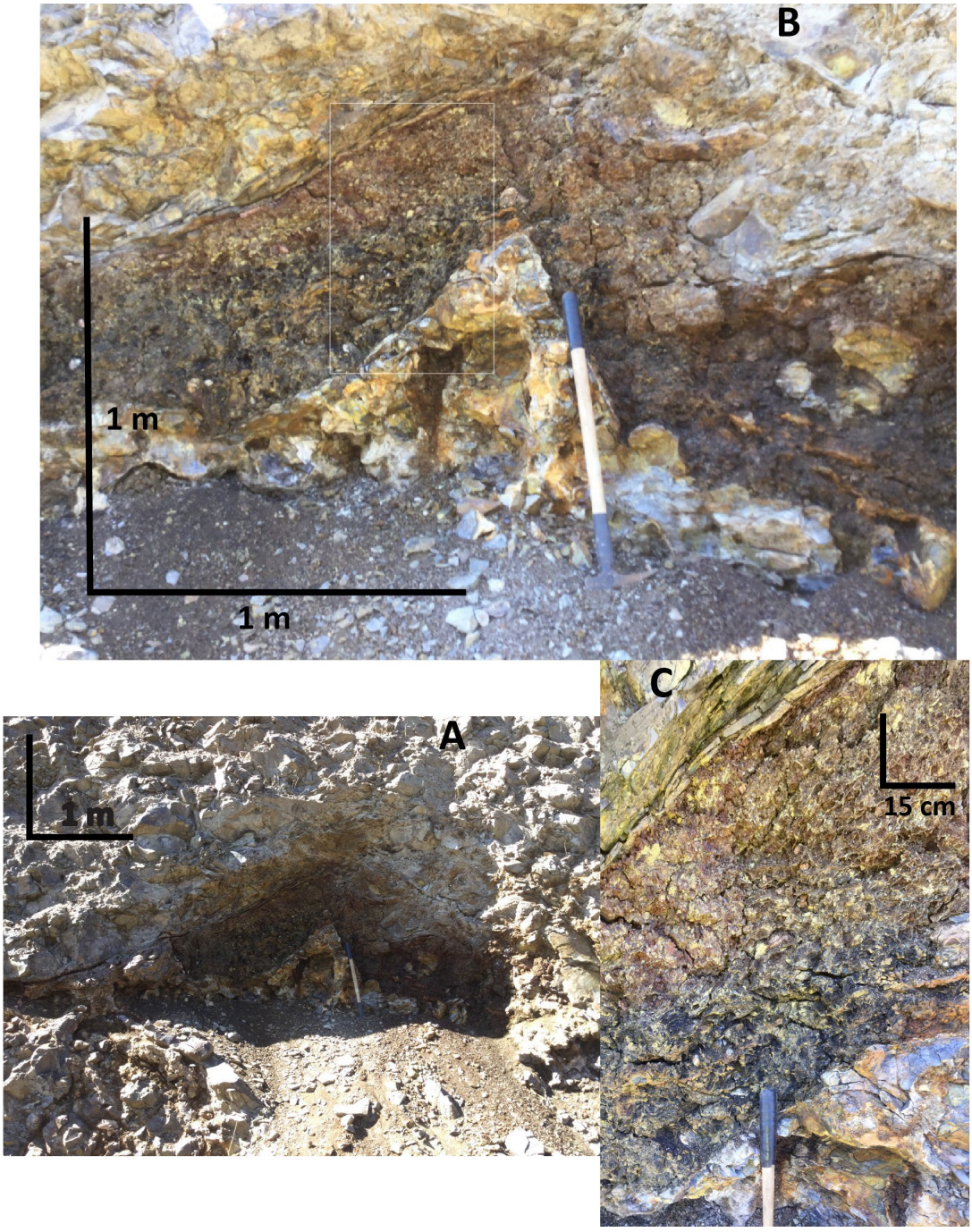

Figure 5-43. Large body of grey siliceous sinter filling void in the Basalt of Sand Hollow along U.S. Route 97 southeast of Biggs Junction. Location 669842 N, 5058623 N, view to east.

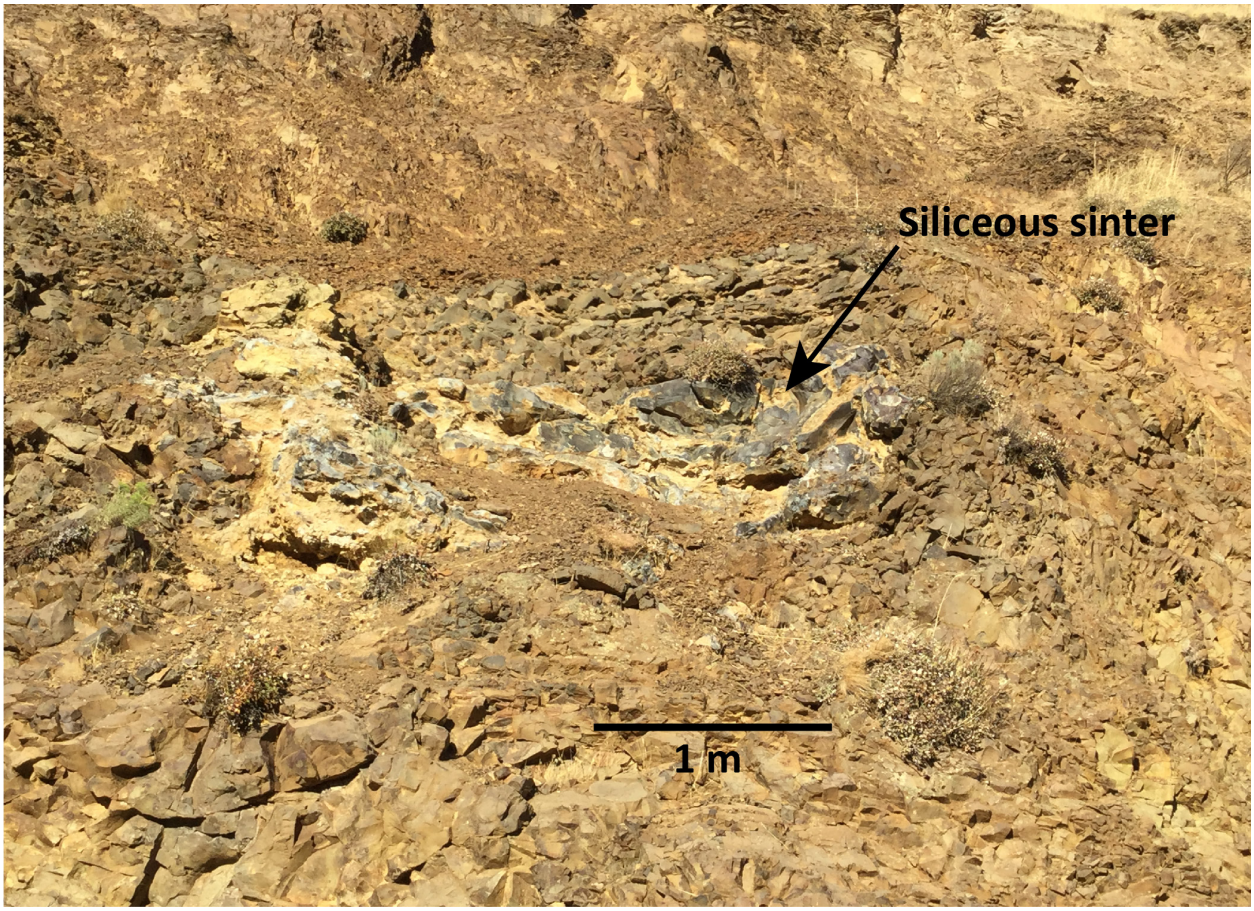

Figure 5-44. Silicified sediments and breccia from upper contact of the Basalt of Sand Hollow. Located at the Hilderbrand China Hollow jasper mine, 672985 E, 5057966 N. (A) Silicified laminated siltstone or claystone, locally called "wascoite." (B) Silicified massive silt or claystone. (C) Silicified breccia. Sample bags 25 cm wide.

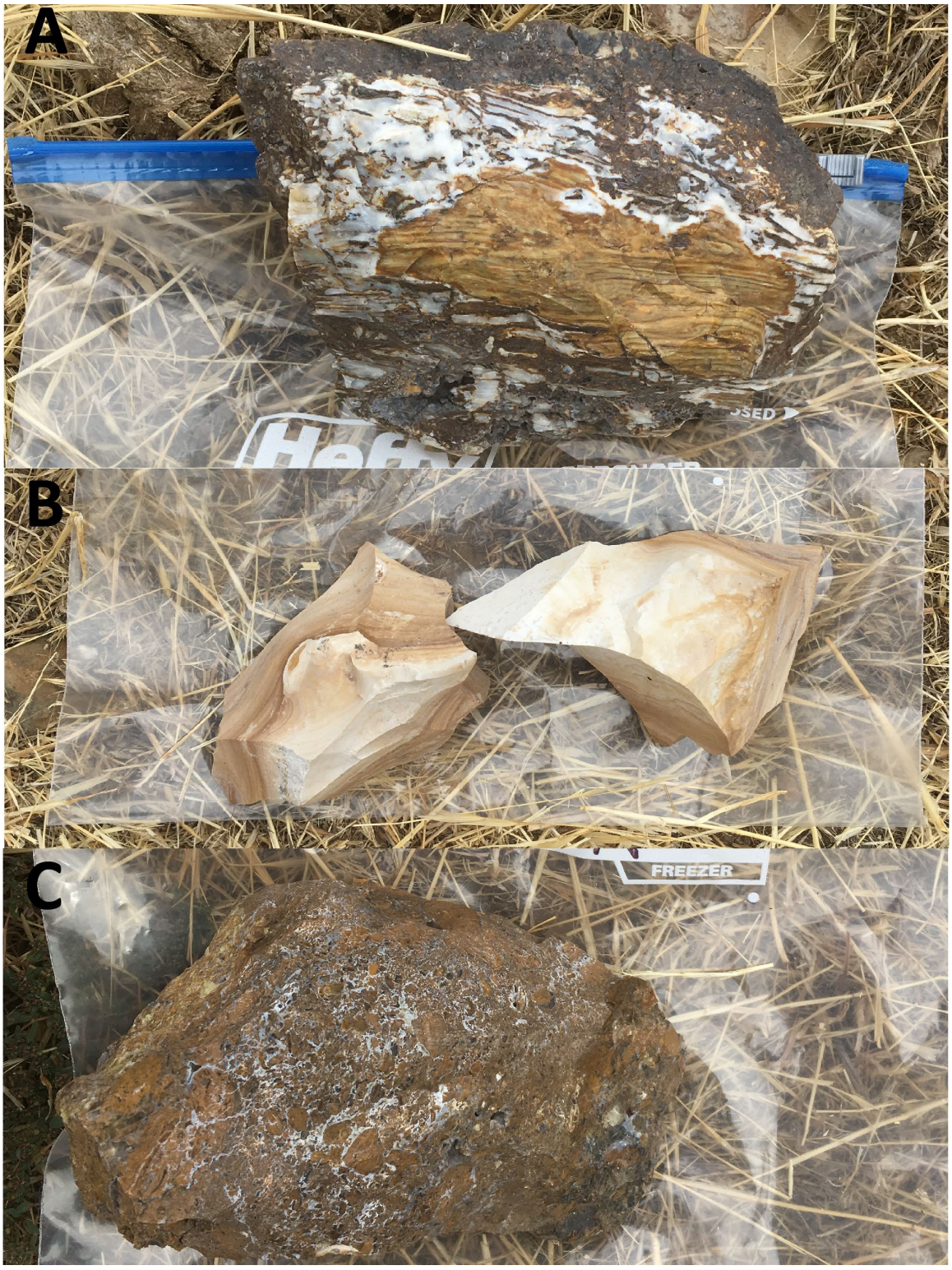

Figure 5-45. Hand samples of the Basalt of Sand Hollow. Smaller specimen is from the dense basal colonnade and is finer grained and has fewer plagioclase microphenocrysts than the majority of the flow, represented by the larger sample.

Figure 5-46. Roadcut exposure of "pegmatoid" Basalt of Sand Hollow at intersection of Scott Canyon and Gerking Canyon Roads. Location 677749 E, 5061963 N, view to west. Orthomosaic projection of 3D model.

Figure 5-47 Hand specimen of "pegmatoid" Basalt of Sand Hollow Yellow and white flecks are lath-shaped plagioclase phenocrysts and microphenocrysts. Sample number BJ18-21, map code G11, location 677749 E, 5061963 N.

Twfg **Basalt of Ginkgo (lower Miocene)**—Two flows of abundantly plagioclase-phyric basalt exposed beneath the Basalt of Sand Hollow (**Twfh**) and above the Sentinel Bluffs Member (**Tgsb**) throughout the entire map area (**Figure 5-14** and **Figure 5-21, Figure 5-17**; Plate 1). The Basalt of Ginkgo is moderately well exposed at the base of the cliffs of the Columbia River Gorge, but generally does not have a flood-scoured bench marking the top of the unit, as is the case with overlying flows (**Figure 5-17**), and it is typically partially buried by colluvium derived from the overlying Basalt of Sand Hollow (**Twfh**). Two flows are recognized throughout most of the area, and the thickness of the unit varies significantly. The total thickness ranges from ~ 40 m (130 ft) at Frank Fulton Canyon (**Figure 5-21**) to about 10 m (33 ft) at Biggs Junction, and 27 m (90 ft) at the John Day River. The unit is completely absent along the Biggs-Rufus Highway just east of Biggs Junction, where the Basalt of Sand Hollow (**Twfh**) rests directly on the Sentinel Bluffs Member (**Tgsb**). The lower flow is consistently the thickest, and the upper flow, where exposed, is typically about 7 m (24 ft) thick.

The lower flow typically has a colonnade with irregular columns ~0.5 m in diameter, overlain by entablature jointing (**Figure 5-39**) and a flow top characterized by horizontal layers of highly vesicular lava. The upper flow forms columns 1.5–2 m in diameter, and its upper half is pillowed at the Fulton Canyon exposure (**Figure 5-39**). The abundance of plagioclase phenocrysts is variable, and the Basalt of Ginkgo is aphyric at one location in Biggs Junction but has thousands of phenocrysts per square meter near Rufus (**Figure 5-49**). Anderson (1987) also noted that the Basalt of Ginkgo may be aphyric to depths of 5 to 10 m (16.4 to 32.8 ft) from upper surfaces. Regionally, the Frenchman Springs Member is separated from the underlying Grande Ronde Basalt by a sedimentary interval referred to as the Vantage Member of the Ellensburg Formation (Swanson and others, 1979b) (**Figure 5-14**). Sediments of the Vantage Member were not observed in outcrop, but logs of wells near Biggs Junction (OWRD GRID numbers SHER 285, SHER 223) report clay, gravel, boulders, and sandstone a few meters thick between the Basalt of Ginkgo and the Sentinel Bluffs Member (**Tgsb**). The colonnade of the Basalt of Ginkgo rests directly on the weathered scoriaceous rubbly top of the underlying Sentinel Bluffs Member (**Tgsb**) along the Biggs-Rufus Highway southwest of Biggs Junction (**Figure 5-48**). Just east of Biggs Junction along the Biggs-Rufus Highway, a local high in the upper surface of the Sentinel Bluffs Member (**Tgsb**) causes the Basalt of Ginkgo to thin and pinch out, with the Basalt of Sand Hollow (**Twfh**) resting directly on the Sentinel Bluffs Member (**Tgsb**) over a small area (**Figure 5-17**, Plate 1).

Typical hand samples are medium dark gray (N4) to dark gray (N2) abundantly to sparsely porphyritic and microporphyritic basalt (**Figure 5-49** and **Figure 5-50**). The basalt contains ~ 3–5 percent euhedral to subhedral, prismatic to lath-shaped, yellow brown (5YR 5/6) to very pale orange (10YR 8/2) plagioclase phenocrysts and glomerocrysts up to 3 cm (1.2 in) in length and conspicuous blocky to lath-shaped plagioclase microphenocrysts contained within a microvesicular, diktytaxitic fine-grained crystalline to glassy groundmass.

Samples obtained from the Basalt of Ginkgo have a basaltic to basaltic andesite chemical composition with 51.37 to 52.37 weight percent SiO_2, 3.12 to 3.27 weight percent TiO_2, 3.7 to 4.24 weight percent MgO, 0.57 to 0.68 weight percent P_2O_5, and 10 to 13 ppm Cr (**Table 5-1** and **Figure 5-19**; appendix). These lavas are distinguished from other Frenchman Springs units on the basis of abundant plagioclase phenocrysts and relatively high amounts of TiO_2 and P_2O_5 and lower amounts of Cr (**Figure 5-19**; **Table 5-1**; appendix).

Outcrops of the Basalt of Ginkgo measured in this study have normal magnetic polarity and the unit is assigned an early Miocene age bracketed by U/Pb dates of 15.895 ± 0.019 Ma for ash between the Basalt of Rosalia and Basalt of Lolo, and 16.066 ± 0.04 Ma for ash between the Basalt of Ginkgo and the Sentinel Bluffs Member (Kasbohm and Schoene, 2018) (**Figure 5-14**). Equivalent to the Ginkgo flows of Mackin (1961) and Beeson and others (1985).

Figure 5-48. Contact between the Basalt of Ginkgo and Sentinel Bluffs Member exposed along the Biggs-Rufus Highway (667287 E, 5058874 N, view to southeast). Basal columns of the Basalt of Ginkgo rest directly on the baked rubbly top of the underlying flow.

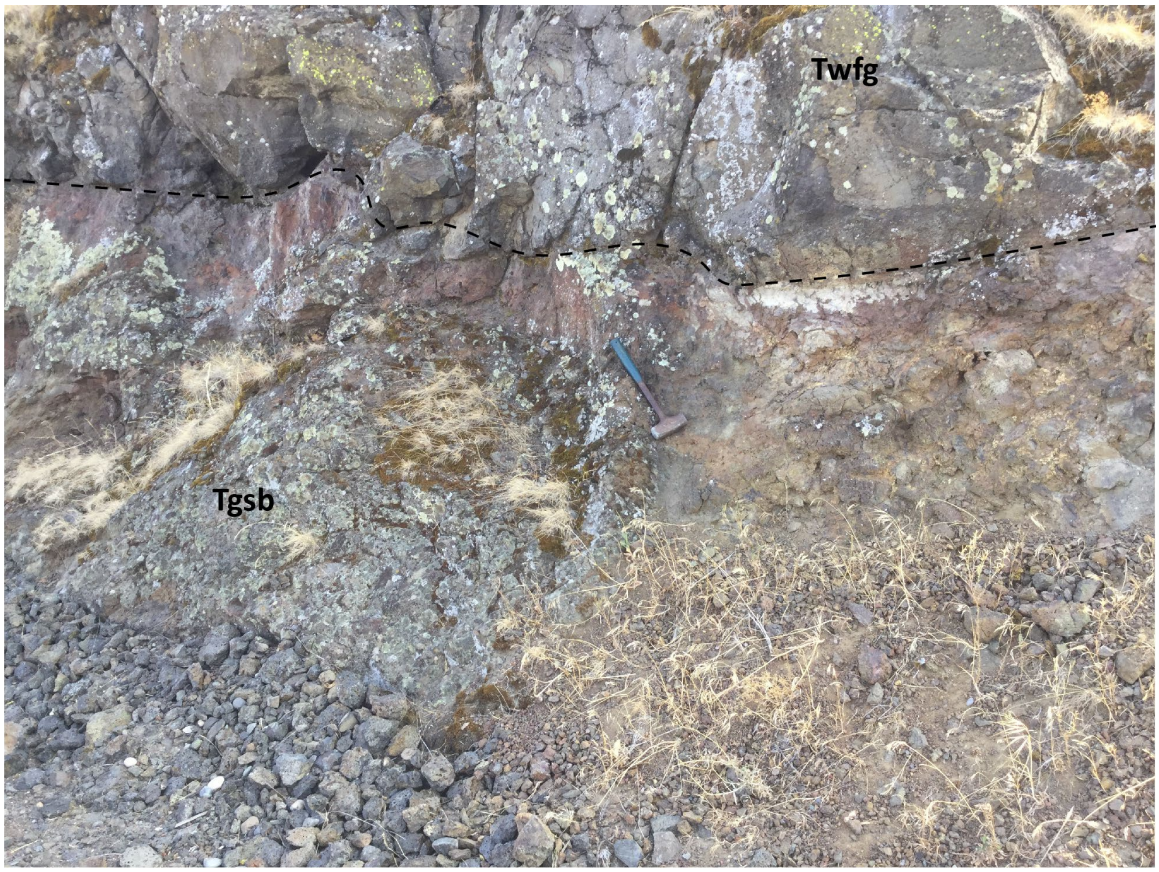

Figure 5-49. Close-up of a weathered surface of the upper flow of the Basalt of Ginkgo, showing unusually abundant plagioclase phenocrysts 2–10 mm in diameter. Location 677412 E, 5063173 N.

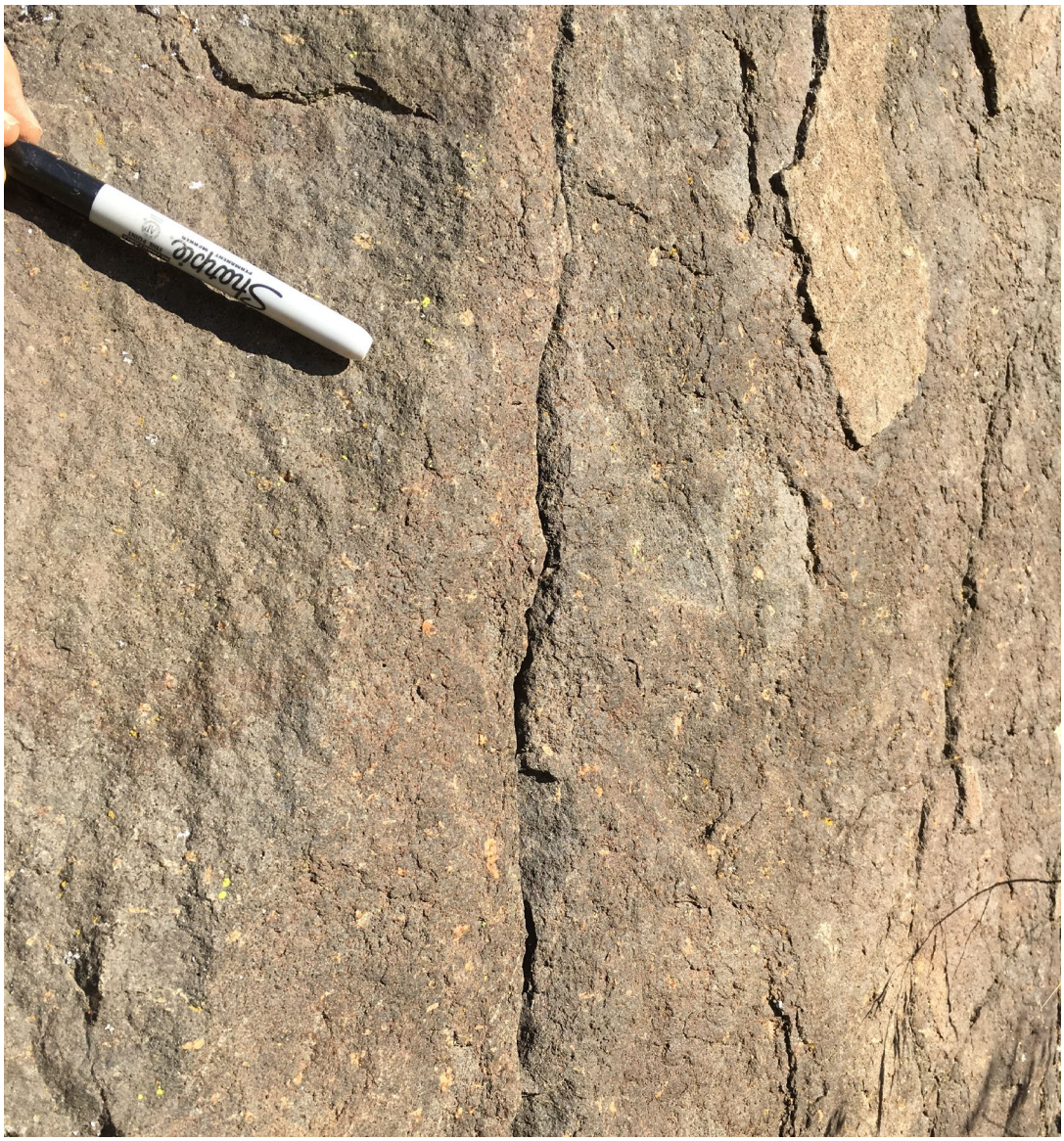

Figure 5-50. Hand samples of the Basalt of Ginkgo. Clear to yellow blocky plagioclase phenocrysts 2–10 mm in diameter occur with varying abundance.

Disconformity—Vantage Member of the Ellensburg Formation

5.2.2.3 Grande Ronde Basalt

The upper part of the Grande Ronde Basalt is the lowermost exposed geologic unit in the Biggs Junction-Rufus area (**Figure 5-14** and **Figure 5-16**; Plate 1). These lavas, erupted between 16.572 ± 018 Ma and 16.066 ± 0.04 Ma (Kasbohm and Schoene, 2018), are the thickest, most voluminous formation of the CRBG (66 percent of total volume erupted; Camp and others, 2003; Camp and Ross, 2004). Effusion of the Grand Ronde Basalt, from vents and fissures in the eastern and southeastern parts of the Columbia Plateau, produced over 150,400 km^3 (36,100 mi^3) of lava that covered an area exceeding 169,600 km^2 (65,500 mi^2) (Tolan and others, 1989; Reidel and others, 1989; Barry and others, 2010; Reidel and Tolan, 2013). The formation spans at least four paleomagnetic zones and has been stratigraphically subdivided into the R1, N1, R2, and N2 magnetostratigraphic units by Swanson and others (1979b) (**Figure 5-14**). The Grande Ronde Basalt exposed in the map area consists of lavas assigned to the Sentinel Bluffs Member (**Tgsb**) of the N2 magnetostratigraphic unit. These lavas are generally monotonously fine-grained, aphyric, and petrographically nondistinctive. Chemical compositions also have a relatively narrow range, but precise

analyses of major and trace elements can be used to correlate individual flows on a regional basis, when used in conjunction with careful geologic mapping (Wells and others, 2009; Hagstrum and others, 2010; Swanson and others, 1981; Reidel and others, 1989, Tolan and others, 1989; Hooper, 2000). Grande Ronde lavas are distinguished from the overlying Wanapum Basalt by the local presence of the intervening Vantage Member of the Ellensburg Formation (Swanson and others, 1979b) (**Figure 5-14** and **Figure 5-16**), the conspicuous absence of large plagioclase phenocrysts and glomerocrysts, and significantly lesser TiO_2 contents (**Figure 5-19a,b**; Hooper, 2000; Tolan and others, 2009b). Composite thickness of the Grande Ronde Basalt in the Biggs Junction-Rufus area exceeds 278 m (910 ft) (**Figure 5-16**; Plate 1).

The Grande Ronde Basalt is subdivided in the map area into the following units:

5.2.2.3.1 Normal-polarity (N2) magnetostratigraphic unit

The N2 magnetostratigraphic unit is the youngest Grande Ronde Basalt magnetostratigraphic unit, made up of chemically distinctive flow packages that cover an area of ~114,500 km^2 (44,208 mi^2) (**Figure 5-14**). The estimated volume of the N2 magnetostratigraphic unit is ~35,300 km^3 (8,469 mi^3) (Reidel and Tolan, 2013).

The N2 magnetostratigraphic unit is locally represented by the following unit:

Tgsb **Sentinel Bluffs Member (lower Miocene)**—Multiple flows of aphyric basaltic andesite lavas present beneath the Basalt of Ginkgo (**Twfg**) throughout the map area (**Figure 5-16, Figure 5-21, Figure 5-17**; Plate 1). The Sentinel Bluffs Member (**Tgsb**) is exposed along the Bigg-Rufus Highway southwest of Biggs Junction, at the base of the cliffs of the just east of Biggs Junction, and as a flood-scoured bench partly buried by colluvium at the base of the cliffs between Rufus and the John Day River.

Individual flows in the unit are composed of thin lava flow lobes, generally <5 to 20 m thick (16.4 to 65.6 ft) that have well-developed vesicular flow tops and basal flow breccia. Flow interiors are typically characterized by massive, meter-scale colonnade jointing with lesser hackly and thick scoriaceous rubble zones at the flow tops (**Figure 5-51**). The Sentinel Bluffs Member is 170 m (556 ft) thick at the John Day Dam (**Figure 5-16**) in the northeast corner of the map area, and 110 m (360 ft) thick at Gordon Ridge 11 km (7 mi) south of the map area (**Figure 5-21, Figure 5-20**).

Typical hand samples are medium light gray (N6) to medium gray (N5) aphyric to very sparsely microporphyritic basaltic andesite containing 1- 2 percent euhedral, prismatic to blocky, clear plagioclase microphenocrysts contained within a glassy to very fine-grained diktytaxitic crystalline groundmass (**Figure 5-52**). The groundmass is often a red to tan mottled color due to alteration along the margins of microvesicles.

No samples of the Sentinel Bluffs Member from within the map area were analyzed, but the uppermost flow in the Gordon Ridge section is the McCoy Canyon flow, based on geochemistry (**Figure 5-21, Figure 5-20**, **Table 5-1**), and it is likely that the McCoy Canyon flow is the flow exposed along the Columbia River Gorge in the map area. Sentinel Bluffs Member is among the most primitive units in the Grande Ronde Basalt and has a basaltic andesite chemical composition with 53.83 to 54.41 weight percent SiO_2, 1.79 to 1.98 weight percent TiO_2, 4.74 to 4.75 weight percent MgO, and 0.32 weight percent P_2O_5 (**Figure 5-18** and **Figure 5-19, Table 5-1**; appendix). The Sentinel Bluffs Member is distinguished from other members of the Grande Ronde Basalt on the basis of lithology and higher contents of MgO (**Figure 5-19, Table 5-1**).

Outcrops of the Sentinel Bluffs Member measured in this study have normal magnetic polarity and the unit is assigned an early Miocene age bracketed by U/Pb dates of 16.066 ± 0.04 Ma for ash from the overlying Vantage Horizon and 16.254 ± 0.034 Ma for ash between the Wapshilla Ridge and Meyer Ridge Members of the underlying R2 magnetostratigraphic unit (Kasbohm and Schoene, 2018). These flows are locally separated from the overlying Frenchman Springs Member by the Vantage Member of the Ellensburg Formation (**Figure 5-14**). The Sentinel Bluffs Member was erupted from a northerly trending vent system in eastern Washington and northern Oregon and flowed west down an ancestral paleoslope (**Figure 5-13**; Tolan and others, 2009b; Reidel and Tolan, 2013). Effusion of the Sentinel Bluffs Member produced ~10,150 km^3 (2,435 mi^3) of lava that covered an area exceeding 167,700 km^2 (64,749 mi^2) (Reidel and Tolan, 2013). Equivalent to the high-MgO flows of Wright and others (1973), the Sentinel Bluffs unit of Reidel and others (1989), and the Sentinel Bluffs Member of Reidel and Tolan (2013).

Figure 5-51. Upper portion of the uppermost flow of the Sentinel Gap Member exposed in cliffs along Interstate 84 between Rufus and the John Day River (678435 E, 5063725 N, view to southeast). Orthomosaic projection from 3D model, full-resolution image in digital appendix.

Figure 5-52. Hand samples of the Sentinel Bluffs Member.

6.0 STRUCTURE

6.1 Introduction

Geologic structure in the Biggs Junction-Rufus area is defined by the mapped traces of contacts of geologic units, topographic lineaments (as observed in 1-m lidar DEMs and orthoimagery), and bedding attitudes (Plate 1; appendix). The only primary structural features observed in the field were contacts and rare minor shear zones. A series of contact surface models were created for each major basalt contact by using intercepts in water wells and mapped surface contacts.

The Oregon portions of the Biggs Junction and Rufus 7.5' quadrangle lies in a moderately to little-deformed structural area situated at the southeastern edge of the Yakima Fold Belt anticlinal ridges/uplifts with the Columbia Hills thrust and anticline immediately north of the map area (Powell, 1982). Within the study area the dips of flow surfaces are so shallow that neither field measurements nor dips measured from lidar topographic data are accurate. For example, the contact between the Basalt of Ginkgo (**Twfh**) and the Sentinel Bluffs Member (**Tgsb**) rises steadily from the northwestern edge of the map to the northeastern edge, a total of 108 m (354 ft) over a distance of 20 km (12 mi), with an overall calculated dip of 0.3 degrees. Structure contour maps on the top and bottom of the Basalt of Sand Hollow (**Twfh**) (**Figure 6-1**) show that the thick stack of CRBG lavas in the map area is characterized by an ~1° regional north-northwest dip with dip directions varying from ~340° to ~297°. There are other minor irregularities in the surfaces defined by the structure contours, which are typically driven by a single well, and are probably not significant. The Roza and Priest Rapids Member flows may have been emplaced in a broad paleo Columbia River channel localized in part by the very minor northward tilting of earlier flows, but the resulting difference in dips is below the level of detection.

This simple structure is in sharp contrast to the Columbia Hills anticline, which occupies the northern shore of the Columbia River north of the map area. There, the same package of CRBG flows is folded into a sharp anticline as they are thrust south along the Columbia Hills thrust fault (Powell, 1982).

Figure 6-1. Structure contours for the Basalt of Sand Hollow. Contours are in feet and are based on water well intercepts and high-confidence points along mapped contacts. (A) Lower contact with Basalt of Ginkgo (Twfg). (B) Upper contact with Basalt of Sentinel Gap (Twfs).

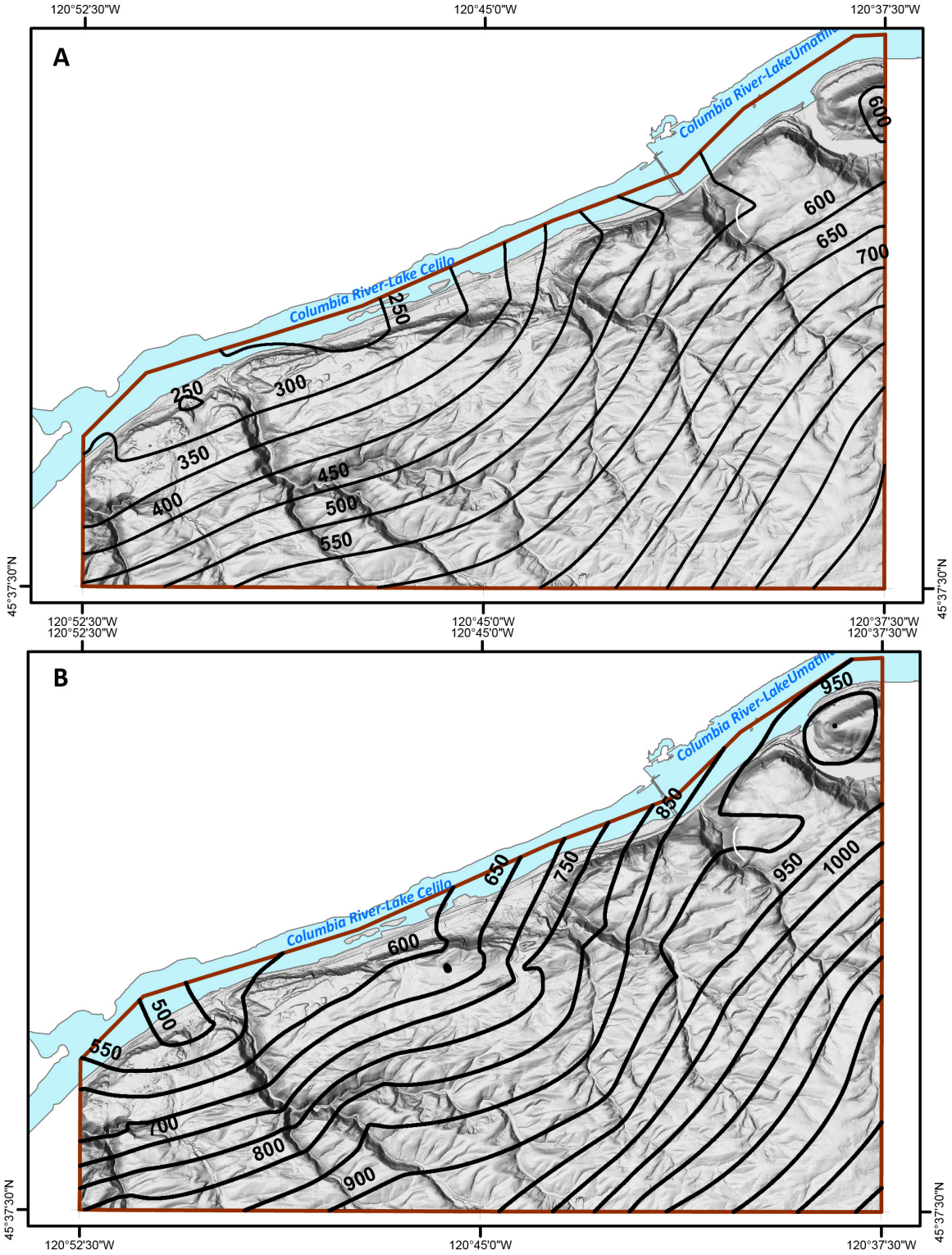

6.2 Northwest- to southeast-trending lineaments

No faults were mapped within the study area. The contacts between the CRBG flows are generally very slightly dipping, planar, and show no evidence of significant vertical offset on faults. There are a few aeromagnetic lineaments (**Figure 4-2, Plate 1**) that resemble other local lineaments known to be faults, but there was no evidence of offset of flows, although the lineaments occur in areas with relatively poor control on the location of contacts. The most prominent of these lineaments is coincident with Helm Canyon, which opens almost directly at the Oregon footing of the John Day Dam. At Helm Canyon, continuous cliff and vertical cut exposures of the Sentinel Bluffs Member (**Tgsb)** along the freeway are interrupted by cut slopes made in colluvium. However, there is no apparent difference in elevation of the prominent bench formed along the top of Sentinel Bluffs Member (**Tgsb)** to the east and west, and there is continuous unfaulted exposure of the top of Sentinel Bluffs Member (**Tgsb)** along the northern shore of the Columbia where the lineament projects.

Vertical discontinuities in basalt flows were observed rarely in some roadcut outcrops but generally the flows did not have evidence of offset. These features may have been cooling joints enhanced by hydrothermal alteration or weathering.

7.0 GEOLOGIC HISTORY

Late Cenozoic volcanic and sedimentary rocks and surficial deposits exposed in the Biggs Junction-Rufus area provide a partial record of the volcanic, depositional, and deformational history east of the axis of the Cascades volcanic arc since the early Miocene (**Figure 2-1** and **Figure 2-2**). Basalt and basaltic andesite lavas of the early Miocene CRBG are the oldest known rock-units exposed in the area (**Figure 2-2** and **Figure 5-1**). In the western part of the Columbia River Gorge, CRBG units unconformably overlie volcanogenic rocks of the early Western Cascades, including the lower Miocene (ca. 19 Ma) Eagle Creek Formation (Williams, 1916; Allen, 1932), and older rocks thought to be equivalent to the late Eocene and early Oligocene Ohanapecosh Formation (Waters, 1973; Beaulieu, 1977). To the south and east rocks beneath the CRBG include the lower Eocene and upper Paleocene Herren Formation, and volcanic and sedimentary sequences of the middle Eocene Clarno Formation, and the Eocene and Oligocene John Day Formation (see OGDC-6, Smith and Roe, 2015). Farther to the southwest, in the southern Willamette Valley, the CRBG unconformably overlies rocks of the early Western Cascades assigned to the Little Butte Volcanics (McClaughry and others, 2012). Between the southern Willamette Valley and the western part of the Columbia River Gorge, rocks of the Western Cascades sequence are poorly exposed and the nature of bedrock beneath the CRBG is not well understood. This area has been referred to as the Columbia Trans-Arc Lowland which, prior to eruption of younger Cascades volcanic sequences, provided a more southerly drainage to the sea (Beeson and others, 1985).

7.1 Early Miocene (~16.6 to 16.0 Ma)

The CRBG is an extensive succession of tholeiitic basalt and basaltic andesite lavas that cover more than 210,000 km^2 (130,500 mi^2) in parts of Washington, Oregon, and Idaho (**Figure 5-13**, **Figure 5-14**, and **Figure 5-15**; Tolan and others, 1989; Reidel and others, 2013). These lavas were erupted from north-northwest-trending linear fissure systems in the eastern part of the Columbia Plateau, largely between ca. 17 and 14 Ma, and flowed westward through the Columbia Trans-Arc Lowland toward the low-relief topography of western Oregon (**Figure 2-1**; Tolan and Beeson, 1984; Beeson and others, 1985, 1989;

Tolan and others, 1989; Wells and others, 1989, 2009). The Columbia Trans-Arc Lowland was a generally southwest-northeast directed, ~60-km-wide (37 mi) topographic low that extended across the ancestral Cascade Range during the early Miocene (Beeson and others, 1989; Beeson and Tolan, 1990). The lowland was likely structural in origin, related to fold-deformation of Eocene to early Miocene rocks underlying western Oregon, and probably was not related to the development of the early Cascades volcanic arc (Beeson and Tolan, 1990). The position of the lowland, however, may have influenced later development and growth of the volcanic arc in this area (Beeson and Tolan, 1990).

The first flows of the CRBG to enter the Columbia Trans-Arc Lowland on their way to the Pacific coast were part of the Grande Ronde Basalt, erupted between 16.066 ± 0.04 Ma and 16.572 ± 018 Ma (Kasbohm and Schoene, 2018). The earliest flows erupted in eastern parts of the Columbia Plateau and flowed westward, following pre-CRBG ancestral Columbia River channels, which were probably located along the northern edge of the Columbia Trans-Arc Lowland (**Figure 2-1;** Beeson and others, 1989; Wells and others, 2009). Flows in the Grande Ronde Basalt are locally separated by thin, discontinuous sedimentary interbeds, indicating brief intervals of erosion and deposition between eruptions.

Subsequent flows of Grand Ronde Basalt, including those of the Winter Water and Sentinel Bluffs (**Tgsb**) Members locally overlie or grade into intervals of pillow lava and hyaloclastite. These flows largely overwhelmed topographic lows that had formed in pre-early Miocene strata, forming a relatively uniform distribution of lavas across the lowland. The youngest part of the Grande Ronde Basalt, the Sentinel Bluffs Member (**Tgsb**), largely flowed across a relatively muted terrain, covering the most extensive area of any CRBG unit (Beeson and others, 1989). Emplacement of the Sentinel Bluffs Member (**Tgsb**) was followed by an eruptive hiatus and a period of erosion on the upper surface of the CRBG, leaving a regionally widespread unconformity known as the Vantage Member of the Ellensburg Formation. Ancestral Columbia River channels developed through the Columbia Trans-Arc Lowland above this unconformity, creating new pathways for younger CRBG flows to reach western Oregon. The Sentinel Bluffs Member is the only Grand Ronde Basalt exposed in the Biggs Junction and Rufus quadrangles.

7.2 Early Miocene (~16.0 to 15.9 Ma)

The Basalt of Ginkgo (**Twfg**) was the first flow of the Frenchman Springs Member of the Wanapum Basalt to extend from the Columbia Plateau into the Biggs Junction-Rufus area. The relatively uniform thickness and nearly flat orientation of the entire Frenchman Springs Member in the area provides no information about structural or topographic controls on emplacement, in contrast to other parts of the mid-Columbia Basin. The localized high in the upper surface of the Sentinel Bluffs Member (**Tgsb**) that causes the Basalt of Ginkgo (**Twfg**) to thin and pinch out near Biggs Junction is probably due to a feature of emplacement, rather than subsequent deformation. To the west, between Mosier (32 km [20 mi] northwest of Biggs Junction-Rufus) and the Willamette Valley of western Oregon, the basalt encountered the canyon of the ancestral Columbia River, as suggested by the common occurrence of pillows and hyaloclastite at the base of the unit in those areas (McClaughry and others, 2012). Subsequent flows of the Basalt of Sand Hollow (**Twfh**) covered a more extensive area than earlier Ginkgo lavas (**Twfg**) (**Figure 5-14**). Sentinel Gap flows (**Twfs**), forming the upper part of the Frenchman Springs Member in the area, were confined to the northern part of the Columbia Trans-Arc Lowland and forced the ancestral Columbia River to establish a new course along the axis of the Mosier syncline (**Figure 2-1**, **Figure 5-14**; Beeson and others, 1989; Tolan and others 2009; McClaughry and others, 2012). Flows in the Frenchman Springs Member are locally separated by thin and discontinuous sedimentary interbeds, indicating intervals of erosion between eruptions.

7.3 Early to Middle Miocene (~15.9 to ca. 6 Ma)

Eruption of the last of the Frenchman Springs lavas was followed by an ~600,000 year lull in CRBG volcanism and ensuing period of erosion and sedimentation across the Columbia Trans-Arc Lowland. Continued deformation and uplift of Yakima Fold Belt anticlines and reoccupation and downcutting by ancestral channels of the Columbia River across the lowland generated a deep river canyon ~1 to 2 km wide (0.6 to 1.2 mi) that was incised through the Frenchman Springs Member and into the Sentinel Bluffs Member in areas west and north of Biggs Junction-Rufus (Anderson and Vogt, 1987; McClaughry and others, 2012). Early flows of the Roza and Priest Rapids Members of the Wanapum Basalt were partly confined to this paleocanyon as they traversed the area of the present-day Cascade Range around 14.5 Ma (**Figure 5-14** and **Figure 5-19b-d**; Anderson and Vogt, 1987). In the Biggs Junction and Rufus quadrangles, the pinchout of both the Roza and Priest Rapids Members suggests that the edge of the paleo canyon may have traversed across the southeastern portion of the map area.

7.4 Late Miocene to Holocene (~6 Ma to present)

During the late Miocene to early Pliocene, volcanic centers in the High Cascades shed large volumes of volcaniclastic debris to the east, building up hundreds of meters of the Dalles Formation (**Tmdl**). In the map area, this period was represented by the deposition of a distal sedimentary facies composed largely of sandstone, siltstone, tuff, and conglomerate that was probably partly composed of material reworked from the volcaniclastic facies of the Dalles Formation and fluvial sediments derived from basins to the east.

Deeply incised Miocene and Neogene geologic units exposed in the Biggs Junction-Rufus area are capped by a variably thick and discontinuous blanket of Pleistocene loess (**Qlc**). Loess has accumulated in this area as a result of episodic transport of airborne silt by southwesterly winds during the Quaternary. Loess deposits in the Biggs Junction-Rufus area are assigned a Pleistocene age on the basis of stratigraphic position and may be as old as ca. 600 ka. Medley (2012) interpreted loess deposits and Missoula Flood deposits exposed along U.S. Highway 197 between Dufur and The Dalles to lie above a series of older paleosols that contain pumice correlated to the ca. 600 ka Dibekulewe tuff from Nevada (Cordero, 1997). Pluhar and others (2014a,b) reported paleomagnetically reversed paleosols at the base of U.S. Highway 197 section, so loess in this area may in some places be older than 0.78 Ma.

Microrelief features, known as Mima mounds, are a prevalent geomorphic feature in the Biggs Junction-Rufus area, preserved mantling the landscape in areas between cultivated loess (**Qlc**) and steep canyon slopes, but very few examples are preserved in the Biggs Junction and Rufus quadrangles. Mima mounds scattered across north-central Oregon formed during multiple cycles in the Pleistocene, occurring on a variety of landscapes, including plateau and ridge caps, as well as moderate to steep slopes, at differing elevations, on differing bedrock and soil substrates, and in areas of variable saturation (Nelson, 1977). Ideas on the formation of Mima mounds are numerous, and the causative forces remain controversial (see Appendix D of Johnson and Horwath Burnham, 2012). Mima mounds in the Pacific Northwest are ascribed a polygenetic and complex origin, due to both biological and physical causes including but probably not limited to one or a complex combination of: 1) bioturbation by animals (such as pocket gophers), plants, fungi, protoctists, microbes, etc. (Johnson and Horwath Burnham, 2012; Cox, 2012); 2) bioturbationally modified and shaped erosional remnants of a thicker soil mantle (Johnson and Johnson, 2012); 3) a relatively shallow soil mantle overlying an impermeable permafrost or bedrock layer (Nelson, 1977); 4) frost sorting and runoff flushing of stone gutters intervening between mounds

(Johnson and Johnson, 2012); 5) intense frost action under former periglacial conditions (Nelson, 1977); 6) erosion, including snowmelt and surface runoff from mounds (Johnson and Johnson, 2012); 7) occasional eolian inputs (Johnson and Johnson, 2012). Downslope elongation of many of the mounds and stone rings in north-central Oregon is likely the result of mass wasting as slope increases (Nelson, 1977).

The northwestern half of the map area was inundated by the late Pleistocene Missoula floods (Plate 1). These catastrophic flood landscapes and deposits are the result of multiple late Pleistocene glacial-outburst floods that originated from Glacial Lake Missoula in western Montana between ca. 19 and 15 ka (Bretz and others, 1956; Baker and Nummedal, 1978; Waitt, 1985; Allen and others, 1986, Benito and O'Connor, 2003; Waitt, 2016) and repeatedly swept down the Columbia River Gorge, with water levels in the Biggs Junction and Rufus areas reaching elevations of about ~340 m (1,115 ft). Along the Columbia River Gorge severe scour removed all loose material and eroded the CRBG flows into a landscape of pronounced cliffs and benches. The upland areas are mantled with thin layers of fine-grained sediments deposited by the floods, and bar deposits (**Qm**) are present at the mouths of and some distance upstream along the major canyons tributary to the Columbia River.

Steep slopes and valley bottoms have accumulated late Pleistocene and Holocene surficial units including stream alluvium (**Qa, Qt**), fan deposits (**Qaf**), landslide deposits (**Qls**), and colluvium (**Qc**). These units reflect late Pleistocene and Holocene landscape adjustments to the huge geomorphic changes caused by the Missoula floods.

8.0 GEOLOGIC RESOURCES

8.1 Aggregate materials and industrial minerals

Aggregate, in the form of crushed rock and gravel, is the major mineral resource now being mined in the Biggs Junction-Rufus area. Available locations for aggregate and crushed rock resources in the area are given by Niewendorp and Geitgey (2009; http://www.oregongeology.org/sub/milo/index.htm). The entire area is underlain by flows of the CRBG. Aggregate-rock quarry sites within the area are sited mainly within the Sentinel Gap (**Twfs**) and Sand Hollow (**Twfh**) flows of the Frenchman Springs Member, primarily because those units cover the majority of the area. Quarries along the Columbia River also mine Ginkgo flows (**Twfg**). (Plate 1). The Sand Hollow flow (**Twfh**) commonly has very closely spaced platy or prismatic joints that facilitate crushing. The basal colonnade of the Basalt of Sand Hollow (**Twfh**) and some areas of the Basalt of Sentinel Gap (**Twfs**) can produce large column sections that may be suitable for use as riprap for stabilization and erosion control purposes. Sand and gravel suitable for use as aggregate has been mined from Missoula Flood deposits (**Qm**) at Biggs Junction, Rufus, and the mouth of Helm Canyon and the John Day River, but these deposits are largely mined out or covered by development. Columbia River alluvium was extensively mined near Rufus in areas now inundated by Lake Celilo.

No industrial minerals are known to occur in the map area (Niewendorp and Geitgey, 2009), but there is a small deposit of diatomite present (**Figure 5-24**).

8.1.1 Semiprecious gemstones

Several semiprecious gem material localities, containing deposits of silicified sediment, sinter, and brecciated sinter, have been mined in the Biggs Junction-Rufus area. Virtually all of the mines exploit material deposited at the contact between the Basalt of Sand Hollow (**Twfh**) and the overlying Basalt of Sentinel Gap (**Twfs**) **(Figure 5-30**). The locally mined material has been known in the lapidary community

as "Biggs jasper" and "wascoite" (**Figure 8-1**). Half a dozen occurrences are reported by Niewendorp and Geitgey (2009), and there are one active and two closed mine sites permitted by DOGAMI. At the China Hollow jasper mine operated by Mr. Don Hilderbrand, several kinds of material were observed being mined from the **Twfh**-**Twfs** contact. At one site, the source was flooded, but the float consisted of two general types of material. One was a massive pink-tan fine-grained silicified ash or siltstone, and the other was a combination of jasper and agate stained in brown to yellow hues. Some of the jasper material showed evidence of brecciation, or remnants of centimeter scale bedding, and this is reportedly the most valuable in the lapidary market (**Figure 5-44**) (Don Hilderbrand, personal communication 2018). The second site located several hundred meters away and on the same contact exposed a 0.5–1 m (1.5–3 ft) thick layer of silicified or jasperized fine-grained sediment at the contact between the two lava flows. The material at this site displays varied and bright colors and complex textures.

The closed mine site in Biggs Junction was visited, but there was no jasper, agate or other silicified material observed in place or in float throughout a very large pit excavated in the Basalt of Sand Hollow (**Twfh**) (**Figure 5-36**).

Similar deposits occurring within the CRBG are reported from Spanish Hollow Canyon near Wasco, just south of the boundary of the map area (Lowry and others, 1946, DOGAMI department mining records, http://www.oregongeology.org/sub/milo/ohmi-Sherman.htm). The Spanish Hollow locality is reported to contain a variety of intermixed, massive to locally banded chalcedony and opal occurring in various shades of brown, reddish brown, and white; some samples contain numerous limonite inclusions (Lowry and others, 1946, DOGAMI department mining records, http://www.oregongeology.org/sub/milo/ohmi-Sherman.htm). Samples submitted for analysis to DOGAMI in 1946 by Mr. Ryland O. Scott, and reputedly collected from locations in Spanish Hollow, were determined to contain anomalously high values for both gold (1.8 to 21.2 oz Au/ton) and silver (1.0 to 12.9 oz Ag/ton) (Lowry and others, 1946, DOGAMI department mining records, http://www.oregongeology.org/sub/milo/ohmi-Sherman.htm).. Verification samples subsequently collected and assayed by DOGAMI geologists in 1946 (Lowry and others, 1946) show high amounts of iron (>10 percent), but nil to trace amounts of gold (Au) and silver (Ag); one DOGAMI sample assayed at 0.02 oz Au/ton. Additional occurrences of chalcedonic material are known from the CRBG in the vicinity of Biggs and Wasco in Sherman County, and DOGAMI assays of samples from those areas determined they contain neither gold nor silver (Lowry and others, 1946).

Figure 8-1. Polished jasper from China Hollow Mine. (A) "Biggs jasper" and (B) "wascoite." Samples courtesy of Mr. Don Hilderbrand, owner of the China Hollow Biggs Jasper mine.

8.2 Water resources

A full discussion of the geologic controls on surface and groundwater resources in the Biggs Junction-Rufus area is beyond the scope of this report. The reader is directed to previous reports published by Piper (1932), Sceva (1966), Newcomb (1969), Grady (1983), Lite and Grondin (1988), Lindsey and others (2009), Burns and others (2012), and Lite (2013) for a more thorough discussion of groundwater resources and hydrogeology in the Middle Columbia Basin.

Groundwater resources are strongly influenced by permeability differences between stratigraphic units and geologic structures, such as folds and faults. The majority of the groundwater flow system in the map area lies within lavas of the CRBG (Piper, 1932; Newcomb, 1969). Overlying the CRBG are thin, discontinuous locally permeable Quaternary surficial units.

8.2.1 Columbia River Basalt Group aquifers

The extensive series of relatively stratiform units in the CRBG, many of which can be traced laterally from the Columbia Plateau west through the Columbia River Gorge, are a major host for groundwater supplies in the Middle Columbia Basin, including the Biggs Junction-Rufus area (Piper, 1932; Newcomb, 1969; Grady, 1983). Wells producing from these units typically intercept aquifers residing at multiple levels within the flow succession (Newcomb, 1963). However, interconnecting multiple aquifers in wells within the CRBG has elsewhere been shown to contribute to large water level declines in the aquifers (Lite and Grondin, 1988; Lindsey and others, 2009; Burns and others, 2012). Water-bearing horizons in the CRBG are generally associated with open-framework interflow zones including vesicular flow-top breccia, and flow-foot breccia, pillow lavas, and hyaloclastite complexes occurring near the base of a unit (**Figure 8-2**; Newcomb, 1969; Lite and Grondin, 1988; Tolan and others, 2009a; Lindsey and others, 2009). These horizons serve as horizontal to subhorizontal pathways for groundwater flow. Interiors of thick flow complexes typically have extremely low permeability and act as confining units unless secondary permeability exists due to fractures created by faults or folds, flow pinchouts, or erosional windows. Sedimentary interbeds can act as either a confining unit or a porous media serving as a pathway for lateral transport of groundwater. Permeability contrasts created by heterogeneities in flow successions create a series of stacked confined aquifers in the CRBG aquifer system (**Figure 8-2**). Although some characteristics of CRBG flows are considered remarkably homogenous throughout their extent, hydrogeologic characteristics vary on local scales due to a difference in the environment of emplacement for each successive flow and the geologic setting of an area (Lite, 2013). Newcomb (1963) reported regional well yields from 300 gallons per minute to 800 gallons per minute from wells constructed in various formations of the CRBG in the nearby Mosier area. Grady (1983) reported yields of a few hundred to a few thousand gallons per minute for wells in the Hood River basin.

In the Biggs Junction-Rufus area, most water wells produce from the contact between the Basalt of Sand Hollow (**Twfh**) and the Basalt of Sentinel Gap (**Twfh**). This contact, which is present through nearly the entire area, commonly includes sedimentary interbeds and strong hydrothermal alteration and silicification. This contact forms prominent spring and vegetation lines in canyon walls (**Figure 5-2**), probably due to the permeability contrast between the **Twfh** flow top and overlying sedimentary interbeds, and the body of the **Twfh** flow. The ~100 m (328 ft) thick body of the Sand Hollow flow is generally impermeable, and where the **Twfh**/**Twfs** contact is absent or shallow, wells must extend to the contact between the Basalt of Ginkgo (**Twfg**) and the Basalt of Sand Hollow (**Twfh**). Wells in the lowlands along the Columbia River typically originate in **Twfg** or **Tgsb** and produce from interflow zones within **Tgsb**. Few wells produce from contacts between **Twfs** and overlying units.

Figure 8-2. Schematic stratigraphic section of Columbia River Basalt Group lava flows showing typical intraflow structures and vertical relationships of colonnade, entablature, and blocky columnar jointing, vesicular flow top, flow-top breccia, and pillow lava. Modified from Figure 5-1 of Tolan and others (2009a). K values represent the typical hydraulic conductivity ranges in meters per second (m/s) and feet per day (ft/d).

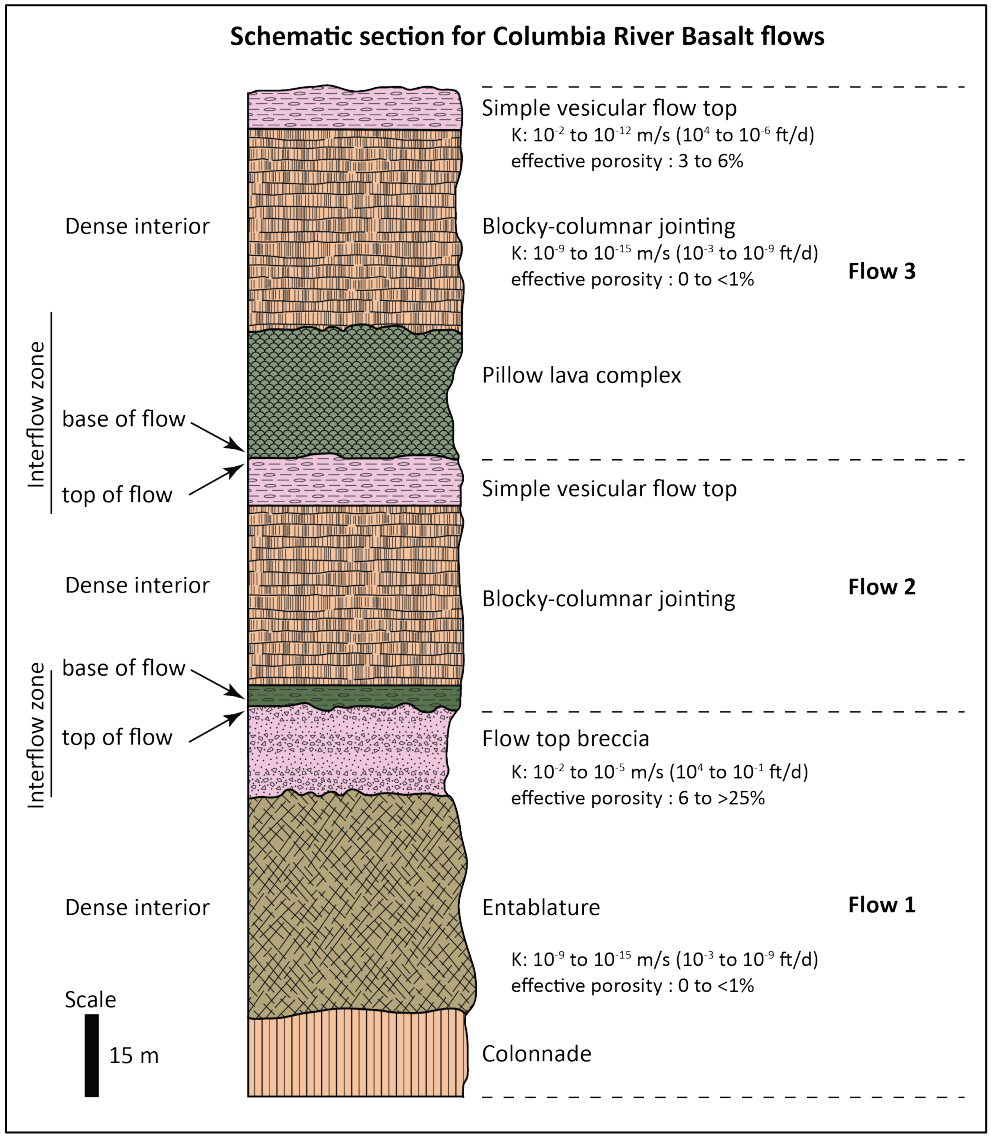

8.2.2 Alluvial deposits

Most of the unconsolidated to partly consolidated surficial deposits are too thin to constitute significant aquifers. The exception is the sand and gravel alluvium of the Columbia River floodplain (**Qac**), which hosts an unconfined aquifer that is in hydraulic connection with the river. The deposits are typically thin (10–20 m) but are very permeable, as indicated by the fact that the small ponds and lakes along the floodplain developed only after the filling of Lake Celilo, which raised the local water table to the level of the lake.

8.3 Geologic hazards

8.3.1 Earthquakes and active faults

Numerous studies in the Pacific Northwest indicate the recent occurrence of large, regional earthquakes and the possibility of significant local events (e.g., Atwater, 1987; McCaffrey and Goldfinger, 1995; Atwater and Hemphill-Haley, 1997; Clague, 1997; McCaffrey and others, 2007, Frankel and Peterson, 2008). There has been little in the way of historic seismic activity in the Biggs Junction-Rufus area during the period 1850–2019 (**Figure 8-3**, https://earthquake.usgs.gov/earthquakes/search/). Only one event (M2.7) occurred within the project area. The majority of the regional seismicity is to the north in Washington. (Goter, 1994; Niewendorp and Neuhaus, 2003). Historical (1896 to 2008) earthquake epicenters in the project area show events generally ranging in magnitude from 1.0 to 2.9 (Richter scale) with several larger events (M4.0 to M4.9) having occurred between Biggs Junction-Rufus and The Dalles in historic times (Beaulieu, 1977; Niewendorp and Neuhaus, 2003). Larger earthquake swarms are known nearby, beneath the volcanic edifice at Mount Hood (75 km [45 mi] west-southwest) and near Maupin (57 km [34 mi] south-southwest) and Condon (79 km [47 mi] south-southeast) (https://earthquake.usgs.gov/earthquakes/search/). Communities in the Biggs Junction-Rufus area may be at risk from four different types of earthquakes: 1) Cascadia subduction zone earthquakes, 2) crustal fault earthquakes, 3) those related to volcanic activity, and 4) deeper intraplate earthquakes occurring within the region (**Figure 8-4**). The 2014 USGS National Seismic Hazard Map (https://earthquake.usgs.gov/static/lfs/nshm/conterminous/2014/2014pga2pct.pdf) estimates that the peak ground acceleration for the area with a 2 percent chance of exceedance in 50 years is 0.18 g. The probabilistic ground shaking is dominated by local crustal sources.

Figure 8-3. Historic seismicity in the project area and surrounding region. Data from USGS earthquake search page, https://earthquake.usgs.gov/earthquakes/search/). Study area shown in black outline.

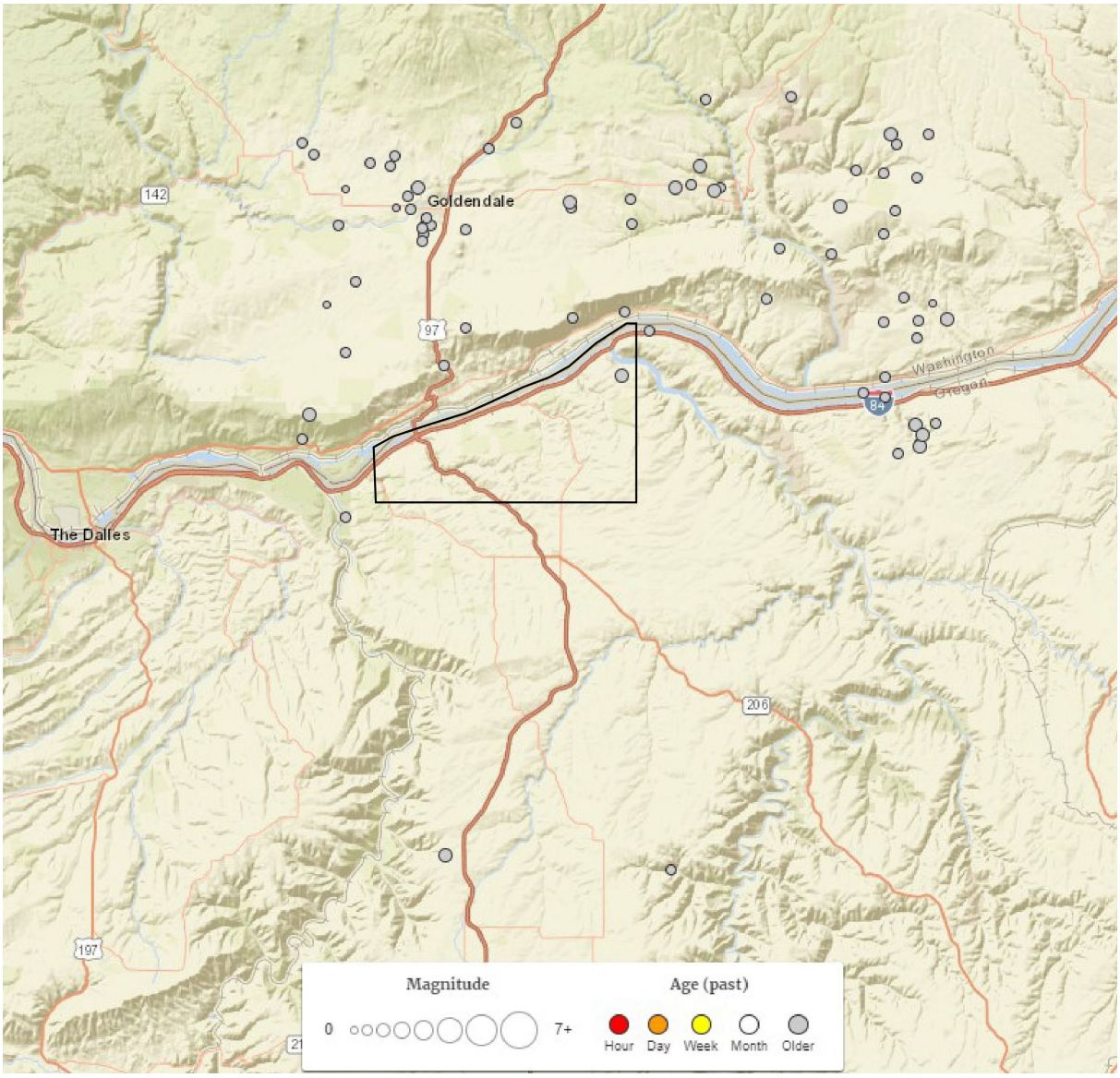

Figure 8-4. Schematic diagram showing tectonic setting of the Pacific Northwest and idealized locations of the four earthquake types described in the text. Modified from Madin and Wang (2000).

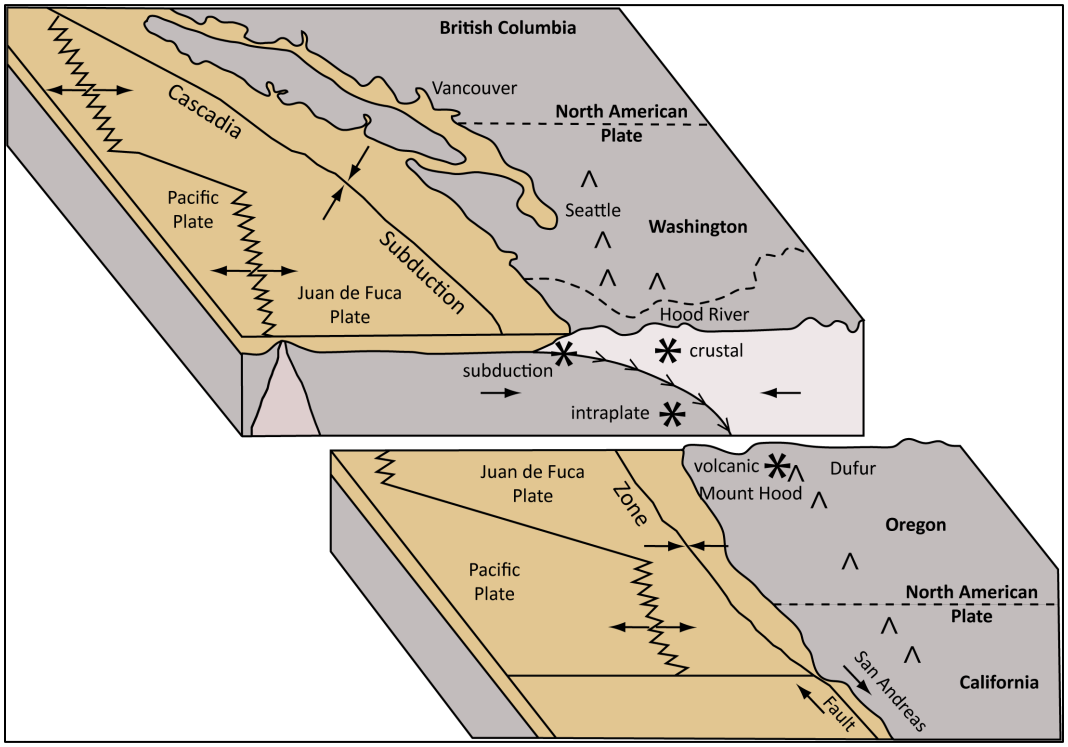

8.3.2 Subduction zone earthquakes

Subduction zone earthquakes occur where one crustal plate overrides an adjacent plate along a dipping interface, commonly known as a subduction zone. The Biggs Junction-Rufus area sits ~310 km (185 mi) east of the Cascadia subduction zone, which marks the plate boundary between the North American plate on the east and the underlying, smaller Juan de Fuca plate on the west (**Figure 2-1, Figure 8-4**). Beneath the Earth's surface, this zone extends eastward from the base of the continental slope, beneath western Oregon, and, as the lower plate continues to slide deeper into the Earth, it drives the processes that result in the eruption of volcanoes in the Cascade Range. The Cascadia subduction zone is generally considered to be at high risk from large subduction zone earthquakes. Goldfinger and others (2003) and Nelson and others (2006) indicated evidence of a number of great Cascadia subduction zone earthquakes, with the most recent occurring in 1700 A.D. (Satake and others, 1996). The Cascadia subduction zone is thought to produce earthquakes as a large as M9.0 every 400 to 500 years (Frankel and Peterson, 2008). More recent work by Goldfinger and others (2012) indicated more frequent intervals of ~240 years, with a 7 to 12 percent chance of a M9.0 Cascadia event in the next 50 years. Priest and others (2009) reported that at least 20 great subduction earthquakes have occurred on the Cascadia subduction zone during the last ~10,000 years. These events, with magnitudes in the range of M8.0 to M9.0 likely caused long-duration, moderately strong shaking throughout much of the region, with intensity decreasing eastward from the epicenter. Site effects from such an event, including earthquake induced liquefaction, landsliding, and amplification of shaking by low-velocity surficial deposits could dramatically enhance damage in the area. Madin and Burns (2013) indicated that a M9.0 Cascadia event would result in light to very light damage in the Biggs Junction-Rufus area (see Plate 7 of Madin and Burns, 2013).

8.3.3 Crustal earthquakes

Crustal earthquakes result from shallow sources within the North American plate (**Figure 8-4**). Epicenters are located at relatively shallow depths of 10 to 20 km (6 to 12 mi) below land surface. East of the Cascades, the majority of earthquake shaking hazard comes from crustal earthquakes (Madin and Mabey, 1996). In the western part of the Columbia River flood basalt province, focal mechanisms of small magnitude (< M3) earthquakes are associated with some northwest-trending wrench faults in the Yakima fold belt, providing direct evidence that some of these faults could remain active (Bela, 1982; USDOE, 1988; Yelin and Patton, 1991). The presence of other possible Quaternary faults in north-central Oregon is indicated by new geologic mapping and compilations published by previous workers (Geomatrix Consultants Inc., 1995; Madin and Mabey, 1996; Weldon and others, 2003; Lidke and others, 2003; Personius and others, 2003; McClaughry and others, 2012). No active crustal faults have been identified in or near the map area.

8.3.4 Volcanic earthquakes

Volcanic earthquakes in the area are usually small in magnitude and occur over infrequent intervals; earthquakes of this type of at least M4.5 or larger can occur around Mount Hood (**Figure 2-1**, **Figure 8-4**).. During 2002 a swarm of earthquakes ranging from M3.2 to M4.5 occurred on the southeast flank of Mount Hood (Burns and others, 2011). These types of earthquake swarms are known to occur periodically within the vicinity of the volcano; they do not necessarily indicate impending eruptions. The USGS Cascades Volcano Observatory (CVO) continuously monitors earthquakes in the Cascades through a regional seismograph network and will provide warning, as possible, if activity suggests potential for volcanic eruptions.

8.3.5 Intraplate earthquakes

The Biggs Junction-Rufus area may also experience site effects from deeper intraplate earthquakes, which result from movement within the underlying Juan De Fuca plate (**Figure 2-1**, **Figure 8-4**). These earthquakes could occur beneath much of the Pacific Northwest at depths of 40 to 60 km (25 to 37 mi). The large earthquakes that caused significant damage in the Puget Sound region in 1949 (Olympia), 1965 (Puget Sound), and 2001 (Nisqually) are considered to have been deep intraplate earthquakes (Haugerud and others, 1999).

8.3.6 Site effects

Ground shaking, soil liquefaction, landslides, surface ruptures, and seiches are all possible causes of damage during an earthquake affecting the Biggs Junction-Rufus area. The damaging effects of earthquakes can be enhanced by proximity to epicenters, amplification of shaking in soft soils, by liquefaction, or by induced landslides. Detailed relative hazard maps that incorporate all of these hazards into single risk categories have not been compiled for the Biggs Junction-Rufus area, but Madin and Burns (2013) have produced regional seismic hazard maps generated on the basis of statewide geologic data. Liquefaction hazards occur where the shaking of a water-saturated soil causes its material properties to change from a solid to a liquid. Soils that liquefy tend to be loose, granular soils that are saturated with water. Unsaturated soils will not liquefy but may settle. Areas underlain by artificial fill (**Hcf**) and alluvium (**Qa**), (Plate 1) have a moderate liquefaction susceptibility (see liquefaction susceptibility map of Madin and Burns, 2013). Where bedrock (volcanic rock or lithified sedimentary rock) is exposed at the surface, such as in uplands or in the bottoms of incised drainages, the liquefaction hazard is negligible (Madin and Burns, 2013).

8.4 Volcanic hazards

The Biggs Junction-Rufus area lies ~45 km [28 mi] east-northeast of the axis of the intermittently active volcanic zone along Cascades volcanic arc and Quaternary Mount Hood volcano. Unlike other geologic hazards discussed in this report (e.g., earthquakes) which may occur over several seconds to minutes, a volcanic episode can last days to decades and may include multiple syn- and inter-eruptive events. Volcanic hazards for the Biggs Junction-Rufus area identified by the USGS and by DOGAMI are restricted to fallout of tephra and lava flows.

8.4.1 Tephra fall

Tephra (volcanic ash) generated by larger eruptions at Mount Hood or other nearby Cascade volcanoes may fall on areas up to several hundred kilometers downwind. Such events are inferred to pose little risk to communities in the vicinity of Mount Hood (Scott and others, 1997). On the basis of Mount Hood's past tephra production, it is estimated that nearby communities such as Biggs Junction-Rufus and The Dalles would likely receive a tephra thickness up to 1.5 cm (0.6 in) in any one event (Scott and others, 1997). The 30-year probability of accumulation of 1 cm (0.4 in) or more tephra in the Biggs Junction-Rufus area from eruptions in the Cascade Range is 1 in 30; the 30-year probability of accumulation of 10 cm (4 in) or more tephra in the Biggs Junction-Rufus area from eruptions in the Cascade Range is 1 in 150 (Scott and others, 1997). However, no such thickness of tephra in the map area is known from a Holocene eruption at Mount Hood. Hazards associated with tephra falls include tens of minutes or more of darkness, paint damage, clogging of engine filters with fine particles, short-circuiting of electric transformers and power lines, and disruption of air traffic (e.g., Mount St. Helens eruptions, May 1980). Larger events may include the possibility of roof collapse of structures.

8.5 Landslide hazards

Relatively few landslide deposits (**Qls**) were recognized and mapped in the study area. The majority were rockfall or debris flow/debris avalanche deposits originating on the cliffs or steep slopes of the Columbia River gorge or tributary canyons. The thick colluvial wedges present at the base of these cliffs and steep slopes have accumulated in part though rockfall and debris flow events. All areas at the base of cliffs or on or near areas mapped as colluvium (**Qc**) should be considered at high risk from future landslides. Throughout the rest of the area, there is widespread occurrence of loess (**Qlc**), which can be susceptible to landslides where it is on moderate to steep slopes and saturated. However, over most to the map area the loess is too thin to present significant landslide hazard, as evidenced by the presence of only one landslide that originates in loess (Plate 1).

In upland areas covered by loess, small alluvial fans are common at the mouths of ephemeral streams and are the result of debris flows triggered by intense local rainfall. The areas mapped as alluvial fans and the mouths of all minor drainages should be considered to have significant risk of damaging debris flows.

8.6 Flooding hazards

Flooding hazards in the study area typically result from a combination of steep topography, low bedrock infiltration rates, and the periodic occurrence of high-precipitation weather events or late fall and winter marine storms that place warm rain across significant accumulations of low-elevation snow. Other sources of flooding include flash floods associated with locally intense (summer) thunderstorms,

channel migration, ice or debris jams and, much less frequently, artificial-dam or landslide-dam failures. A number of notable floods have occurred in the Pacific Northwest as a result of high-precipitation or rain-on-snow-events during the years 1861-1862, 1894, 1948, 1964/1965, 1977, 1996, and 2005/2006 (Oregon Department of Land Conservation and Development, 2015). Five flood events have been declared major disasters in Wasco County since 1964 (1964, 1974, 1995, 1996, and 2007). The flood of 1894 on the Columbia completely destroyed the community of Grant located between Rufus and Biggs Junction (Oregon Department of Land Conservation and Development, 2015). The 1964 flood primarily affected tributary streams, and there was extensive damage and fatalities in Rufus and Biggs Junction due to flooding on Scott, Spanish Hollow, and Gerking canyons, and highway damage at Frank Fulton Canyon (Beaulieu, 1977). Flooding in 1996 (February) occurred when warming and intense precipitation (5 to 6.4 cm [2 to 2.5 in]) initiated rapid snowmelt across the Middle Columbia Basin. Infiltration of intense rainfall was limited by several factors, including frozen soils, iced-over creeks, and hard-crusted snow. The resulting overland flows scoured soils and filled upland drainages where ice-jams, clogged culverts, and bridges had reduced stream capacity. The combination of these conditions led to widespread flooding, landslides, erosion, and debris flows downstream.

Floods cause damage to buildings and infrastructure through inundation by water and by erosion and deposition of sediment and debris. Significant hazards related to channel migration are present in the area. Channel migration hazards can occur slowly, for example, by continuous erosion along a cutbank meander and deposition onto a point bar during high flows, or very rapidly during storm events through avulsion (the rapid abandonment of the current river channel for a new one) (Beaulieu, 1977; Easterbrook, 1993; Rapp and Abbe, 2003). Channel migration hazards in the drainages may be substantial within the narrow inner gorges of streams due to the large volume of loose sediment are added to the fluvial system from frequent upslope debris flows or loosely consolidated constructed fills (Plate 1). This loose sediment is easily eroded and transported through flood torrents, thereby amplifying the channel migration process downstream. Infrequent torrential floods accompanying periodic thunderstorms, should also be expected in the map area, where steep gradient canyons are incised into the CRBG. These canyons have narrow floodplains and are characterized by catastrophic streamflow, erosion, and deposition. Hazards along these channels include erosion of roads, fills, and bridge pilings, and plugging of culverts. Both Rufus and Biggs Junction are built on alluvial fans that have been deposited in the later Quaternary and Holocene by repeated torrential floods in Scott and Spanish Hollow canyons.

9.0 ACKNOWLEDGMENTS

This study was supported in part by a grant from the STATEMAP component of the National Cooperative Geologic Mapping Program (G18AC00136). Additional funds were provided by the State of Oregon. XRF geochemical analyses were prepared and analyzed by Dr. Scott Burroughs at the GeoAnalytical Lab at Washington State University The authors appreciate critical information shared by Charles Cannon, Jim O'Connor, and James Anderson on the geology of adjacent quadrangles and region. Informative discussions and field trips with Ray Wells, Jim O'Connor, Charlie Cannon, Danielle Woodring, and Andrew Meigs added to our knowledge of Quaternary surficial deposits and CRBG stratigraphy and structure in the Columbia River Gorge. Donald Hilderbrand provided access to his Biggs jasper gem mine and contributed his extensive knowledge of the distribution of hydrothermal deposits in the map area. Cartography for the map plates was provided by Jon Franczyk and GIS assistance was provided by Carlie

Duda. Critical and insightful reviews by Nancy Calhoun, (DOGAMI), Jim O'Connor (USGS), Charles Cannon (USGS), and Ray Wells (USGS), greatly enriched the final manuscript, geodatabase, and geologic maps.

10.0 REFERENCES

Allen, J. E., 1932, Contribution to the structure, stratigraphy, and petrography of the lower Columbia River Gorge: Eugene, Oreg., University of Oregon, M.S. thesis, 53 p.

Allen, J. E., 1966, The Cascade Range volcano-tectonic depression of Oregon, *in* Benson, G. T, ed., Transactions of the Lunar Geological Field Conference, Bend, Oregon, August 1965: Oregon Department of Geology and Mineral Industries Open-File Report O-66-01, p. 21–23. https://www.oregongeology.org/pubs/ofr/O-66-01.pdf

Allen, J. E., Burns, M., and Sargent, S.C., 1986, Cataclysms on the Columbia: Portland, Oreg., Timber Press, 211 p.

Anderson, J. L., 1987, The structure and ages of deformation of a portion of the southwest Columbia Plateau, Washington and Oregon: Los Angeles, University of Southern California, Ph.D. dissertation, 272 p.

Anderson, J. L., and Vogt. B.F., 1987, Intracanyon flows of the Columbia River Basalt Group in the southwestern part of the Columbia Plateau and adjacent Cascade Range, Oregon and Washington, *in* Schuster, J. E., ed., Selected papers on the geology of Washington: Washington Division of Geology and Earth Resources Bulletin 77, p. 249–267. http://www.dnr.wa.gov/publications/ger_b77_papers_on_wa_geology_pt1of3.pdf

Anderson, J. L., Tolan, T.L., and Wells., R. E., 2013, Strike-slip faults in the western Columbia River flood basalt province, Oregon and Washington, *in* Reidel, S. P., Camp, V., Ross, M. E., Wolff, J. A., Martin, B. E., Tolan, T. L., and Wells, R. E., eds., The Columbia River Flood Basalt Province: Geological Society of America Special Paper 497, p. 325–347. https://doi.org/10.1130/2013.2497(13)

Atwater, B. F., 1987, Evidence for great Holocene earthquakes along the outer coast of Washington State: Science, v. 236, p. 942–944. https://science.sciencemag.org/content/236/4804/942

Atwater, B. F., and Hemphill-Haley, E., 1997, Recurrence intervals for great earthquakes of the past 3,500 years at northeastern Willapa Bay, Washington: U.S. Geological Survey Professional Paper 1576, 108 p. http://pubs.er.usgs.gov/publication/pp1576

Baker, V. R., and Nummedal, D., eds., 1978, The Channeled Scabland; a guide to the geomorphology of the Columbia Basin, Washington, prepared for the Comparative Planetary Geology Field Conference held in the Columbia Basin, June 5–8, 1978: Washington, D.C., National Aeronautics and Space Administration, 186 p. https://ntrs.nasa.gov/archive/nasa/casi.ntrs.nasa.gov/19780019521.pdf

Barnett, D. B., Fecht, K. R., Reidel, S. P., Bjornstad, B. N., Lanigan, D. C., and Rust, C. F., 2007, Geology of the Waste Treatment Plant site seismic boreholes: Richland, Wash., Pacific Northwest National Laboratory, PNNL-16407, 107 p.

Barry, T. L., Self, S., Kelley, S. P., Reidel, S., Hooper, P., and Widdowson, M., 2010, New $^{40}Ar/^{39}Ar$ dating of the Grande Ronde lavas, Columbia River Basalts, USA: Implications for duration of flood basalt eruption episodes: LITHOS, v. 118, no. 3-4, p. 213–222. https://doi.org/10.1016/j.lithos.2010.03.014

Beaulieu, J. D., 1977, Geologic hazards of parts of northern Hood River, Wasco, and Sherman Counties, Oregon: Oregon Department of Geology and Mineral Industries Bulletin 91, 95 p. 11 pl., scale 1:62,500. https://www.oregongeology.org/pubs/B/B-091.pdf

Beeson, M. H., and Tolan, T. L., 1990, The Columbia River Basalt Group in the Cascade Range: A middle Miocene reference datum for structural analysis: Journal of Geophysical Research, v. 95, p. 19,547–19,559. https://doi.org/10.1029/JB095iB12p19547

Beeson, M. H., Fecht, K. R., Reidel, S. P., and Tolan, T. L., 1985, Regional correlations within the Frenchman Springs Member of the Columbia River Basalt Group: new insights into the middle Miocene tectonics of northwestern Oregon: Oregon Geology, v. 47, no. 8, p. 87–96. https://www.oregongeology.org/pubs/og/OGv47n08.pdf

Beeson, M. H., Tolan, T. L., and Anderson, J. L., 1989, The Columbia River Basalt Group in western Oregon: Geologic structures and other factors that controlled flow emplacement patterns, *in* Reidel, S. P., and Hooper, P. R., eds., Volcanism and tectonism in the Columbia River Flood-Basalt Province: Geological Society of America Special Paper 239, p. 223–246. https://doi.org/10.1130/SPE239-p223

Bela, J. L., 1982, Geologic and neotectonic evaluation of north-central Oregon: The Dalles 1° × 2° quadrangle: Oregon Department of Geology and Mineral Industries GMS-27, 2 plates, scale 1:250,000. https://www.oregongeology.org/pubs/gms/GMS-027.pdf

Benito, G., and O'Connor, J. E., 2003, Number and size of last-glacial Missoula Floods in the Columbia River valley between the Pasco Basin, Washington, and Portland, Oregon: GSA Bulletin, v. 115, no. 5, p 624–638. https://doi.org/10.1130/0016-7606(2003)115<0624:NASOLM>2.0.CO;2

Bretz, J. H., Smith, H. T. U., and Neff, G. E., 1956, Channeled Scabland of Washington: New data and interpretations: GSA Bulletin, v. 67, no. 8, p. 957–1049. https://doi.org/10.1130/0016-7606(1956)67[957:CSOWND]2.0.CO;2

Burns, E. R., Morgan, D. S., Lee, K. K., Haynes, J. V., and Conlon, T. D., 2012, Evaluation of long-term water-level declines in basalt aquifers near Mosier, Oregon: U.S. Geological Survey Scientific Investigations Report 2012-5002, 134 p., GIS files. http://pubs.usgs.gov/sir/2012/5002/

Burns, W. J., Hughes, K. L. B., Olson, K. V., McClaughry, J. D., Mickelson, K. A., Coe, D. E., English, J. T., Roberts, J. T., Lyles Smith, R. R., and Madin, I. P., 2011, Multi-hazard and risk study for the Mount Hood region, Multnomah, Clackamas, and Hood River Counties, Oregon: Oregon Department of Geology and Mineral Industries Open-File Report O-11-16, 179 p., 7 pl., scale 1:72,000, spreadsheets. http://www.oregongeology.org/pubs/ofr/p-O-11-16.htm

Camp, V. E., 1981, Geologic studies of the Columbia Plateau: Part II. Upper Miocene basalt distribution reflecting source locations, tectonism, and drainage history of the Clearwater embayment, Idaho: Geological Society of America Bulletin, v. 92, no. 9, p. 669–678.

Camp, V. E., and Ross, M. E., 2004, Mantle dynamics and genesis of mafic magmatism in the intermontane Pacific northwest: Journal of Geophysical Research, v. 109, B08204. https://doi.org/10.1029/2003JB002838

Camp, V. E., Ross, M.E., Hanson, W. E., 2003, Genesis of flood basalts and basin and range volcanic rocks from Steens Mountain to the Malheur River Gorge, Oregon: The Geological Society of America Bulletin, v. 115, p. 105–128.

Cande, S. C., and Kent, D. V., 1992, A new geomagnetic polarity time scale for the Late Cretaceous and Cenozoic: Journal of Geophysical Research, v. 97, p. 13,917–13,951. https://doi.org/10.1029/92JB01202

Clague, J. J., 1997, Evidence for large earthquakes at the Cascadia subduction zone: Reviews in Geophysics, v. 35, p. 439–460.

Cohen, K. M., Finney, S.C., Gibbard, P. L. and Fan, J.-X., 2013 (updated 2015), The ICS International Chronostratigraphic Chart: Episodes 36, p. 199–204. http://www.stratigraphy.org/index.php/ics-chart-timescale

Conrey, R. M., Sherrod, D.R., Uto, K., and Uchiumi, S., 1996, Potassium-argon ages from Mount Hood area of Cascade Range, northern Oregon: Isochron/West, no. 63, p. 10–20.

Conrey, R. M., Sherrod, D. R., Hooper, P. R., and Swanson, D. A., 1997, Diverse primitive magmas in the Cascade Arc, northern Oregon and southern Washington: The Canadian Mineralogist, v. 35, no. 2, p. 367–396.

Conrey, R. M., Taylor, E. M., Donnelly-Nolan, J. M., and Sherrod, D. R., 2002, North-central Oregon Cascades: Exploring petrologic and tectonic intimacy in a propagating intra-arc rift, in Moore, G. W., ed., Field guide to geologic processes in Cascadia: Oregon Department of Geology and Mineral Industries Special Paper 36, p. 47–90. http://www.oregongeology.org/pubs/sp/p-SP.htm

Cordero, D. I., 1997, Early to Middle Pleistocene catastrophic flood deposits, The Dalles, Oregon: Portland, Portland State University, M.S. thesis, 162 p.

Cox, G. W., 2012, Alpine and montane Mima mounds of the western United States, *in* Horwath Burnham, J. L. and Johnson, D. L., eds., Mima mounds: The case for polygenesis and bioturbation: Geological Society of America Special Paper 490, p. 63–70. https://doi.org/10.1130/2012.2490(03)

Cox, K. G., Bell, J. D., and Pankhurst, R. J., 1979, The interpretation of igneous rocks: London, George Allen and Unwin, 450 p.

Duncan, R. A., Hooper, P. R., Rehacek, J., Marsh, J. S., and Duncan, A. R., 1997, The timing and duration of the Karoo igneous event, southern Gondwana: Journal of Geophysical Research, v. 102, no. B8, p. 18,127–18,138. https://doi.org/10.1029/97JB00972

Easterbrook, D. J., 1993, Surface processes and landforms: New York, Macmillan, 520 p.

Fecht, K. R., Reidel, S. P., and Tallman, A. M., 1987, Paleodrainage of the Columbia River system on the Columbia Plateau off Washington State—a summary, *in* Schuster, J. E., ed., Selected Papers on the Geology of Washington: Washington Division of Geology and Earth Resources Bulletin 77, p. 219–248. http://www.dnr.wa.gov/Publications/ger_b77_papers_on_wa_geology_pt2of3.pdf

Ferns, M. L., and McClaughry, J. D., 2013, Stratigraphy and volcanic evolution of the middle Miocene to Pliocene La Grande–Owyhee eruptive axis in eastern Oregon, *in* Reidel, S. P., Camp, V., Ross, M. E., Wolff, J. A., Martin, B. E., Tolan, T. L., and Wells, R. E., eds., The Columbia River Flood Basalt Province: Geological Society of America Special Paper 497, p. 401–427. https://doi.org/10.1130/2013.2497(16)

Frankel, A. D., and Peterson, M. D., 2008, Cascadia subduction zone, Appendix L in the Uniform California Earthquake Rupture Forecast, version 2 (UCERF2): U.S. Geological Survey Open File Report 2007-1437L and California Geological Survey Special Report 203L, 7 p. http://pubs.usgs.gov/of/2007/1437/

Geomatrix Consultants, Inc., 1995, Seismic design mapping, State of Oregon: technical report to Oregon Department of Transportation, Salem, Oregon, under contract 11688, January 1995, unpaginated, 5 plates, scale 1:1,250,000.

Gillespie, M. R., and Styles, M. T., 1999, BGS rock classification scheme, v. 1, Classification of igneous rocks: British Geological Survey Research Report RR99-06 (2nd ed.), 52 p.

Goldfinger, C., Nelson, C. H., Johnson, J. E., and the Shipboard Scientific Party, 2003, Deep-water turbidites as Holocene earthquake proxies: The Cascadia subduction zone and Northern San Andreas Fault systems: Annuals of Geophysical Research, v. 46, no. 5, p. 1169–1194.

Goldfinger, C., Nelson, C. H., Johnson, J. E., Morey, A. E., Gutiérrez-Pastor, J., Karabanov, E., Eriksson, A. T., Gràcia, E., Dunhill, G., Patton, J., Enkin, R. J., Dallimore, A., Vallier, T., and the Shipboard Scientific Parties, 2012, Turbidite event history—methods and implications for Holocene paleoseismicity of the Cascadia subduction zone: U.S. Geological Survey, Professional Paper 1661–F, 170 p. http://pubs.usgs.gov/pp/pp1661f/

Goter, S. K., 1994, Earthquakes in Washington and Oregon: 1872–1993: U. S. Geological Survey Open-File Report 94-226-A, 1 p., 1 pl., scale 1:1,000,000. http://pubs.er.usgs.gov/publication/ofr94226A

Gradstein, F. M., and others, 2004, A geologic time scale 2004, Cambridge University Press, 589 p.

Grady, S. J., 1983, Ground-water resources in the Hood Basin, Oregon: U.S. Geological Survey Water-Resources Investigations Report 81-1108, 68 p., 2 plates, scale 1:62,500. http://pubs.er.usgs.gov/publication/wri811108

Gray, L. B., Sherrod, D.R., and Conrey, R. M., 1996, Potassium-argon ages from the northern Oregon Cascade Range: Isochron/West, no. 63, p. 21–28.

Green, G. L., 1981, Soil survey of Hood River County area, Oregon: Natural Resources Conservation Service Soil Conservation Survey 629, 66 p. https://www.nrcs.usda.gov/Internet/FSE_MANUSCRIPTS/oregon/OR629/0/or629_text.pdf

Green, G. L., 1982, Soil survey of Wasco County, Oregon, northern part: Natural Resources Conservation Service Soil Conservation Survey 673, 83 p. https://www.nrcs.usda.gov/Internet/FSE_MANUSCRIPTS/oregon/OR673/0/or673_text.pdf

Hagstrum, J. T., Sawlan, M. G., Wells, R. E., Evarts, R. C., and Niem, A. R., 2010, New paleomagnetic and geochemical reference sections in Miocene Grande Ronde Basalt flows on the Columbia Plateau are fundamental to stratigraphic, structural, and tectonic studies in the Portland Metro area and Coast Ranges of Oregon and Washington: American Geophysical Union Fall Meeting 2010, abstract #GP11A-0745.

Hallsworth, C. R., and Knox, R. W. O'B., 1999, BGS rock classification scheme, v. 3, Classification of sediments and sedimentary rocks: British Geological Survey Research Report 99-03, 44 p.

Haugerud, R. A., Ballantyne, D., Weaver, C. S., Meagher, K., and Barnett, E. A., 1999, Lifelines and earthquake hazards in the greater Seattle area: U.S. Geological Survey, Open-File Report 99-387, 10 p., http://geomaps.wr.usgs.gov/pacnw/lifeline/index.html

Hodge, E. T., 1938, Geology of the lower Columbia River: Geological Society of America Bulletin, v. 49, no. 6, p. 831–930. https://doi.org/10.1130/GSAB-49-831

Hooper, P. R., 2000, Chemical discrimination of Columbia River Basalt flows: Geochemistry, Geophysics, and Geosystems, v. 1, no. 1, p. 1–14. https://doi.org/10.1029/2000GC000040

Johnson, A. K., 2011, Dextral shear and north-directed crustal shortening defines the transition between extensional and contractional provinces in north-central Oregon: Corvallis, Oregon State University, master's thesis, 77 p., 3 pl., scale 1:24,000. http://ir.library.oregonstate.edu/xmlui/handle/1957/20928

Johnson, D. L., and Horwath Burnham, J. L., 2012, Introduction: overview of concepts, definitions, and principles of soil mound studies, *in* Horwath Burnham, J. L. and Johnson, D. L., eds., Mima mounds: the case for polygenesis and bioturbation: Geological Society of America Special Paper 490, p. 1–19. https://doi.org/10.1130/2012.2490(00)

Johnson, D. L., and Johnson, D. N., 2012, The polygenetic origin of prairie mounds in northeastern California, *in* Horwath Burnham, J. L. and Johnson, D. L., eds., Mima mounds: the case for polygenesis and bioturbation: Geological Society of America Special Paper 490, p. 135–159. https://doi.org/10.1130/2012.2490(06)

Johnson, D. M., Hooper, P. R., and Conrey, R. M., 1999, XRF analysis of rocks and minerals for major and trace elements on a single low dilution Li-tetraborate fused bead: Advances in X-ray Analysis, v. 41, p. 843–867. http://cahnrs.wsu.edu/soe/facilities/geolab/technotes/xrf_method/

Kasbohm, J., and Schoene, B., 2018, Rapid eruption of the Columbia River flood basalt and correlation with mid-Miocene climate optimum; Science Advances v. 4, no. 9 https://advances.sciencemag.org/content/4/9/eaat8223

Korosec, M. A., 1987, Geologic map of the Hood River quadrangle, Washington and Oregon: Washington Division of Geology and Earth Resources Open File Report 87-6, 41 p., 1 plate, scale 1:100,000. http://ngmdb.usgs.gov/Prodesc/proddesc_30784.htm

Kuehn, S. C., 1995, The Olympic-Wallowa lineament, Hite fault system, and Columbia River Basalt Group stratigraphy in northeast Umatilla County, Oregon: Pullman, Wash., Washington State University, master's thesis, 170 p.

Le Bas, M. J., and Streckeisen, A. L., 1991, The IUGS systematics of igneous rocks: Journal of the Geological Society, v. 148, p. 825–833. https://doi.org/10.1144/gsjgs.148.5.0825

Le Bas, M. J., Le Maitre, R. W., Streckeisen, A., and Zanettin, B., 1986, A chemical classification of volcanic rocks based on the total alkali-silica diagram: Journal of Petrology, v. 27, part 3, p. 745–750. https://doi.org/10.1093/petrology/27.3.745

Le Maitre, R. W., Bateman, P., Dudek, A., Keller, J., Lemeyre, J., Le Bas, M. J., Sabine, P. A., Schmid, R., Sorenson, H., Streckeisen, A., Wooley, A. R., and Zanettin, B., 1989, A classification of igneous rocks and glossary of terms: Oxford, Blackwell, 193 p.

Le Maitre, R.W. (ed.), Streckeisen, A., Zanettin, B., Le Bas, M.J., Bonin, B., Bateman, P., Bellieni, G., Dudek, A., Efremova, S., Keller, J., Lameyre, J., Sabine, P.A., Schmid, R., Sørensen, H., and Woolley, A.R., 2004, Igneous rocks: A classification and glossary of terms: Recommendations of the International Union of Geological Sciences, Subcommission on the Systematics of Igneous Rocks: Cambridge University Press, 236 p.

Lidke, D. J., Johnson, S. Y., McCrory, P. A., Personius, S. F., Nelson, A. R., Dart, R. L., Bradley, L., Haller, K. M., and Machette, M. N., 2003, Map and data for Quaternary faults and folds in Washington State: U.S. Geological Survey Open-File Report 03-428, 579 p., 1 plate, scale 1:750,000. http://pubs.usgs.gov/of/2003/428/

Lindsey, K., Morgan, D., Vlassopoulos, D., Tolan, T. L., and Burns, E., 2009, Hydrogeology of the Columbia River Basalt Group in the Columbia Plateau: road log and field trip stop descriptions, *in* O'Connor, J. E., Dorsey, R. J., and Madin, I. P., eds., Volcanoes to vineyards: geologic field trips through the dynamic landscape of the Pacific Northwest: Geological Society of America Field Guide 15, p. 673–696. https://doi.org/10.1130/2009.fld015(30)

Lite, K. E., 2013, The influence of depositional environment and landscape evolution on groundwater flow in Columbia River Basalt—examples from Mosier, Oregon, *in* Reidel, S. P., Camp, V. E., Martin, M. E., Ross, M. E., Wolff, J. A., Martin, B. S., Tolan, T. L., and Wells, R. E., eds., Geological Society of America Special Paper 497, p. 429–440. https://doi.org/10.1130/2013.2497(17)

Lite, K. E., and Grondin, G. H., 1988, Hydrogeology of the basalt aquifers near Mosier, Oregon: A ground water resource assessment: Oregon Water Resources Department Ground Water Report 33, 119 p., 5 plates, scale 1:24,000. http://www.oregon.gov/owrd/pages/gw/gw_pubs.aspx

Lux, D. R., 1982, K-Ar and $^{40}Ar/^{39}Ar$ ages of mid-Tertiary volcanic rocks from the West Cascades Range, Oregon: Isochron/West, no. 33, p. 27–32.

Mackenzie, W. S., Donaldson, C. H., and Guilford, C., 1997, Atlas of igneous rocks and their textures, 7th ed.: Addison Wesley Longman Limited, 148 p.

Mackin, J. H., 1961, A stratigraphic section in the Yakima Basalt and the Ellensburg Formation in south-central Washington: Washington Division of Mines and Geology Report of Investigations No. 19, 45 p. http://www.dnr.wa.gov/Publications/ger_ri19_strat_yakima_basalt_ellensburg_form.pdf

Madin, I. P., and Burns, W. J., 2013, Ground motion, ground deformation, tsunami inundation, coseismic subsidence, and damage potential maps for the 2012 Oregon resilience plan for Cascadia subduction zone earthquakes: Oregon Department of Geology and Mineral Industries Open-File Report O-13-06, 39 p., 38 pl., various scales. http://www.oregongeology.org/pubs/ofr/p-O-13-06.htm

Madin, I. P., and Mabey, M. A., 1996, Earthquake hazard maps for Oregon: Oregon Department of Geology and Mineral Industries Geological Map GMS-100, 1 pl., various scales. https://www.oregongeology.org/pubs/gms/GMS-100.pdf

Madin, I.P., and Wang, Z., 2000, Relative earthquake hazard maps for selected areas in western Oregon: Oregon Department of Geology and Mineral Industries Interpretive Map 7 (IMS-7), scale 1:24,000. http://www.oregongeology.org/pubs/ims/p-ims.htm

Martin, B. S., 1989, The Roza Member, Columbia River Basalt Group; Chemical stratigraphy and flow distribution, *in* Reidel, S. P., and Hooper, P. R., eds., Volcanism and tectonism in the Columbia River Flood-Basalt Province: Geological Society of America Special Paper 239, p. 85–105. https://doi.org/10.1130/SPE239-p85

Martin, B. S., Tolan, T. L., and Reidel, S. P., 2013, Revisions to the stratigraphy and distribution of the Frenchman Springs Member, Wanapum Basalt, *in* Reidel, S. P., Camp, V. E., Martin, M. E., Ross, M. E., Wolff, J. A., Martin, B. S., Tolan, T. L., and Wells, R. E., eds., Geological Society of America Special Paper 497, p. 155–180. https://doi.org/10.1130/2013.2497(06)

McCaffrey, R., and Goldfinger, C., 1995, Forearc deformation and great subduction earthquakes: Implications for Cascadia offshore earthquake potential, Science, v. 267, p. 856–859. http://www.jstor.org/stable/2886147

McCaffrey, R., Qamar, A. I., King, R. W., Wells, R., Khazaradze, G., Williams, C. A., Stevens, C. W., Vollick, J. J., and Zwick, P. C., 2007, Fault locking, block rotation and crustal deformation in the Pacific Northwest: Geophysical Journal International, v. 169, issue 3, p. 1315–1340. https://doi.org/10.1111/j.1365-246X.2007.03371.x

McClaughry, J. D., Wiley, T. J., Ferns, M. L., and Madin, I. P., 2010, Digital geologic map of the southern Willamette Valley, Benton, Lane, Linn, Marion, and Polk Counties, Oregon: Oregon Department of Geology and Mineral Industries Open-File Report O-2010-03, 116 p., 1 pl., scale 1:63,360, Esri ArcGIS geodatabase, GIS files, spreadsheets. http://www.oregongeology.org/pubs/ofr/p-O-10-03.htm

McClaughry, J. D., Wiley, T. J., Conrey, R. C., Jones, C. B., and Lite, K. E., 2012, Digital geologic map of the Hood River Valley, Hood River and Wasco Counties, Oregon: Oregon Department of Geology and Mineral Industries Open-File Report O-12-03, 142 p., 1 plate, scale 1:36,000, Esri ArcGIS geodatabase, GIS files, spreadsheets. http://www.oregongeology.org/pubs/ofr/p-O-12-03.htm

McDonald, E. V., Sweeney, M. R., and Busacca, A. J., 2012, Glacial outburst floods and loess sedimentation documented by Oxygen Isotope Stage 4 on the Columbia Plateau, Washington State: Quaternary Science Reviews, v. 45, p. 18–30. https://doi.org/10.1016/j.quascirev.2012.03.016

Medley, E., 2012, Ancient cataclysmic floods in the Pacific Northwest: Ancestors to the Missoula Floods: Portland, Portland State University, M.S. thesis, 174 p. http://pdxscholar.library.pdx.edu/open_access_etds/581/

Mertzman, S. A., 2000, K-Ar results from the southern Oregon–northern California Cascade Range: Oregon Geology, v. 62, p. 99–122. http://www.oregongeology.org/pubs/og/p-OG.htm

Miyashiro, A., 1974, Volcanic rock series in island arcs and active continental margins: American Journal of Science, v. 274, p. 321–355.

NCGMP (USGS National Cooperative Geologic Mapping Program), 2010, NCGMP09—Draft standard format for digital publication of geologic maps, version 1.1, *in* Soller, D. R., ed., Digital Mapping Techniques '09—Workshop Proceedings: U.S. Geological Survey Open-File Report 2010–1335, p. 93–146. https://pubs.usgs.gov/of/2010/1335/pdf/usgs_of2010-1335.pdf

NCGMP (USGS National Cooperative Geologic Mapping Program), 2018, GeMS (Geologic Map Schema)—a standard format for digital publication of geologic maps: U.S. Geological Survey, version 2, draft 7, 78 p. https://ngmdb.usgs.gov/Info/standards/GeMS/docs/GeMSv2_draft7g_ProvisionalRelease.pdf

Nelson, A. R., Kelsey, H. M., and Witter, R. C., 2006, Great earthquakes of variable magnitude at the Cascadia subduction zone: Quaternary Research, v. 65, p. 354–365. https://doi.org/10.1016/j.yqres.2006.02.009

Nelson, C. A., 1977, The origin and characteristics of soil mounds and patterned ground in north central Oregon: Corvallis, Oregon State University, M.S. thesis, 51 p.

Newcomb, R. C., 1963, Ground water in the Orchard syncline, Wasco County, Oregon: The Ore Bin, v. 25, no. 8, p. 133–138. https://www.oregongeology.org/pubs/og/OBv25n08.pdf

Newcomb, R. C., 1966, Lithology and eastward extension of the Dalles Formation, Oregon and Washington: U.S. Geological Survey Professional Paper 550-D, p D59–D63. https://doi.org/10.3133/pp550D

Newcomb, R. C., 1969, Effect of tectonic structure on the occurrence of groundwater in the basalt of the Columbia River Group of The Dalles area, Oregon and Washington: U.S. Geological Survey Professional Paper 383-C, 33 p., 1 pl., scale 1:62,500. https://doi.org/10.3133/pp383C

Niewendorp, C. A., and Geitgey, R. P., 2009, Mineral information layer for Oregon (MILO, release 2), GIS files. http://www.oregongeology.org/sub/milo/index.htm

Niewendorp, C.A., and Neuhaus, M. E., 2003, Map of selected earthquakes for Oregon, 1841 through 2002: Oregon Department of Geology and Mineral Industries Open-File Report O-03-02, 1 pl. http://www.oregongeology.org/pubs/ofr/p-OFR.htm

Ogg, J. G., Ogg, G., and Gradstein, F. M., 2008, The concise geologic time scale: Cambridge, Cambridge University Press, 177 p.

Oregon Department of Land Conservation and Development, 2015, Oregon Natural Hazards Mitigation Plan: Floods, p. 123–134. http://www.oregon.gov/LCD/HAZ/Pages/nhmp.aspx#Oregon_Natural_Hazards_Mitigation_Plan

Personius, S. F., Dart, R. L., Bradley, L.-A., and Haller, K. M., 2003, Map and data for Quaternary faults and folds in Oregon: U.S. Geological Survey Open-File Report 03-095, 16 p., 1 pl., scale 1:750,000. http://pubs.usgs.gov/of/2003/ofr-03-095/

Phillips, W. M., Korosec, M. A., Schasse, H. W., Anderson, J. L., and Hagen, R. A., 1986, K-Ar ages of volcanic rocks in southwest Washington: Isochron/West, v. 47, p. 18–24.

Piper, A. M., 1932, Geology and ground-water resources of The Dalles region, Oregon: U.S. Geological Survey Water-Supply Paper 659-B, p. 107–189, 2 pl., scale 1:62,500. https://pubs.er.usgs.gov/publication/wsp659B

Pluhar, C. J., Carpenter, B., Yazzie, K., Melton, D., and Burns, S., 2014a. Early and middle Pleistocene cataclysmic flood deposits at The Dalles, OR: Geological Society of America Abstracts with Programs, v. 46, no. 6, p. 591.

Pluhar, C. J., Burns, S., Carpenter, B., Yazzie, K., and Melton, D., 2014b. Paleomagnetism of early and middle Pleistocene cataclysmic flood deposits in the Pacific Northwest: American Geophysical Union, Fall Meeting 2014, abstract #GP21A-3653. http://adsabs.harvard.edu/abs/2014AGUFMGP21A3653P

Powell, J. E., 1982, Geology of the Columbia Hills, Klickitat County, Washington: University of Idaho master's thesis, 56 p, 4 pl.

Priest, G. R., Goldfinger, C., Wang, K.., Witter, R. C., Zhang, Y., and Baptista, A. M., 2009, Tsunami hazard assessment of the northern Oregon coast: A multi-deterministic approach tested at Cannon Beach, Clatsop County, Oregon: Oregon Department of Geology and Mineral Industries Special Paper 41, 87 p., GIS files, time histories, animations. Compressed file: https://www.oregongeology.org/pubs/sp/SP-41.zip

Rapp, C. F., and Abbe, T. B., 2003, A framework for delineating channel migration zones: Olympia, Wash., Washington State Department of Ecology Publication 03-06-027, 65 p. https://fortress.wa.gov/ecy/publications/documents/0306027.pdf

Reidel, S. P., and Campbell, N. P., 1989, Structure of the Yakima Fold Belt, central Washington, *in* Joseph, N. L. and others, eds., Geologic guidebook for Washington and adjacent areas: Washington Division of Geology and Earth Resources Information Circular 86, p. 275–303. http://www.dnr.wa.gov/Publications/ger_ic86_geol_guide_wa_area.pdf

Reidel, S. P., and Tolan, T. L., 2013, Grande Ronde Basalt, Columbia River Basalt Group, *in* Reidel, S. P., Camp, V. E., Martin, M. E., Ross, M. E., Wolff, J. A., Martin, B. S., Tolan, T. L., and Wells, R. E., eds., Geological Society of America Special Paper 497, p. 117–154. https://doi.org/10.1130/SPE497

Reidel, S. P., Tolan, T. L., Hooper, P. R., Beeson, M. H., Fecht, K. R., Bentley, R. D., and Anderson, J. L., 1989, The Grande Ronde Basalt, Columbia River Basalt Group; Stratigraphic descriptions and correlations in Washington, Oregon, and Idaho, *in* Reidel, S. P., and Hooper, P. R., eds., Volcanism and tectonism in the Columbia River Flood-Basalt Province: Geological Society of America Special Paper 239, p. 21–53. https://doi.org/10.1130/SPE239-p21

Reidel, S. P., Johnson, V. G., and Spane, F. A., 2002, Natural gas storage in basalt aquifers of the Columbia Basin, Pacific Northwest USA: A guide to site characterization: Richland, Wash., Pacific Northwest National Laboratory, PNNL-13962, 277 p. https://www.pnnl.gov/main/publications/external/technical_reports/PNNL-13962.pdf

Reidel, S. P., Camp, V. E., Tolan, T. L., and Martin, B. S., 2013, The Columbia River flood basalt province: Stratigraphy, areal extent, volume, and physical volcanology, *in* Reidel, S. P., Camp, V. E., Martin, M. E., Ross, M. E., Wolff, J. A., Martin, B. S., Tolan, T. L., and Wells, R. E., eds., Geological Society of America Special Paper 497, p. 1–43. https://doi.org/10.1130/2013.2497(01)

Robertson, S., 1999, BGS rock classification scheme, v. 2, Classification of metamorphic rocks: British Geological Survey Research Report 99-02, 24 p.

Satake, K., K. Shimazaki, Y. Tsuji, and K. Ueda, 1996, Time and size of a giant earthquake in Cascadia inferred from Japanese tsunami records of January 1700: Nature, v. 379, p. 246–249.

Sceva, J. E., 1966, A reconnaissance of the ground-water resources of the Hood River Valley and the Cascade Locks area, Hood River County, Oregon: State of Oregon Groundwater Resources Report 10, 45 p, 1 pl. https://digital.osl.state.or.us/islandora/object/osl:14684

Scott, W. E., Pierson, T. C., Schilling, S. P., Costa, J. E., Gardner, C. A., Vallance, J. W., and Major, J. J., 1997, Volcano hazards in the Mount Hood region, Oregon: U.S. Geological Survey Open-File Report 97-89, 14 p., 1 map. https://pubs.usgs.gov/of/1997/0089/

Seims, B. A., Bush, J. G., and Crosby, J. W., 1974, TiO_2 and geophysical logging criteria for Yakima Basalt correlation, Columbia Plateau: Geological Society of America Bulletin, v. 85, no. 7, p. 1061–1068. https://doi.org/10.1130/0016-7606(1974)85<1061:TAGLCF>2.0.CO;2

Shannon and Wilson, Inc., 1973, Geologic studies of Columbia River basalt structures and age of deformation; the Dalles-Umatilla region Washington and Oregon; Boardman Nuclear Project: Portland, Oreg., report to Portland General Electric Company, 52 p.

Sherrod, D. R., and Scott, W. E., 1995, Preliminary geologic map of the Mount Hood 30- by 60-minute quadrangle, Northern Cascade Range, Oregon: U.S. Geological Survey Open-File Report 95-219, 36 p., scale 1:100,000. Web: http://pubs.usgs.gov/of/1995/of95-219/

Sherrod, D. R., and Smith, J. G., 2000, Geologic map of upper Eocene to Holocene volcanic and related rocks of the Cascade Range, Oregon: U.S. Geological Survey Map I-2569, 17 p., 2 pl., scale 1:500,000. http://pubs.usgs.gov/imap/i-2569/

Smith, G. A., 1987, The influence of explosive volcanism on fluvial sedimentation: the Deschutes Formation (Neogene) in central, Oregon: Journal of Sedimentary Petrology, v. 57, no. 4, p. 613–629. http://dx.doi.org/10.1306/212F8BBB-2B24-11D7-8648000102C1865D

Smith, G. A., and Taylor, E. M., 1983, The central Oregon High Cascade graben: what? where? when?: Geothermal Resources Council Transactions, v. 7, p. 275–279.

Smith, R. A., and Roe, W. P., compilers, 2015, Oregon Geologic Data Compilation [OGDC], release 6 (statewide): Oregon Department of Geology and Mineral Industries Digital Data Series OGDC-6, Esri geodatabase. http://www.oregongeology.org/pubs/dds/p-OGDC-6.htm

Swanson, D. A., Anderson, J. L., Bentley, R. D., Byerly, G. R., Camo, V. E., Gardner, J. N., and Wright, T. L., 1979a, Reconnaissance geologic map of the Columbia River Basalt Group in eastern Washington and northern Idaho: U.S. Geological Survey Open-File Report 79-1363, 44 p., 12 pl., scale 1:250,000. https://doi.org/10.3133/ofr791363

Swanson, D. A., Wright, T. L., Hooper, P. R., and Bentley, R. D., 1979b, Revisions in stratigraphic nomenclature of the Columbia River Basalt Group: U.S. Geological Survey Bulletin 1457-G, 59 p., 1 pl. https://doi.org/10.3133/b1457G

Swanson, D. A., Anderson, J. A., Camp, V. E., Hooper, P. R., Taubeneck, W. H., and Wright, T. L., 1981, Reconnaissance geologic map of the Columbia River Basalt Group, northern Oregon and western Idaho: U.S. Geological Survey Open-File Report 81-797, 35 p., 6 pl., scale 1:250,000. https://doi.org/10.3133/ofr81797

Taylor, E. M., 1981, Central High Cascade roadside geology—Bend, Sisters, McKenzie Pass, and Santiam Pass, Oregon, in Johnston, D.A., and Donnelly-Nolan, J., eds., Guides to some volcanic terranes in Washington, Idaho, Oregon, and northern California: U.S. Geological Survey Circular 838, p.55–83. https://doi.org/10.3133/cir838

Timm, S., 1979, The structure and stratigraphy of Columbia River Basalt in the Hood River valley: Portland, Portland State University, M.S. thesis, 56 p.

Tolan, T. L., and Beeson, M. H., 1984, Intracanyon flows of the Columbia River Basalt Group in the lower Columbia River Gorge and their relationship to the Troutdale Formation: Geological Society of America Bulletin, v. 95, no. 4, p. 463–477. https://doi.org/10.1130/0016-7606(1984)95<463:IFOTCR>2.0.CO;2

Tolan, T. L., and Reidel, S. P., compilers, 1989, Structure map of a portion the Columbia-River Flood-Basalt Province, *in* Reidel, S. P., and Hooper, P. R., eds., Volcanism and tectonism in the Columbia River Flood-Basalt Province: Geological Society of America Special Paper 239, scale 1:576,000, 1 pl.

Tolan, T. L., Reidel, S. P., Beeson, M. H., Anderson, J. L., Fecht, K. R., and Swanson, D. A., 1989, Revisions to the estimates of the areal extent and volume of the Columbia River Basalt Group, *in* Reidel, S. P., and Hooper, P. R., eds., Volcanism and tectonism in the Columbia River Flood-Basalt Province: Geological Society of America Special Paper 239, p. 1–20. https://doi.org/10.1130/SPE239-p1

Tolan, T. L., Martin, B. S., Reidel, S. P., Anderson, J. L., Lindsey, K. A., and Burt, W., 2009a, An introduction to the stratigraphy, structural geology, and hydrogeology of the Columbia River Flood-Basalt Province: A primer for the GSA Columbia River Basalt Group field trips, *in* O'Connor, J. E., Dorsey, R. J., and Madin, I. P., eds., Volcanoes to vineyards: geologic field trips through the dynamic landscape of the Pacific Northwest: Geological Society of America Field Guide 15, p. 599–643. https://doi.org/10.1130/2009.fld015(28)

Tolan, T. L., Martin, B. S., Reidel, S. P., Kauffman, J. D., Garwood, D. L., and Anderson, J. L., 2009b, Stratigraphy and tectonics of the central and eastern portions of the Columbia River Flood-Basalt Province: An overview of our current state of knowledge, *in* O'Connor, J. E., Dorsey, R. J., and Madin, I. P., eds., Volcanoes to vineyards: Geologic field trips through the dynamic landscape of the Pacific Northwest: Geological Society of America Field Guide 15, p. 645–672. https://doi.org/10.1130/2009.fld015(29)

USDOE (U.S. Department of Energy), 1988, Site characterization plan, reference repository location, Hanford site, Washington—consultation draft: Washington, D.C., Office of Civilian Radioactive Waste Management, DOE/RW-0164, v. 1 and 2, 1245 p.

Verplanck, E. P., and Duncan, R. A., 1987, Temporal variations in plate convergence and eruption rates in the Western Cascades Oregon: Tectonics, v. 6, p. 197–209. https://doi.org/10.1029/TC006i002p00197

Vogt, B. F., 1981, The stratigraphy and structure of the CRBG in the Bull Run Watershed, Oregon: Portland, Oreg., Portland State University, master's thesis, 151 p.

Waananen, A. O., Harris, D. D., and Williams, R. C., 1971, Floods of December 1964 and January 1965 in the Far Western States: U.S. Geological Survey Water-Supply Paper 1866-A. https://doi.org/10.3133/wsp1866A

Waitt, R. B., 1985, Case for periodic, colossal jokulhlaups from Pleistocene glacial Lake Missoula: Geological Society of America Bulletin, v. 96, no. 10, p. 1271–1286.

Waitt, R. B., 2016, Megafloods and Clovis cache at Wenatchee, Washington: Quaternary Research, v. 85, p. 430–444. https://doi.org/10.1016/j.yqres.2016.02.007

Waters, A. C., 1968, Reconnaissance geologic map of the Dufur quadrangle, Hood River, Sherman, and Wasco Counties, Oregon: U.S. Geological Survey Miscellaneous Geologic Investigations Map I-556, scale 1:125,000. http://pubs.er.usgs.gov/publication/i556

Waters, A. C., 1973, The Columbia River Gorge, basalt stratigraphy, ancient lava dams and landslide dams, *in* Beaulieu, J. D., ed., Geologic field trips in northern Oregon and southern Washington: Oregon Department of Geology and Mineral Industries Bulletin 77, p. 133–162. https://www.oregongeology.org/pubs/B/B-077.pdf

Watters, T. R., 1989, Periodically spaced anticlines of the Columbia Plateau, *in* Reidel, S. P., and Hooper, P. R., eds., Volcanism and tectonism in the Columbia River flood-basalt province: Geological Society of America Special Paper 239, p. 283–292. https://doi.org/10.1130/SPE239-p283

Weldon, R. J., II, Fletcher, D. K., Weldon, E. M., Scharer, K. M., and McCrory, P. A., 2003, An update of Quaternary faults of central and eastern Oregon: U.S. Geological Survey Open-File Report 2002-301, version 1.0. http://pubs.usgs.gov/of/2002/of02-301/

Wells, R. E., Simpson, R. W., Bentley, R. D., Beeson, M. H., Mangan, M. T., and Wright, T. L., 1989, Correlation of Miocene flows of the Columbia River Basalt Group from the central Columbia River Plateau to the coast of Oregon and Washington, *in* Reidel, S. P., and Hooper, P. R., eds., Volcanism and tectonism in the Columbia River Flood-Basalt Province: Geological Society of America Special Paper 239, p. 113–129. https://doi.org/10.1130/SPE239-p113

Wells, R. E., Niem, A. R., Evarts, R. C., and Hagstrum, J. T., 2009, The Columbia River Basalt Group—from the gorge to the sea, *in* O'Connor, J. E., Dorsey, R. J., and Madin, I. P., eds., Volcanoes to vineyards: geologic field trips through the dynamic landscape of the Pacific Northwest: Geological Society of America Field Guide 15, p. 737–774. https://doi.org/10.1130/2009.fld015(32)

Williams, D. L., Hull, D. A., Ackerman, H. D., and Beeson, M. H., 1982, The Mt. Hood region: volcanic history, structure, and geothermal potential: Journal of Geophysical Research, v. 87, p. 2767–2781. https://doi.org/10.1029/JB087iB04p02767

Williams, I. A., 1916, The Columbia River Gorge – its geologic history interpreted from the Columbia River Highway, *in* Mineral resources of Oregon, v. 2: Oregon Bureau of Mines and Geology, p. 7–130, 2 pl., scale 1:24,000.

Wright, T. L., Maurice, J. G., and Swanson, D. A., 1973, Chemical variation related to the stratigraphy of the Columbia River Basalt: Geological Society of America Bulletin, v. 84, p. 371–386. https://doi.org/10.1130/0016-7606(1973)84<371:CVRTTS>2.0.CO;2

Yelin, T. S., and Patton, H. J., 1991, Seismotectonics of the Portland, Oregon, region: Seismological Society of America Bulletin, v. 81, p. 109–130.

Zdanowicz, C. M., Zeilinski, G. A., and Germani, M. S., 1999, Mount Mazama eruption: calendrical age verified and atmospheric impact assessed: Geology, v. 27, no. 7, p. 621–624. https://doi.org/10.1130/0091-7613(1999)027<0621:MMECAV>2.3.CO;2

11.0 APPENDIX

This appendix is divided into two sections:

- Section 11.1 describes the digital databases included with this publication.
- Section 11.2 contains a summary of analytical and field methods. Tables list descriptions of the fields in associated spreadsheets.

11.1 Geographic Information Systems (GIS) database

Geodatabase specifications

Digital data created for the Oregon portions of the Biggs Junction and Rufus 7.5'quadrangles are stored in an Esri format geodatabase. The geodatabase structure follows that outlined by the U.S. Geological Survey (USGS) Geologic Map Schema (GeMS), version 2.7 (USGS National Cooperative Geologic Mapping Program, 2018). The following information describes the overall database structure, the feature classes, and supplemental tables

The data are stored in a file geodatabase feature dataset (GeologicMap). Accessory file geodatabase tables (DataSources, DescriptionOfMapUnits, GeoMaterialDict, and Glossary) were created by using ArcGIS version 10.6 (SP 1). The GeologicMap feature dataset contains all the spatially oriented data (feature classes) created for the Biggs Junction and Rufus 7.5' quadrangles. The file geodatabase tables are used to hold additional geologic attributes. Additional information and complete descriptions of the "GeMS" — Geologic Map Schema (formerly "NCGMP09") can be found at https://ngmdb.usgs.gov/Info/standards/GeMS/#docs.

Figure 11-1. Biggs Junction and Rufus 7.5' quadrangle geodatabase feature datasets and data tables.

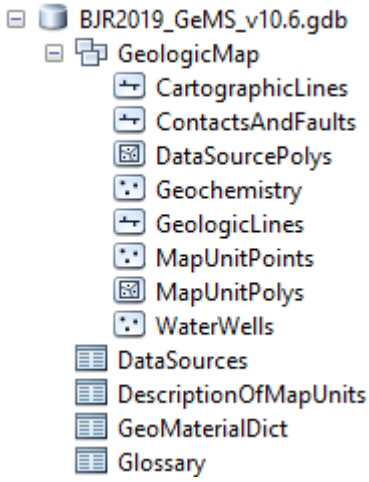

Geodatabase feature class specifications

Each feature class within the GeologicMap feature dataset in the geodatabase contains detailed metadata. Please see the metadata for detailed information such as process descriptions, accuracy specifications, and entity attribute descriptions. **Figure 11-1**, **Figure 11-2, Figure 11-3,** and companion **Table 11-1** are provided below as a summary description for each feature class within the GeologicMap feature dataset.

Figure 11-2. Geodatabase feature classes.

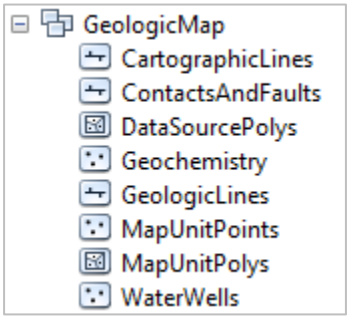

Table 11-1. Feature class description.

Name	Description
CartographicLines	Vector lines that have no real-world physical existence and do not participate in map-unit topology. The feature class includes cross section lines used for cartography.
ContactsAndFaults	The vector lines in this feature class contains geologic content including contacts and fault locations used to create the map unit polygon boundaries. The existence and location confidence for the faults are provided in the feature class attribute table.
DataSourcePolys	This feature class contains polygons that delineate data sources for all parts of the geologic map. These sources may be a previously published map, new mapping, or mapping with a certain technique. For a map with one data source, for example all new mapping, this feature class contains one polygon that encompasses the map area.
Geochemistry	This feature class represents point locations where whole-rock samples have been analyzed by X-ray fluorescence (XRF) techniques. Includes data collected by the authors during the course of this study or compiled from previous studies. These data are also contained in the geochemistry database described in more detail below.
GeologicLines	These vector lines represent known fold axis locations in the map area. The existence and location confidence for the fold axes are provided in the feature class attribute table.
MapUnitPoints	This feature class represents points used to generate the MapUnitPolys feature class from the ContactsAndFaults feature class.
MapUnitPolys	A polygon feature class representing the geologic map units as defined by the authors.
WaterWells	This feature class represents point locations where water wells were located. Includes data obtained by the authors from the Oregon Department of Water Resources (OWRD). These data are also contained in the water well database described in more detail below.

Geodatabase table specifications

Figure 11-3. Geodatabase data tables.

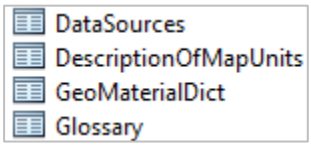

Table 11-2. Geodatabase tables.

Name	Description
DataSources	Data table that contains information about data sources used to compile the geology of the area. Relates to polygons displayed in the DataSourcePolys feature class.
DescriptionOfMapUnits	This table captures the content of the Description of Map Units (DMU), or equivalent List of Map Units and associated pamphlet text, included in a geologic map.

GeoMaterialDict	Data table providing definitions and hierarchy for GeoMaterial names prescribed by the GeMS database schema.
Glossary	Data table that contains information about the definition of terms used in the geodatabase.

Geodatabase projection specifications

All spatial data are stored in the Oregon Statewide Lambert Conformal Conic projection. The datum is NAD83 HARN. The linear unit is international feet. See detailed projection parameters below:

Projection: Lambert_Conformal_Conic
False_Easting: 1312335.958005
False_Northing: 0.000000
Central_Meridian: -120.5
Standard_Parallel_1: 43.0
Standard_Parallel_2: 45.5
Latitude_Of_Origin: 41.75
Linear Unit: Foot (0.3048)
Geographic Coordinate System: GCS_North_American_1983_HARN
Angular Unit: Degree (0.0174532925199433299)
Prime Meridian: Greenwich (0.0)
Datum: D_North_American_1983_HARN
Spheroid: GRS_1980
Semimajor Axis: 6378137.0
Semiminor Axis: 6356752.3141403561
Inverse Flattening: 298.257222101

Geologic map

This report is accompanied by a map plate displaying the surficial and bedrock geology at a scale of 1:24,000, and accompanying geologic cross sections (Plate 1) for the Oregon portions of the Biggs Junction and Rufus 7.5' quadrangles. The map plate has been generated from detailed geologic data (scale of 1:8,000 or better) contained in the accompanying Esri format geodatabase. Both bedrock and surficial geologic interpretations can be recovered from the geodatabase and can be used to create a variety of additional thematic maps.

Plate 1. Geologic map of the Oregon portions of the Biggs Junction and Rufus 7.5’quadrangles, Sherman and Gilliam Counties, Oregon (Plate 1). Plate dimensions are 42 by 42 inches, scale 1;24,000. See digital folder for map plate.

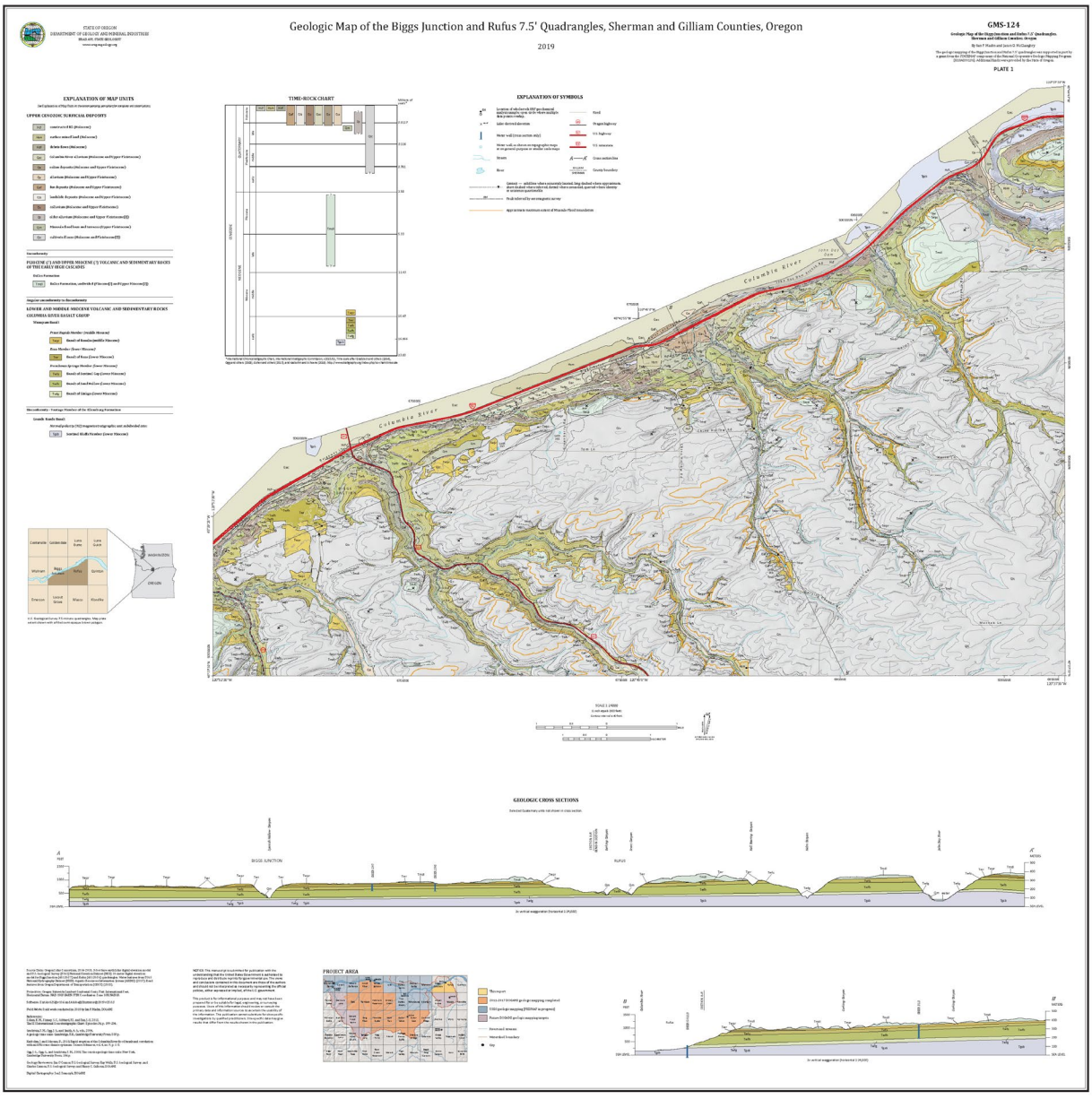

11.2 Methods

Geochemical analytical methods

Geologic mapping in the Biggs Junction-Rufus area was supported by numerous new and compiled X-ray fluorescence (XRF) geochemical analyses of whole-rock samples. Descriptive rock unit names for igneous rocks are based on normalized major element analyses plotted on the total alkalis ($Na_2O + K_2O$) versus silica (SiO_2) diagram (TAS) of Le Bas and others (1986), Le Bas and Streckeisen (1991), and Le Maitre and others (1989, 2004). New and compiled XRF-geochemical analyses are included in the geodatabase, a separate shapefile named BJR2019_Geochemistry, and are also provided in a Microsoft Excel® workbook BJR2019_DATA.xlsx (sheet BJR2019_Geochemistry). **Table 11-3** contains descriptions for the fields in the shapefile and spreadsheet. The locations of all geochemical samples are given in five coordinate systems: UTM Zone 10 (datum = NAD 27, NAD 83, units = meters), Geographic (datum = NAD 27, NAD 83, units = decimal degrees), and Oregon Lambert (datum = NAD 83, HARN, units = international feet).

Samples denoted by lab abbreviation WSU were analyzed by XRF at the Washington State University GeoAnalytical Lab, Pullman, Washington. Analytical procedures for the Washington State University GeoAnalytical Lab are described in Johnson and others (1999) and can be obtained online at http://www.sees.wsu.edu/Geolab/note/xrf.html. Notes for spreadsheet: -9 = no data for numerical fields for analytical data; nd = no data in text fields; na = information not applicable for text fields.

Table 11-3. Geochemical database spreadsheet columns.

Field	Description
SAMPLE_NO	A unique number identifying the sample – e.g., BJ18-219.
WELL ID	Well log number for wells. Wells in Wasco County preceded by acronym WASC – e.g., WASC 53799.
MAP_NO	A unique number identifying the sample on the map plates – e.g., G21.
QUADRANGLE	The USGS 7.5' quadrangle in which the sample is located – e.g., Biggs Junction-Rufus West.
ELEV_FT	Elevation of sample location in feet – e.g., 1928.
UTMN_NAD27	Meters north in NAD 27 UTM projection, zone 10.
UTME_NAD27	Meters east in NAD 27 UTM projection, zone 10.
LAT_NAD27	Latitude in NAD 27 geographic coordinates.
LONG_NAD27	Longitude in NAD 27 geographic coordinates.
UTMN_NAD83	Meters north in NAD 83 UTM projection, zone 10.
UTME_NAD83	Meters east in NAD 83 UTM projection, zone 10.
LAT_NAD83	Latitude in NAD 83 geographic coordinates.
LONG_NAD83	Longitude in NAD 83 geographic coordinates.
N_83HARN	Feet north in Oregon Lambert NAD 83, HARN, international feet.
E_83HARN	Feet east in Oregon Lambert NAD 83, HARN, international feet.
TERRANE_GR	Geologic group that the sample is assigned to. See GeologicMap, MapUnitPolys in the geodatabase – e.g., Columbia River Basalt Group. See DescriptionOfMapUnits table in the geodatabase.
FORMATION	Geologic formation that the sample is assigned to. See GeologicMap, MapUnitPolys in the geodatabase – e.g., Wanapum Basalt. See DescriptionOfMapUnits table in the geodatabase.
MEMBER	Geologic member that the sample is assigned to. See GeologicMap, MapUnitPolys in the geodatabase – e.g., Frenchman Springs Member. See DescriptionOfMapUnits table in the geodatabase.
MAP_UNIT_N	Geologic unit that the sample is assigned to. See GeologicMap, MapUnitPolys in the geodatabase – e.g., Basalt of Sand Hollow. See DescriptionOfMapUnits table in the geodatabase.
MAP_UNIT_L	Unique label identifying the geologic unit that the sample is assigned to. See GeologicMap, MapUnitPolys in the geodatabase – e.g., Twfg. See DescriptionOfMapUnits table in the geodatabase.
VOLCANIC_FIELD	Volcanic field that the unit is assigned to. In igneous provinces, a well-defined area covered with volcanic rocks with a common geologic history.
TAS_LITHOLOGY	Rock name assigned based on the total alkalis ($Na_2O + K_2O$) versus silica (SiO_2) diagram (TAS) of Le Bas and others (1986), Le Bas and Streckeisen (1991), and Le Maitre and others (1989) – e.g., basalt, rhyolite.
MAJOR ELEMENTS	SiO_2, Al_2O_3, TiO_2, FeO*, MnO, CaO, MgO, K_2O, Na_2O, P_2O_5. In wt. percent.
TRACE ELEMENTS	Ni, Cr, Sc, V, Ba, Rb, Sr, Zr, Y, Nb, Ga, Cu, Zn, Pb, La, Ce, Th, Nd, U, Co. In ppm.
LOI	Value for loss on ignition as reported by the lab.
FE2O3	Iron (III) oxide or ferric oxide reported in original analysis.
FeO	Iron (II) oxide or ferrous oxide reported in original analysis.
REFERENCE	Publication reference, keyed to the reference list in this report.
METHOD	Analytical method used by laboratory that analyzed the sample – e.g., XRF.
LABORATORY	Analytical laboratory that analyzed the sample – e.g., WSU.

Natural remanent magnetization (magnetic polarity) methods

Field measurements of natural remanent magnetization (the magnetic field of a sample measured when induced magnetic fields are absent or zeroed out by probe; Butler, 1992) were determined from strongly magnetized lavas exposed in the Biggs Junction and Rufus 7.5′ quadrangles during the course of this study in order to distinguish between flow units with normal and reversed magnetic polarity. Magnetic polarity values were determined using a MEDA, Inc. μMag handheld digital fluxgate magnetometer.

The natural remanent magnetization (magnetic polarity) of strongly magnetized lavas was determined using the following method:

1. A north-pointing arrow and near horizontal line were drawn on and around (to the extent possible) an approximately fist-sized equidimensional sample that was then removed from the outcrop (**Figure 11-4**a).
2. The magnetometer was placed on the most level ground available in a relatively magnetically clean area. The probe was then placed in a fixed position in the horizontal plane and rotated to null the local magnetic field (μMag reads zero). This procedure was done incrementally beginning with minimum range sensitivity (2,000 mG [milliGauss]), increasing the sensitivity (20 mG) and re-rotating the probe until maximum sensitivity was reached. Magnetic polarity was then checked with the north end of a locked compass needle. Total field value will decrease when the compass needle is moved horizontally toward and remains parallel to the probe.
3. The polarity of a sample was determined by placing the oriented sample in a path parallel to the probe. The north-verging line drawn to represent the approximate magnetic pole of the sample was held horizontally (approximately) with the north end facing toward the probe at a distance of at least 10 times farther than the measurement distance. A reading was then determined with the sample absent from the probe. The sample was then moved to a point (typically within 1 to 2 cm) toward the probe in order to cause a change of at least several times greater than the minimum resolution of the magnetometer (**Figure 11-4**b). A decrease in the total field value indicated normal-polarity (N); an increase in total field value indicated reversed-polarity (R).
4. The sample was then rotated backward (top away from the probe) about a horizontal axis approximately 45° to see if field strength increased as the sample's inclined magnetic field was rotated into parallel with the probe.
5. The polarity of two to ten representative samples from different portions of an outcrop or from different outcrops was determined to verify the repeatability of results. Erratic results, due to re-magnetization resulting from lighting strikes, obscure post-emplacement alteration, or aberrant declination and inclination are reported as indeterminate (I).

Figure 11-4. Procedure for determining natural remanent magnetism of lavas. (A) Ideal sample is selected and oriented in outcrop. North arrow is drawn on upper surface; horizontal lines are drawn around the exposed edges of the sample. Fist-sized sample is then removed. (B) Magnetometer probe is placed in a fixed position in the horizontal plane and rotated to null the local magnetic field. Sample polarity is determined by moving the oriented sample into the path of the probe.

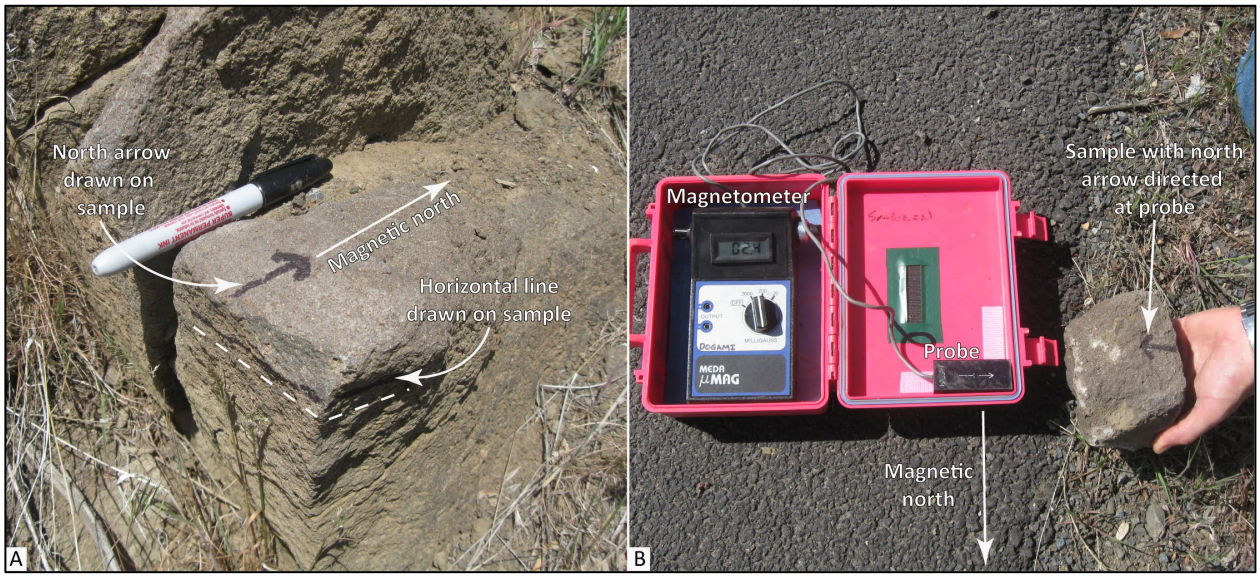

Water well logs

The well log database is derived from written drillers' logs provided by Oregon Department of Water Resources (OWRD). Well logs vary greatly in completeness and accuracy, therefore locally limiting the utility of subsurface interpretations based upon these data. Water well-logs compiled and used for interpretation during the course of this study were not field located. The approximate locations were estimated using tax lot maps, street addresses (coordinates obtained from Google Earth™), and aerial photographs to plot locations on the map. The accuracy of the locations ranges widely, from errors of one-half mile possible for wells located only by section and plotted at the section centroid to a few tens of feet for wells located by address or tax lot number on a city lot with bearing and distance from a corner. At each mapped location the number of the well log is indicated. This number can be combined with the first four letters of the county name (e.g., WASC 5473), to retrieve an image of the well log from the OWRD web site.

Point data are included in the geodatabase, a separate shapefile named BJR2019_WaterWells, and are also provided in a Microsoft Excel® workbook BJR2019_DATA.xlsx (sheet BJR2019_WaterWells). A readme file explaining fields listed in the spreadsheet can be found below in **Table 11-4** and **Table 11-5**. The locations of water well point data are given in six coordinate systems: UTM Zone 10 (datum = WGS 84, NAD 27, NAD 83, units = meters), Geographic (datum = NAD 27, NAD 83, units = decimal degrees), and Oregon Lambert (datum = NAD 83, HARN, units = international feet).

Well intervals listed in the well log database sometimes alternate between consolidated and unconsolidated lithologies and may be listed as alternating between bedrock and surficial geologic units. This may occur where bedrock units are soft, where paleosols or weak zones lie within bedrock, or where cemented or partly cemented zones alternate with unconsolidated zones in surficial deposits.

Table 11-4. Water well database lithologic abbreviations (alphabetical by group).

Unconsolidated Surficial Units	
Abbreviation	**Description**
a	ash
bd	boulders
c	clay
ch	clay, hard (often logged as claystone but probably not bedrock)
g	gravel
gc	cemented gravel
gs	gravel and sand (also sandy gravel)
m	mud
s	sand
sg	sand and gravel (also gravelly sand)
st	silt
Rocl, sedimentary	
a	argillite
bc	breccia
cg	conglomerate
cs	claystone
pbs	pebbly sandstone
sh	shale
sts	siltstone
ss	sandstone
Rock, igneous	
an	andesite

b	basalt
ba	basaltic andesite
cd	cinders
pu	pumice
d	diorite
gb	gabbro
gr	granite
l	lava
r	rhyolite
sc	scoria
t	tuff
v	volcanic, undivided
vb	volcanic breccia
Rock, metamorphic	
mv	meta-volcanic rocks, undivided
ms	meta-sedimentary rocks, undivided
grn	greenstone
gn	gneiss
p	peridotite
ph	phyllite
sch	schist
slt	slate
sp	serpentine
OTHER	
af	artificial fill
cl	coal (lignite)
dg	decomposed granite
o	other (drillers unit listed in notes column of spreadsheet)
rk	rock
sl	soil
u	unknown (typically used where a well has been deepened)

Table 11-5. Water well log database spreadsheet columns.

Field	*Description and Example
TRS	One digit for township, two digits for range, and section; negative if township is south of Willamette baseline – e.g., −10931.
COUNTY	Wasco County – e.g., WASC.
GRID	Well log number for wells. Wells in Wasco County preceded by acronym WASC – e.g., WASC 53799.
WELL_EL_FT	Wellhead elevation in feet as given by Google Earth™ at corresponding WGS 84 location – e.g., 2000.
LOCATED_BY	Google Earth™ elevation for cursor location at a given address – e.g., Google.
	Google Earth™ elevation at house in vicinity of given address – e.g., House.
	Pad identifying approximate well location, visible in air photo – e.g., Pad.
	Approximate taxlot centroid or other best guess for well location using a combination of taxlot maps and aerial photographs – e.g., Taxlot.
	Owner name – e.g., Owner.
	Wells located by Oregon Water Resources Department (OWRD) using handheld GPS – e.g., OWRD.
	GPS coordinates of wellhead included with well log – e.g., GPS.
	Approximate quarter-quarter-section centroid – e.g., qq.
	Approximate quarter-section centroid – e.g., q.
	Approximate fit to sketch map included with well log – e.g., map
LITHOLOGY	Best interpretation of driller's log using abbreviations above – e.g., b.
BASE_FT	Record base of driller's interval or, if lithology abbreviation would not change, similar intervals, in feet below wellhead – e.g., 20.

TOP_FT	Calculated top of driller's interval or similar intervals, in feet below wellhead – e.g., 10.
TOP_EL_FT	Calculated elevation at top of driller's interval, or similar intervals, in feet above sea level – e.g., 1990.
BASE_EL_FT	Calculated elevation at base of driller's interval, or similar intervals, in feet above sea level – e.g., 1980.
BEDRK_LITH	Lists bedrock lithologies, when encountered, abbreviations listed above – e.g., b.
BEDRK_ELEV	Calculated elevation at which bedrock or soil over bedrock was first encountered, in feet above sea level – e.g., 1924.
TAX_LOT	Taxlot number. Where it is determined that a taxlot number is used more than once in the section then the appropriate subdivision of the section is indicated in the notes field – e.g., 800.
COLOR	Color of interval as reported by the well driller – e.g., green.
NOTES	Notes about the stratigraphic interval as originally described by the well driller.
MAP_UNIT_L	Geologic unit interpreted in subsurface on the basis of drillers log and designated by map unit label used in accompanying geodatabase. Intervals labeled "suna" (surface unit not applicable) are those where the lithology as interpreted by the original drillers' log do not correspond; also denotes intervals in the subsurface where a precise unit label cannot be applied.
QUADRANGLE	The USGS 7.5' quadrangle in which the sample is located – e.g., Biggs Junction-Rufus West.
UTMN_WGS84	Meters north in WGS84 UTM projection, zone 10.
UTME_WGS84	Meters east in WGS84 UTM projection, zone 10.
UTMN_NAD27	Meters north in NAD 27 UTM projection, zone 10.
UTME_NAD27	Meters east in NAD 27 UTM projection, zone 10.
LATITUDE_NAD27	Latitude in NAD 27 geographic coordinates.
LONGITUDE_NAD27	Longitude in NAD 27 geographic coordinates.
UTMN_NAD83	Meters north in NAD 83 UTM projection, zone 10.
UTME_NAD83	Meters east in NAD 83 UTM projection, zone 10.
LATITUDE_NAD83	Latitude in NAD 83 geographic coordinates.
LONGITUDE_NAD83	Longitude in NAD 83 geographic coordinates.
N_83HARN	Feet north in Oregon Lambert NAD 83, HARN, international feet.
E_83HARN	Feet east in Oregon Lambert NAD 83, HARN, international feet.

*Well location given in six coordinate systems calculated by reprojecting original WGS 84 UTM, zone 10 locations.

Full-resolution outcrop images

In order to capture the detail and scope of large outcrops, multiple overlapping photographs were taken in the field and processed using Agisoft Metashape structure from motion software. Photographs were taken with an Apple® iPhone® SE or iPad® 2 with a native resolution of 12 megapixels, and photo locations were recorded using the camera GPS system. The photos for each outcrop were aligned in Metashape, and the aligned photos were used to generate a high-resolution point cloud and 3D model. The 3D models were oriented with a view direction that was perpendicular to the outcrop and horizontal, and that orientation was used as the plane of projection for an orthomosaic image. The resulting orthomosaics retain detail in the centimeter range. The full-resolution images are far too large to display in the pamphlet text, so a low-resolution version is embedded in the pamphlet and the full-resolution images are provided in the digital appendix as pdf format files in a folder called Full_Resolution_Images. The image files are named with the figure number from the pamphlet and have the figure caption embedded in the pdf properties.

Full-resolution images:

GMS_124_Figure 5-8_Full_Resolution.pdf
GMS_124_Figure 5-22_Full_Resolution.pdf
GMS_124_Figure 5-27_Full_Resolution.pdf
GMS_124_Figure 5-30_Full_Resolution.pdf
GMS_124_Figure 5-34_Full_Resolution.pdf
GMS_124_Figure 5-35_Full_Resolution.pdf
GMS_124_Figure 5-36_Full_Resolution.pdf
GMS_124_Figure 5-51_Full_Resolution.pdf